Development of non-noble metal-based heterogeneous catalysts for borrowing hydrogen and amidation reactions

Dissertation

in kumulativer Form

zur Erlangung des akademischen Grades

Doctor rerum naturalium (Dr. rer. nat.)

am Leibniz Institut für Katalyse

der Mathematisch-Naturwissenschaftlichen Fakultät

der Universität Rostock

vorgelegt von

Rui Ma

geb. am 25. 06. 1993 in China

Rostock, 19. January.2024

https://doi.org/10.18453/rosdok_id00005098

Gutachter:

Prof. Dr. Matthias Beller, Universität Rostock, Leibniz Institut für Katalyse

Prof. Dr. Shoubhik Das, Universität Bayreuth

Prof. Dr. Malte Behrens, Universität Kiel, Institut für Anorganische Chemie

Jahr der Einreichung: *2024*

Jahr der Verteidigung: *2024*

Declaration

Die vorliegende Arbeit entstand in der Zeit von Oktober 2020 bis heute am Leibniz Institut für Katalyse durchgeführt und von **Dr. Sebastian Wohlrab**, **Prof. Jagadeesh Rajenahally** und **Prof. Matthias Beller** betreut.

This thesis has been performed in Leibniz-Institute for Catalysis in the period from **October 2020** to **Present** and was supervised by **Dr. Sebastian Wohlrab**, **Prof. Jagadeesh Rajenahally** and **Prof. Matthias Beller**

Statement of authorship

I hereby affirm that I have written the present work by myself without side assistance. No other resources were utilized than stated. All references as well as verbatim extracts were quoted, and all sources of information were specifically acknowledged.

Hiermit versichere ich, dass ich die vorliegende Arbeit ohne fremde Hilfe selbst verfasst habe. Es wurden keine anderen Ressourcen als angegeben verwendet. Alle Quellenangaben sowie wörtliche Auszüge wurden zitiert und alle Informationsquellen ausdrücklich genannt.

Rostock, January 2024

Rui Ma

Acknowledgement

First of all, I would like to express my sincere gratitude to Prof. Matthias Beller, Prof. Jagadeesh Rajenahally and Dr. Sebastian Wohlrab for guiding my PhD studies at LIKAT by offering their excellent support, and encouragement throughout the course of this research work.

I am thankful for the China Scholarship Council (CSC) for fellowship to perform PhD studies at LIKAT.

I would also like to extend my sincere thanks to Dr. Helfried Neumann for providing his kind support about using his GC-MS for product analysis. I would like to thank Dr. Jie Gao, Shuoping Ding and Yue Hu for their continued support and timely help. My thanks go to our group members and other colleagues at LIKAT for fruitful discussion that made my stay very pleasant at LIKAT. I would like to give special thanks to the analytical department for excellent analysis and services. Further thanks go to Mr. Torsten Weiss, Dr. Torsten Beweries and Mr. Matthias Auer for their support in chemicals ordering and glass device fabrication. I thank Ms. Anne Tonn and Ms. Nicole Aulerich for their excellent support during research stay at LIKAT.

Finally, I express my deepest gratitude to all my family. They always support my option all the time.

Abstract

This dissertation reports the preparation and application of no-noble metal-based catalysts for the borrowing hydrogen and amidation reactions involving the synthesis of organic compounds. Cobalt-based nanostructured materials are prepared for the *N*-alkylation of primary amides with alcohols through a hydrogen borrowing methodology. Next, iron-zinc bimetal single atoms which enable the α-alkylation reactions of ketones with alcohols is reported. Further, the amide synthesis catalyzed by Ni-nanoparticles is discussed. Regarding the utilization of biomass-based feedstocks, domino reductive amination and amidation of levulinic acid to produce *N*-heterocyclic compounds is performed using cobalt single atom catalysts. Several advanced analytical techniques such as XRD, XPS, BET, Raman, TEM, XAS have been used to investigate the detailed structure of these prepared catalytic materials to understand structure-reactivity relationships.

Diese Dissertation berichtet über die Herstellung und Anwendung von Nanokatalysatoren auf Basis von Nicht-Edelmetallen für die Wasserstoffaufnahme- und Amidierungsreaktionen bei der Synthese organischer Verbindungen. Nanostrukturierte Materialien auf Kobaltbasis werden für die N-Alkylierung primärer Amide mit Alkoholen durch eine Wasserstoff-Borrowing-Methode hergestellt. Als nächstes wird über Eisen-Zink-Bimetall-Einzelatome berichtet, die die α-Alkylierungsreaktionen von Ketonen mit Alkoholen ermöglichen. Darüber hinaus wird die durch Ni-Nanopartikel katalysierte Amidsynthese diskutiert. Im Hinblick auf die Nutzung biomassebasierter Rohstoffe wird die reduktive Domino-Aminierung und Amidierung von Lävulinsäure zur Herstellung N-heterozyklischer Verbindungen unter Verwendung von Kobalt-Einzelatomkatalysatoren durchgeführt. Mehrere fortschrittliche Analysetechniken wie XRD, XPS, BET, Raman, TEM, XAS wurden verwendet, um die detaillierte Struktur dieser vorbereiteten katalytischen Materialien zu untersuchen und Struktur-Reaktivitäts-Beziehungen zu verstehen

List of abbreviation

BET	Brunauer, Emmett and Teller
BH/HA	Borrowing hydrogen / hydrogen auto transfer
C	Vulcan XC-72R carbon powder
CO-IR	Infrared spectroscopy of adsorbed CO
DMF	2,5-Dimethylfuran
FAL	Furfuryl alcohol
FAM	Furfurylamine
FAME	Fatty acid methyl ester
FDCA	2,5-Furandicarboxylic acid
FUR	Furfural
HAADF	High angle annular dark-field imaging
HMF	5-Hydroxymethylfurfural
L	Ligand
LA	Levulinic acid
MA	Maleic anhydride
MHMTHF	(5-Methyltetrahydrofuran-2-yl)methanol
MTHF	2-Methyltetrahydrofuran
mmol	Millimole
mL	Milliliter
NMR	Nuclear magnetic resonance
NPs	Nanoparticles
ORR	Oxygen reduction reaction
Raman	Raman spectroscopy
SAA	Single-atom alloy
SAC	Single atom catalyst
SN	Nucleophilic substitution
STEM	Scanning transmission electron microscopy
TEM	Transmission electron microscopy
THF	Tetrahydrofuran
TMSCl	Trimethylsilyl chloride
XAFS	X-ray absorption fine structure
XPS	X-ray photoelectron spectroscopy
XRD	X-ray powder diffraction
WGSR	Water–gas shift reaction

Contents

List of Figures

List of Schemes

1. Introduction

1.1 Non-noble metal based heterogeneous catalysts

Organic compounds play vital roles in our daily life because they represent important constituents of many essential products including pharmaceuticals, agrochemicals, biomolecules, plastics, and others.[1] In order to synthesize organic compounds, catalysis is crucial, hence around >85% of all chemical products are produced via catalytic proccess.[2] The key to success of catalysis preparation lies in the developing active, selective and stable, recyclable/reusable catalysts.[3] Generally, catalysts are divided into homogeneous and heterogeneous, based on whether these catalysts are in the same phase with the reaction mixture.[2, 4] Homogenous complexes are in the same phase of reactants, while heterogeneous materials are in solid form, and they are not in the same phase as the reactants. Homogeneous complexes exhibit excellent selectivity and activities, but they are unstable at higher temperature and difficult to recover and resue.[2, 4] In contrast, heterogeneous catalysts are relatively practical and can be reused easily; as a result, they are preferable for achieving more sustainable and cost-effective processes. Heterogeneous catalysis typically proceeds on the surface of a solid materials.[5] For example, compared with larger metal particles, the smaller one exposed more to reactants. The degree of exposure not only affects the distribution of metals, but also has a strong impact on selectivity.[5] The first generation heterogeneous catalysts such as bulk materials are composed of many metal atomic particles or heterogeneous aggregates of metal atoms, just a section of them is active for a certain reaction.[5]

The supported metal nanoparticles are then explored as the second-generation of heterogeneous catalysts. The activity of nanoparticle-based materials highly depends on the nature, size and the surface features of supports. Generally, metal oxides (Such as Al_2O_3, SiO_2, TiO_2) and carbon-based materials (carbon nanotube, graphene, carbon nanosheet) are used as common inorganic materials to support nanoparticles.[5]

The new frontiers of heterogeneous materials are the single atom catalysts (SACs), which are considered to be a bridge between homogeneous and heterogeneous. As shown in **Figure 1**, the development of SACs started already from 2003 and they have applied for variety of organic transformations.[6] According to the concept of SACs, each metal atom interacts with heteroatoms in the support and contain isolated single sites with 100% atom efficiency. Hence, they combine both the homogeneous metal complexes and the heterogeneous materials. The stability of single atoms is the key issue. In order to achieve this, creation of micro-environment

around metal atoms is important. In this regard, generation of nitrogen-doped carbon around single atoms plays crucial role to stabilize individual atoms. Usually, nitrogen containing ligands are used to incorporate nitrogen species to the parent carbon materials. The nitrogen atoms in the carbon support not only firmly anchor single metal centers but also could modify the electronic properties of the carbon support.[5] Preparing single atoms with high stability and high metal loading is also a challenging task.[6, 7]

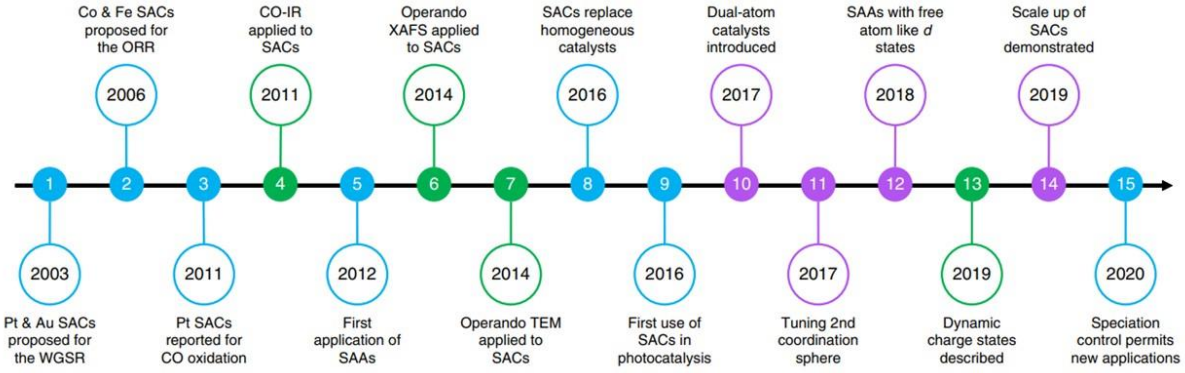

Figure 1. Progress of single-atom catalysis.[6]

Due to inherited advantages of non-noble metals with respect to abundancy and inexpensive, they are more preferred for catalysis applications. To be clear, non-noble metal-based heterogeneous catalysts are critical to advancing sustainable chemical processes for the synthesis of chemicals used in our lives. In this regard, the main objective of this work is developing non-noble metal based supported nanoparticles and single atoms catalysts and exploring their applications in the synthesis of organic compounds.

1.2 Borrowing hydrogen methodology

The hydrogenation has a wide range of application in chemical reactions.[8, 9] Transfer hydrogenation is an important branch of hydrogenation reactions, where hydrogen comes from one molecule to another without involving hydrogen gas.[10] Borrowing hydrogen (BH) methodology, noted as hydrogen auto transfer, related to transfer hydrogenations. However, in BH-methodology one of the substrates itself acts as the hydrogen transfer agent without any additional hydrogen source. The general pathway for the of BH methodology is shown in **Figure 2**. In BH-strategy, first the catalytic dehydrogenation of one substrate took place to generate more reactive intermediate and hydrogen. And then the unsaturated intermediate reduction to the desired product with the hydrogen Notably, BH-methodology offers several advantages, for example, utilization of inexpensive and easily accessible starting materials such

as alcohols or amines, no additional hydrogen required, no any other by-products except water.[11]

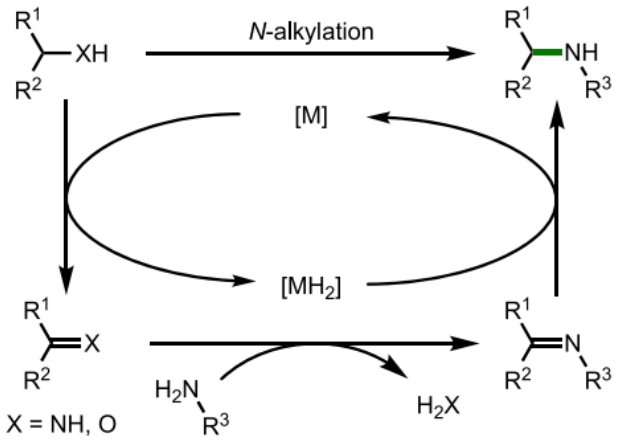

Figure 2. General mechanism for the catalytic borrowing hydrogen methodology.[11]

Most commonly, the functionalization of N-H and C-H bonds can be achieved by borrowing hydrogen methods and this method can also be applied to prepare corresponding mono or di-alkylated products. The concept of borrowing hydrogen was proposed in 2004.[12] An early great work based on nickel catalyzed *N*-alkylation of anilines with alcohols was reported in 1932.[13] Other examples of using the heterogeneous nickel catalysis appeared in subsequent years.[14] The earliest example of hydrogen-borrowed homogeneous catalysis were reported in 1980s, when the ruthenium- and rhodium-based catalysts were demonstrated.[15-17] These seminal results indicated that the borrowing hydrogen approach is very useful and inspired us for further research.

1.2.1 *N*-Alkylation of primary amides

The *N*-alkylation process is a fundamental feature of BH chemistry, which is important in C-N bond formation. The reaction pathway of nucleophilic substitution (SN) and hydrogen transfer are reported.[18] Since amides are less nucleophilic than amines, reactive alcohols (e.g., benzyl, acetylenic, allyl alcohols) are often required as alkylating reagents, SN-type mechanism involving a carbocation intermediate is often proposed.[19, 20] When the non-activated alcohols were used, a hydrogen transfer mechanism can be observed in **Figure 3**.[21]

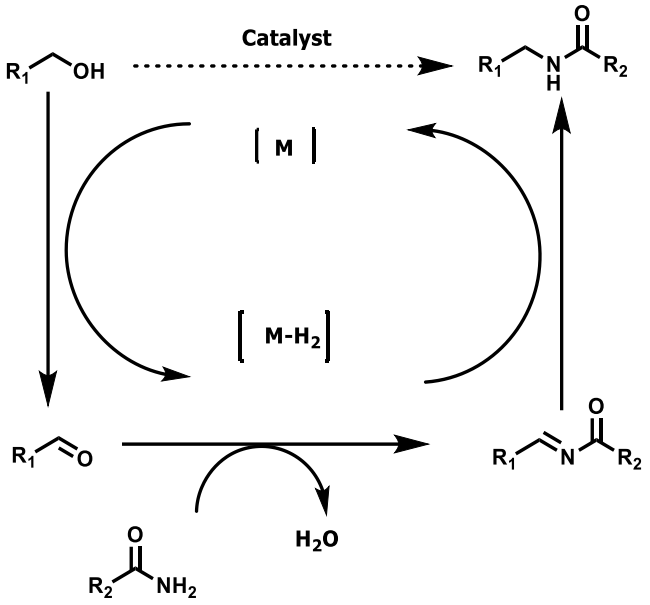

Figure 3. Hydrogen transfer mechanism in *N*-Alkylation of amides with alcohols.[11]

The development of C-N bond by hydrogen borrowing have a long history.[13] An excellent representative example is the use of homogeneous Ir-based complexes in the *N*-benzylation reaction of aniline reported by Yamaguchi and co-workers in 2003.[22] Williams and co-workers performed the same reaction in 2009 on ruthenium p-cymene dichloride dimer.[23] In the same year, supported silver and magnetite were used as alternative catalysts by Satsuma[24] and Ramon[25]. Further studies revealed that many other metals can also be used in the borrowing hydrogen transformation. A heterogeneous palladium was used to synthesize *N*-benzylamine by Sabater and co-workers in 2010.[26] In the same year a gold catalyst was reported, which can also accomplish this transformation.[27] In 2011, a homogeneous palladium(II) acetate was reported by Ramon and co-workers.[28] An osmium PNP complex was reported soon.[29] Another tin catalyst was also demonstrated.[30] The formation of *N*-benzylaniline was achieved using a rhodium catalyst in 2013.[31] Later a heterogeneous nickel-catalyst was demonstrated by Satsuma and co-workers.[32] The diversity of catalysts available for this hydrogen borrowing transformation was further increased.[33] A Rh catalyst was employed for this reaction in 2014.[34]

Among these, homogeneous noble-metal catalysts and acid-catalysts are still dominating. Regarding heterogeneous catalysts, only five examples based on Pd-[35], Re-[36] and Ag-[37] metal have been developed until now. (**Figure 4**).

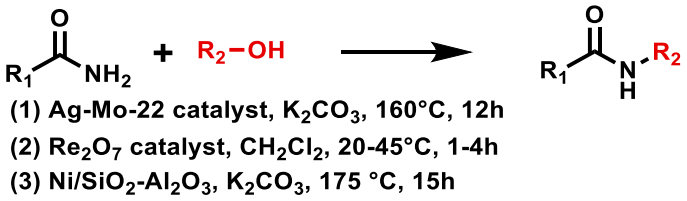

Figure 4. The current three heterogeneous procedure for the *N*-alkylation of primary amides.

1.2.2 C-Alkylation of ketones with alcohols

In parallel with *N*-alkylation studies, many authors also focused on using the borrowing hydrogen approach in C-alkylation processes. The product from C-alkylation process is widely used to synthesis lots of chemicals.[38] At the same time, lots of agents are applied in the process (**Figure 5**).

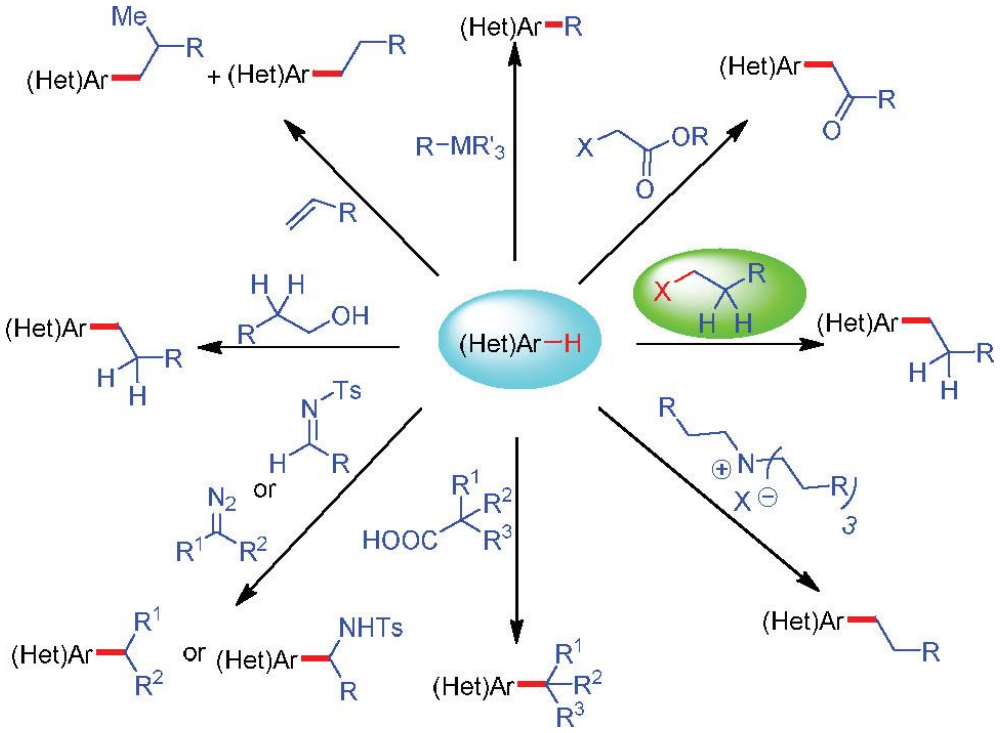

Figure 5. Alkylating agents used in the C-alkylation process.[38]

Precious metal-based catalysts are used in previous reports. For example, a Ru-based catalyst for the C-alkylation of acetophenones was reported in 2002.[39] In addition, 2 years later, Ir based homogeneous protocol is developed and used for this reaction by Ishii and co-workers.[40] A nano catalyst based on palladium was developed too.[41] Hydrogen acceptors (1-dodecene and 1-decene) was employed to prevent the hydrogenation of ketone to alcohol. In

2007, Yus and co-workers did a great work, where nickel nanoparticles is prepared for this reaction.[42] They also reported some good works based on an osmium-catalyzed procedure for the C-alkylation reaction.[43] Mishra and co-workers proposed a heterogeneous copper-catalyzed approach in 2013.[33] A Rh-based catalysts for alkylation between ketones and primary alcohols is also reported.[44] Another approach using rhodium was later realized.[45] In 2015, Sortais and Darcel showed readers that the iron could also enable the α-alkylation reaction between ketones and primary alcohols.[46] Noteworthy, a manganese catalyst could enable the reaction between oxindoles and primary alcohols.[47] A PNP-pincer ligand based on a Rh-, which enable the C-alkylation of acetophenone, is developed too.[48] A cobalt based homogeneous catalysts was developed by Zhang.[49] A homogeneous Ni-based approach was done by Banerjee and co-workers.[50]

Although numerous methods for a-alkylation of alcohol with ketone reaction have been reported, but the current problems are obvious. Such as, the catalysts are based on homogeneous and precious metals in presence of base. In the point view of sustainable synthesis of chemicals, it is quite important to develop practical methods, including new catalysts, new mechanism, and new reaction.

1.3 Synthesis of amides

Amides is widely used in organic and medical filed, and its synthesis is quite hot in organic research. Amides represents lots of chemicals, which are widely used in science fields.[51] For example, they could be used to prepare polymers, drugs and biomolecules.[52] As reported, lots of drugs belongs to the scope of amide chemicals, such as Acetaminophen, Lidocaine and Levobupivacaine, which are very important for our daily life.[53] Hence, to synthesis amides is a very important direction in chemistry. The common approaches to synthesis amides are shown in **Figure 6**.[54, 55] The best method to produce amide is the condensation reaction of carboxylic acid with amine. However, various agents are necessary for reactions between carboxylic acid and amine, which will produce lots of waste chemicals. Thus, the greener approaches for amide creation are attracting attentions of lots of scientists.

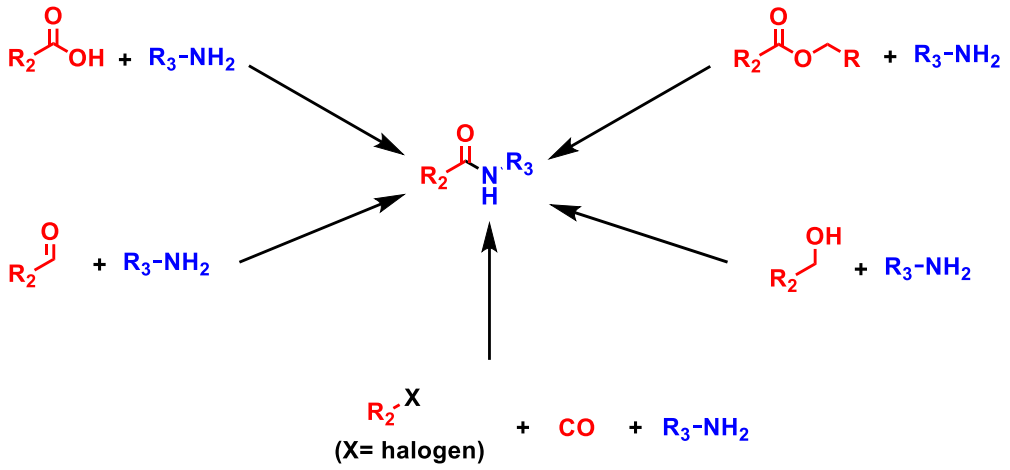

Figure 6. Common amide formation reactions.[54, 55]

The first reaction example from ester and nitro compounds to amide is based on the nickel homogeneous procedure, which is reported by Hu and co-workers.[56] In this catalysis system, they used nickel, phenanthroline, TMSCl, and Zn. Later the mechanism is explored, zinc (Zn) was used to reduce bivalent nickel into zero nickel, which can active ester. While chlorotrimethylsilane (TMSCl) works as Lewis acid in the reaction. By using Zn and TMSCl, an amide anion is produced by the reaction between nickel acyl complex and nitroarene. However, side products, such as Silyl ether (TMS_2O), zinc (II) chlorides and siloxides are formed. A similar work is reported by Ma and co-authors. Typically, a Mn powder and TMSCl is used in this procedure (**Scheme 1**).[57]

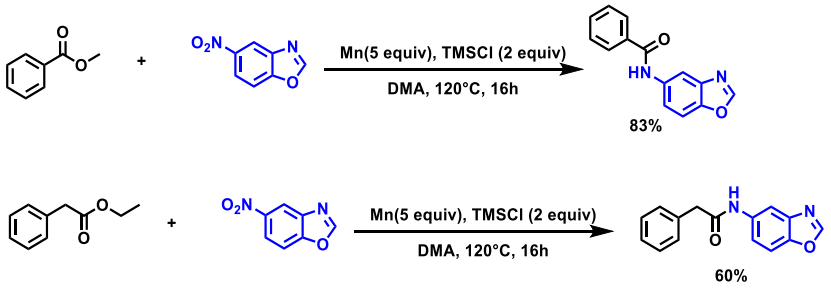

Scheme 1. Mn catalyzed amide synthesis.[57]

In 2019, a chromium based homogeneous system ($CrCl_3$/dtbpy/Mg, TMSCl, THF, 90 °C) for the amidation reaction between esters and nitro compounds is reported.[58] The function of metallic magnesium is to reduce Cr(II) complex to form Cr species with low valence (**Scheme 2**).[58]

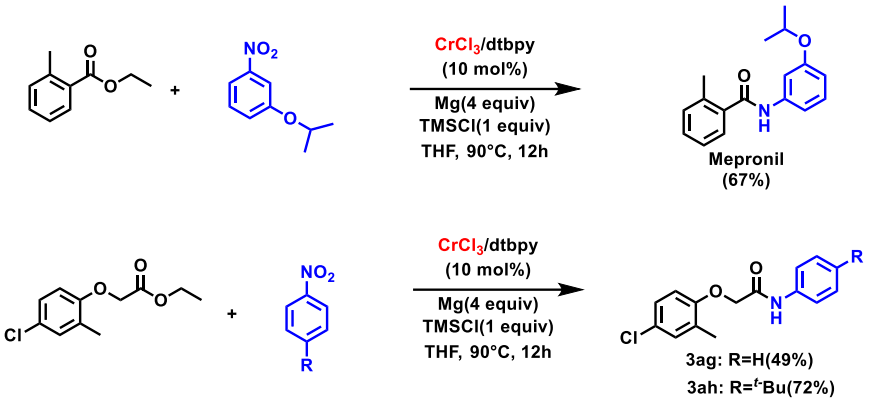

Scheme 2. Applications in the synthesis of amides.[58]

Up to here, we can see TMSCl is a necessary chemical for amide synthesis. The practical methods about designing of heterogeneous catalysts using molecular hydrogen is highly desired. Amide is very important for our life, nylon and paracetamol belongs to amide family. The current method focuses on using expensive starting materials, this is not a good method. People should seek cheaper reactants, such as CO_2, glucose, wood, and straw. Probably, the selectivity will be a bottle neck if we do the reaction using wood, because wood contains lots of different chemicals. However, this method will help to reduce the cost and make the earth green. To make a greener approach in the synthesis of a typical chemicals, people should work hard to explore both the catalysts and reaction method. In another hand, to synthesis useful amide from plastic is also a very interesting method. Plastics contain carbon, oxygen, nitrogen and hydrogen, these elements are same to the current using fossil chemicals. Based on this point, we think it is quite possible to synthesis drugs and pharmaceuticals. Currently, the plastic conversion is very hot in scientific research. So, how to synthesis amides from plastics in one pot under milder conditions is an interesting direction, too.

1.4 Valorization of levulinic acid

The limitation of fossil-based resources encourages us to look for renewable resources. Biomass is a very interesting building blocks, which could be converted into various chemicals.[59] In addition, using biomass to prepare chemicals is a carbon neutral circular framework, too.[60]

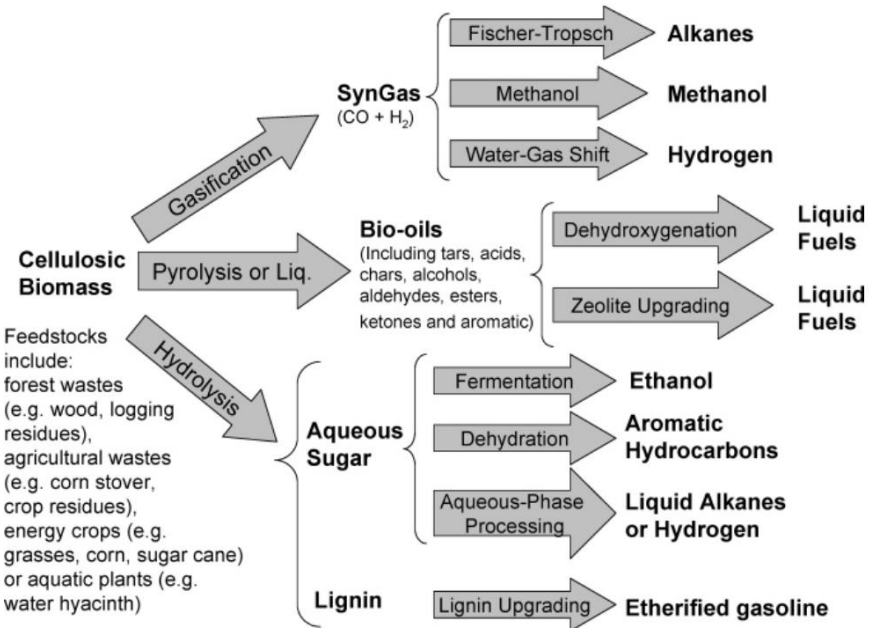

Figure 7. Method for the conversion of biomass.[61]

More and more people know that biomass is a potential source for chemical production, which is necessary to support our life. The method that used for conversion biomass could be found in **Figure 7**.[61] Both syngas, bio-oil, sugars and lignin dimer or monomer units could be given by biomass upgrading.[59] Chemicals including levulinic acid, furfuryl alcohol, 2-Furaldehyde could be given from biomass (**Figure 8**).[62,63] From **Figure 8**, we can see lots of chemicals could be produced from biomass upgrading reactions. Noteworthy, these products represent drugs and pharmaceuticals. Amino acid could also be given form biomass, which is a potential chemical in the production of drugs. But the current limitations for biomass conversion is that the products are very limited. The means to expand the substrate scope is quite important and necessary. Hence, new catalysts and new reaction pathway should be developed by using advanced research methods. So, the hydrogenation of biomass using hydrogen molecular in one pot to produce one certain chemical with relatively higher selectivity is quite interesting.

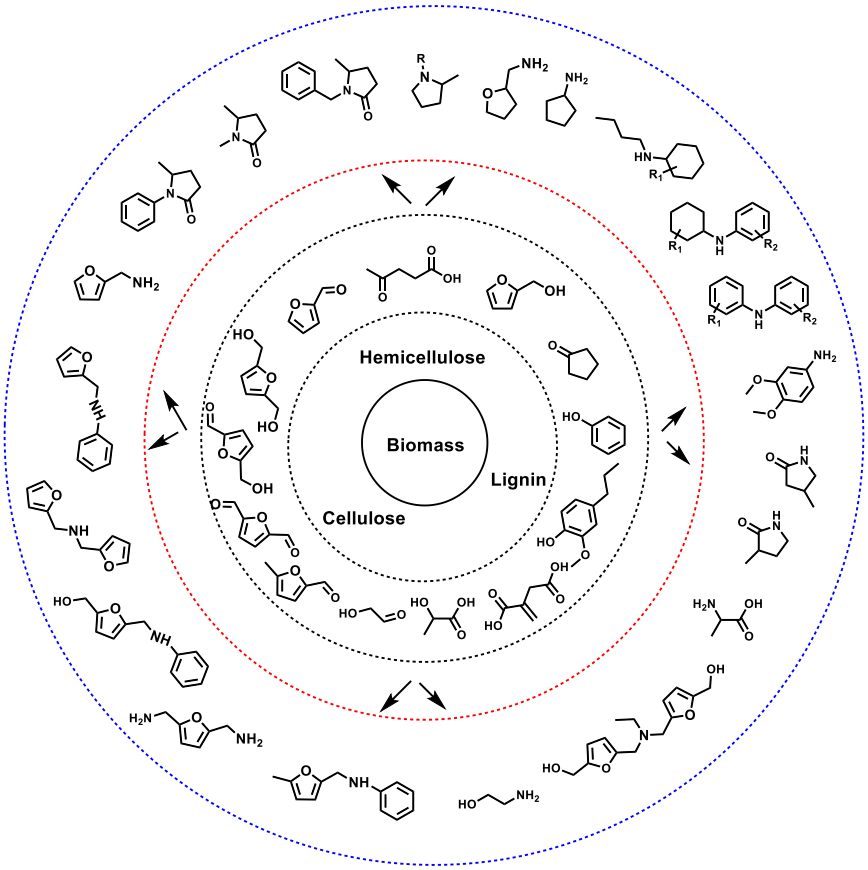

Figure 8. The typical chemicals that could be obtained from biomass.[62]

Cellulose is very useful in the field of biomass. As shown in **Figure 9**, levulinic acid could participates in the formations of many chemicals, these chemicals have typical H-bonding.[64, 65]

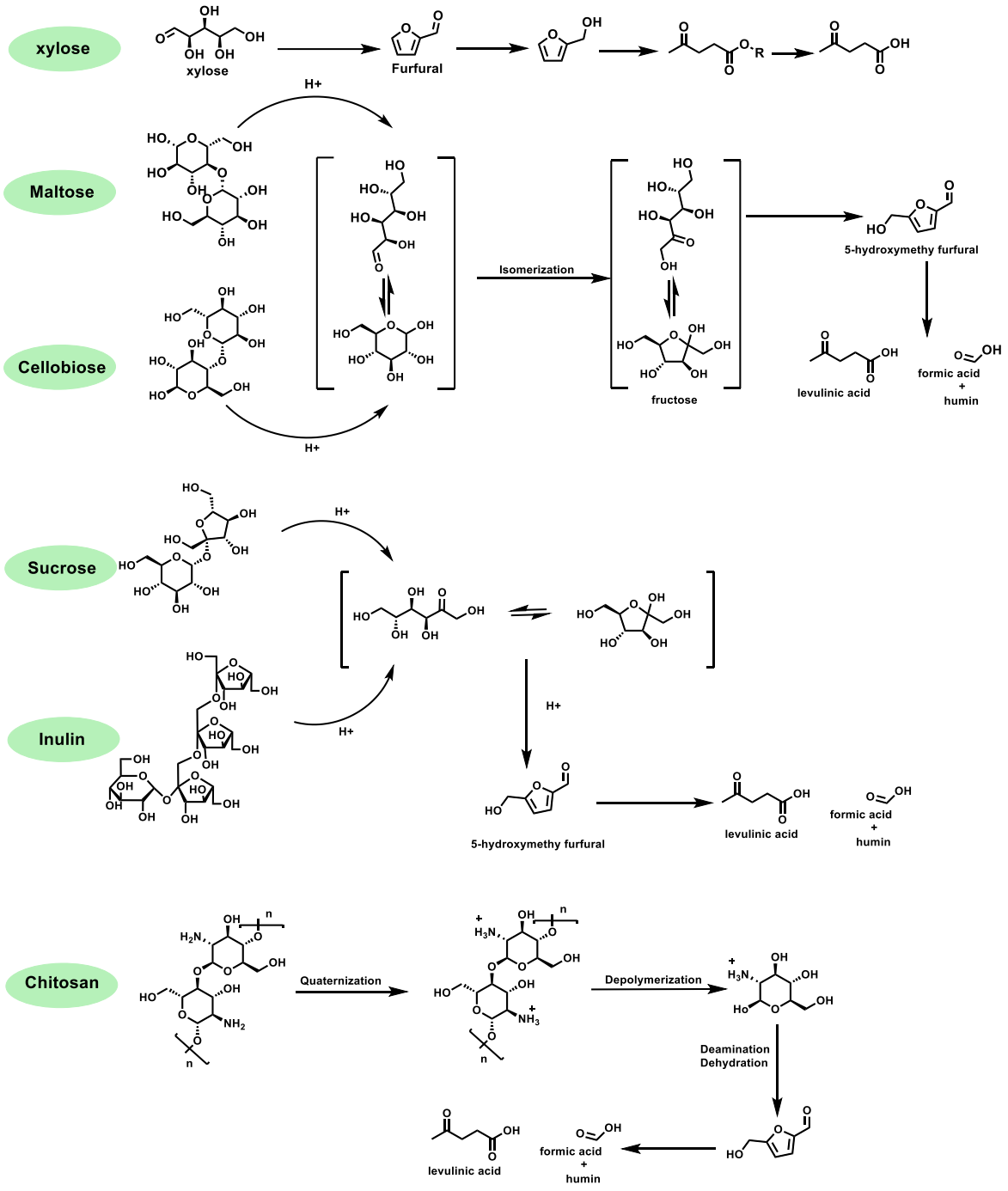

Figure 9. Levulinic acid involved chemicals synthesis from various substrates.[64]

The LA molecular have carboxylic and carbonyl groups.[66] LA has been recognized as an important platform chemical to produce many other chemicals (**Figure 10**).[64]

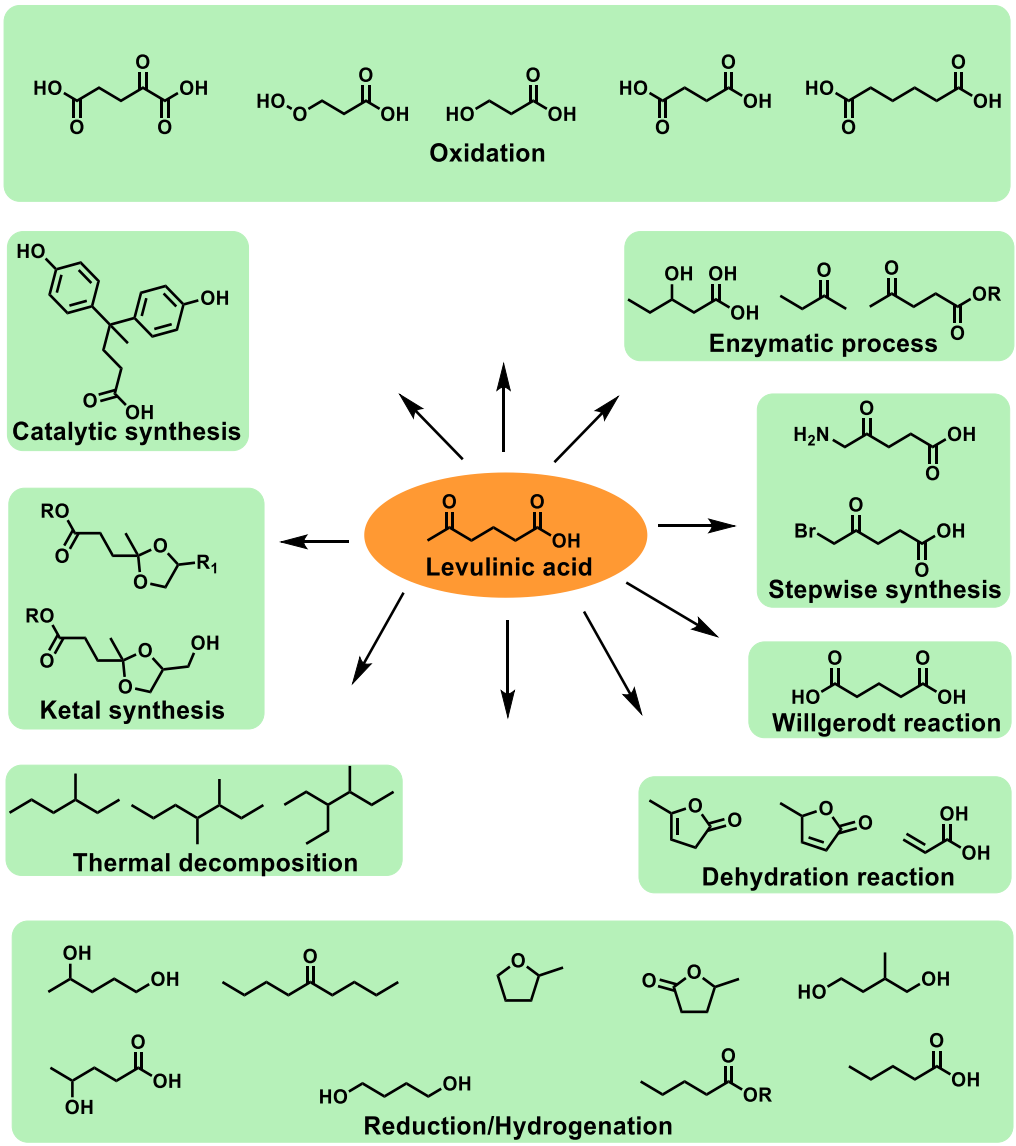

Figure 10. The chemicals that can be produced from levulinic acid upgrading.[64]

The reduction or hydrogenation of LA could yield many products using different approach (**Figure 10**).[64,67] *N*-Alkyl-5-methyl-2-pyrrolidones is a product formed from the reductive amination reaction of levulinic acid (LA), which is commonly serving as industrial solvents, dispersants, and surfactants.[68,69] In industry, pyrrolidinones are given from γ-butyrolactone and butanediol using higher temperatures (>200 °C).[70] Usually, three steps are included: condensation of carbonyl groups by the amino, hydrogenation of imines and intramolecular of aminopentanoic acid (**Scheme 3**).[71,72]

Generally, the reaction mechanism is up to the catalysts, reaction and the involved agents. So, to explore the reaction mechanism is not a good direction, because the reaction is not new, and the selectivity for this reaction is also quite high. So, what we can do in usage of

levulinic acid is to explore new reaction, means, new products will be formed from levulinic acid. This is a very interesting point in the usage of levulinic acid, as the current product for this reaction is very less. Hence, people should expand the products scope of levulinic acid involved reactions. Such as, to prepare ethanol, methanol, acetone, toluene, and fatty acid from levulinic acid will be very valuable. However, people should perform all these conversions in mild conditions. At the same time, people also pursue high selectivity for the reaction of levulinic acid. Totally speaking, both the mild conditions, higher selectivity, and cheaper cost are key point in the research of levulinic acid conversion. In addition, people should also develop new catalysts, to solve the current problems in the production of various chemicals from levulinic acid conversion. The most important thing is the selectivity and the reaction condition. Biomass is a useful resource for production of lots of chemicals. But new reactions should be developed, to obtain more and more products from biomass upgrading. The current work concentrated on using the pure levulinic acid as the starting materials. So, to obtain pyrrolidones from glucose through one pot is quite interesting, too.

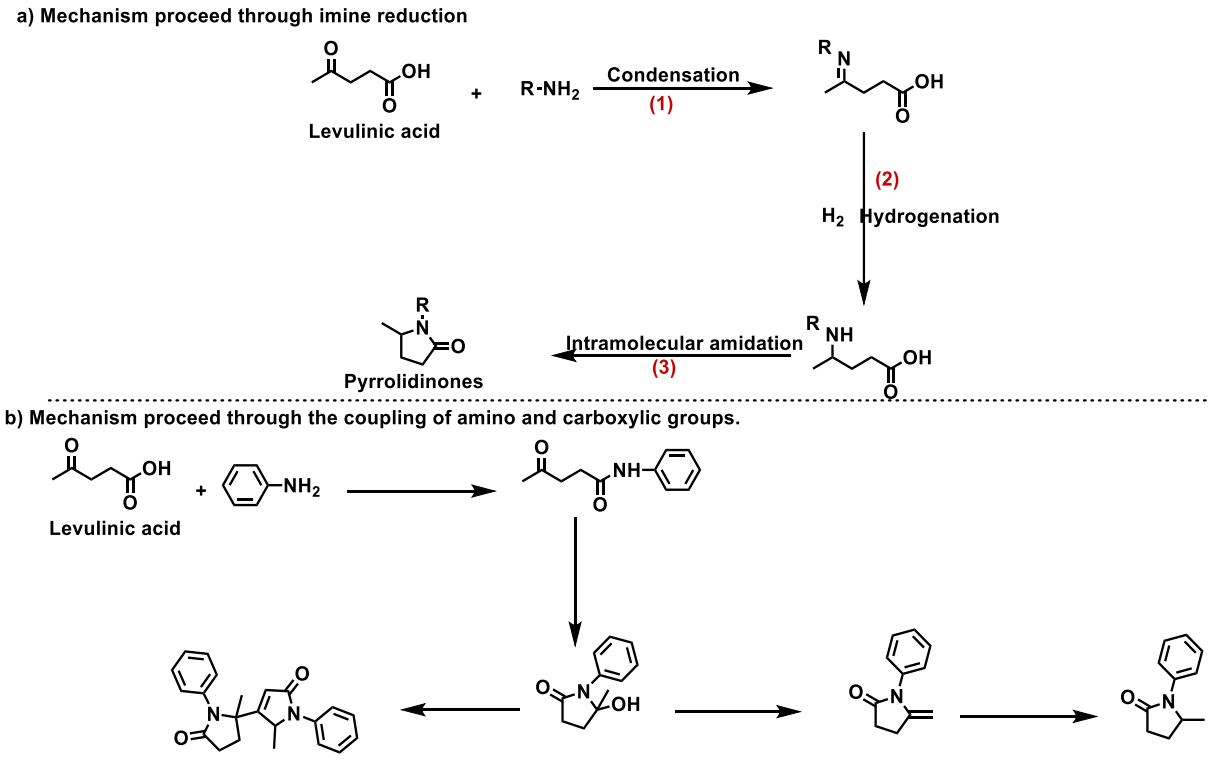

Scheme 3. The reaction roads for reductive amination of LA. a) Mechanism proceed through imine reduction.[71] b) Mechanism proceed through the coupling of amino and carboxylic groups.[72]

In recent years, some groups have contributed great works in the amination reaction of levulinic acid. Here we discuss selected examples on the heterogeneous procedure for the

catalytic reductive amination and amidation of LA to produce different *N*-heterocycles. In 2019, a Pt/P-TiO_2 material could realize the reductive amination of pyrrolidones at ambient conditions(**Figure 11**).[69] Another example, Pt-based nano catalyst used for this reaction is reported in 2020.[73]

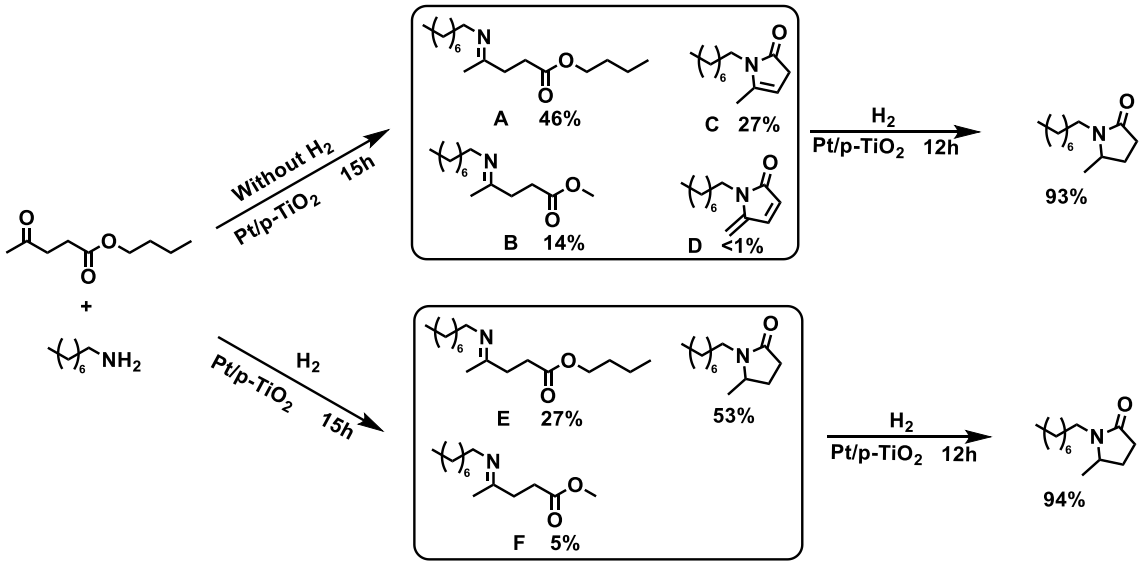

Figure 11. Control experiments in reductive amination of butyl levulinate with n-octylamine.[69]

As the only non-noble metal-based catalyst, CNFx@Ni@CNTs was developed by Gao and co-authors, which can catalyzed the reaction of aniline with LA at 130℃ and 30 bar H_2.[72] From the current works of reductive amination of levulinic acid, we can see the efficient catalysts still relies on the noble metal. Until now, only one nickel catalyst is reported for simple reaction of LA and anilines without extended substrate scope.[72] Thus the preparation of general 3d metal based catalysts are highly important for the reductive amination and amidation of LA for the cost-effective production of pyrrolidinones and related *N*-heterocycles.

Not limited to these, people can do this reaction at ambient conditions, but the catalysts are based on noble metals.[73] Hence, to prepare 3d metal-based catalysts is quite important to produce value-added chemicals. In addition, how to synthesis levulinic acid from biomass with higher selectivity and milder conditions is a current problem. Generally, levulinic acid is produced from glucose and cellulose using strong acid solution. So, new method that enable the production of levulinic acid is quite important for us. In addition, we can also synthesis pyrrolidones from biomass in one pot. So, these products are quite important to support our research in the utilization of levulinic acid.

2. Objectives of this work

As described in the introduction, borrowing hydrogen methodology using alcohols, amidation reactions and the valorization of levulinic acid are very vital transformations are of key importance in fine and bulk chemicals synthesis. The development and applicability of efficient catalysts is necessary for these reactions. Notably, most known catalyst systems for the desired transformations mentioned above are based on precious metals. Hence, the point of this work is to prepare heterogeneous nano catalysts for these reactions. To synthesis nanoparticles (NPs) as well as single atom catalysts (SACs), we followed different approaches by immobilizing suitable metal salts or metal-ligand complexes on heterogeneous supports and subsequently pyrolyzed under argon atmosphere. As example, carbon supported Co-NPs are prepared and show good performance in *N*-alkylation of amides with alcohol. Next, Fe/Zn-single atoms are prepared and exhibit good activity for the base-free selective α-alkylation and α-vinylation of ketones with alcohols. Further, Ni-NPs are designed for the green and practical amides production from esters and nitro compounds. Finally, Co-single atoms on carbon supports are synthesized, and display good applications in the levulinic acid amination.

3. Summary of this work

In this section the following concepts are briefly summarized:

1. Cobalt-nanomaterial used for *N*-alkylation of amides with alcohols.
2. Fe/Zn-SACs for the base-free α-alkylation and α-vinylation of ketones with alcohols.
3. Co-SACs catalyzed upgrading of levulinic acid.
4. Ni-NPs catalyzed amide synthesis from esters and nitro compounds.

3.1 Cobalt-nanomaterial used for *N*-alkylation of amides with alcohols [74]

In this work, we prepared a Co-L5@C-800 catalysts, which displays very good activity and selectivity in *N*-alkylation of amides with alcohols. By comparing the catalysts with and without ligand (**Figure 12-13**), we can find that when using ligand in the preparation procedure some carbon layers will formed on the outer surface of metallic Co, which makes the reaction site more stable. Then, the applicability of the Co-L5@C-800 was demonstrated for synthesis >45 products **(Scheme 4**). The unreported secondary amides can also be obtained in good yield from biological amides by using this method (**Scheme 4, 2j**).

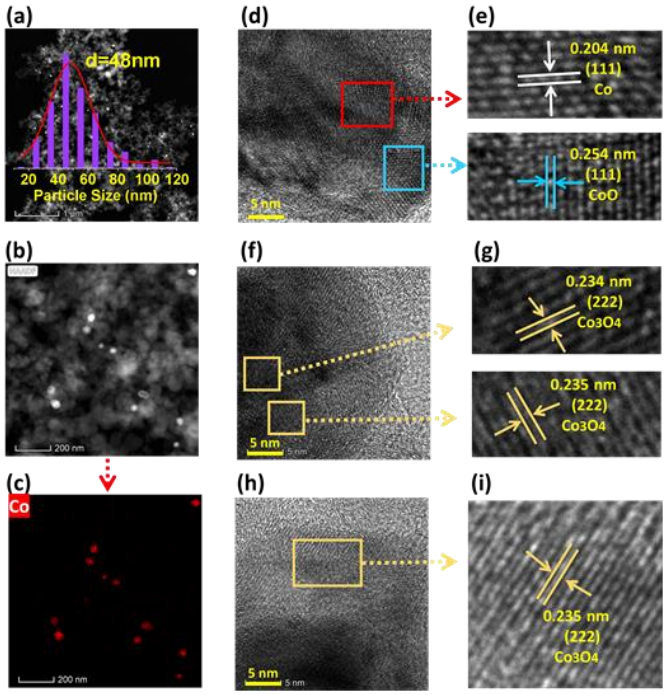

Figure 12. TEM-HAADF and EDX analysis of Co@C-800. (a-b) TEM-HAADF images, (c) EDX element mapping image of Co, (d-i) identified crystal planes of the Co nanoparticles.[74]

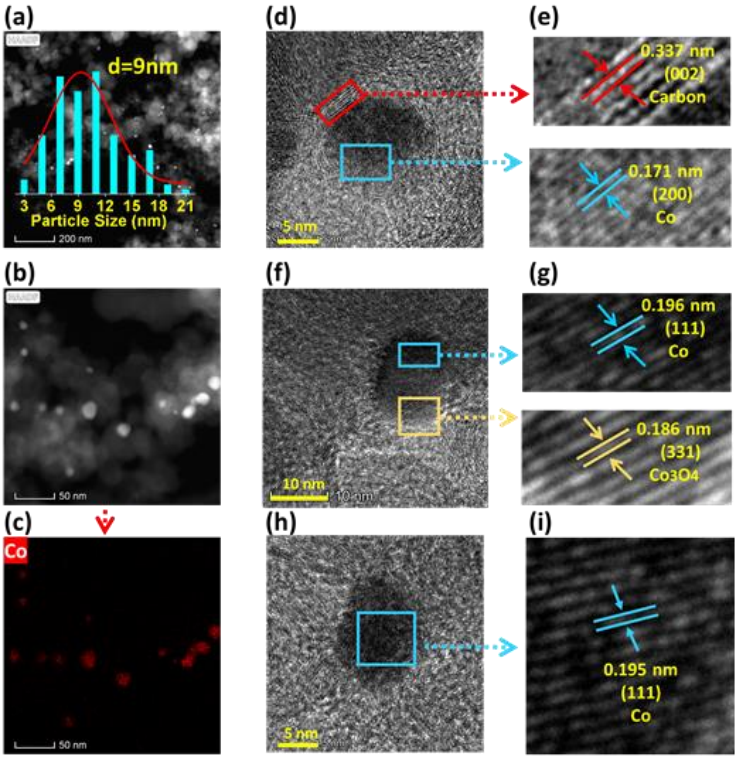

Figure 13. TEM-HAADF and EDX analysis of Co-L5@C-800. (a-b) TEM-HAADF images, (c) EDX element mapping image of Co, (d-i) identified crystal planes of the Co nanoparticles.[74]

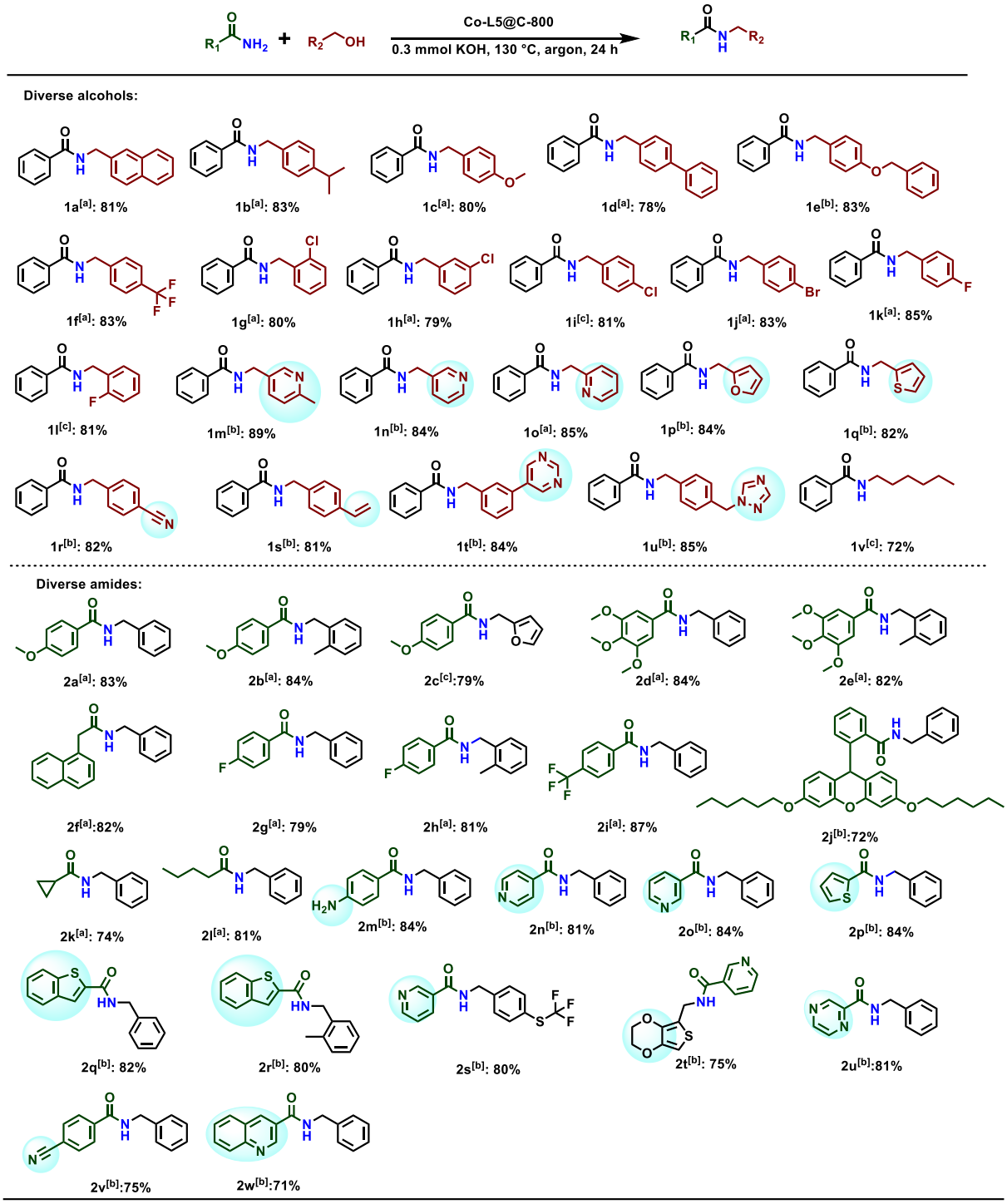

Scheme 4. Substrate scope of Co-L5@C-800. Reaction conditions: [a] 60 mg Co-L5@C-800 (1.9 mol% Co, 0.5 mmol amide, 0.55 mmol alcohol, 0.3 mmol KOH, 3 mL toluene, 130 °C, 24 h, 1 atm argon. Isolated yields. [b] same as [a] at 140 °C. [c] same as [a], GC yield.[74]

3.2 Fe/Zn-SACs for the base-free α-alkylation and α-vinylation of ketones with alcohols

Traditionally, the formation of α-alkylated ketones usually take place by using environmentally harmful alkyl halides in presence of base.[75, 76] Developing non-noble metal based heterogeneous catalytic system, which enable this reaction to occur under mild conditions is challenging. In this work, a novel Fe-Zn single atom material is presented, which catalyze the α-alkylation of ketones with alcohols without using base and hydrogen acceptor.

The success of this Fe/Zn-**L1**@MgO-Al_2O_3-70 catalyst is based on creating Fe and Zn single atoms (**Figures 14-16**) and abundant basic sites (**Figure 17**). The applicability of the Fe/Zn-**L1**@MgO-Al_2O_3-70 was demonstrated for synthesis >50 structurally diverse and functionalized ketones (**Scheme 5**). Utilizing the novel catalyst material different substituted chalcones can also be synthesized (**Scheme 6**). Similarly, our catalyst system is suitable for the synthesis of quinolines, >18 substituted functionalized quinolines were obtained (**Scheme 7**).

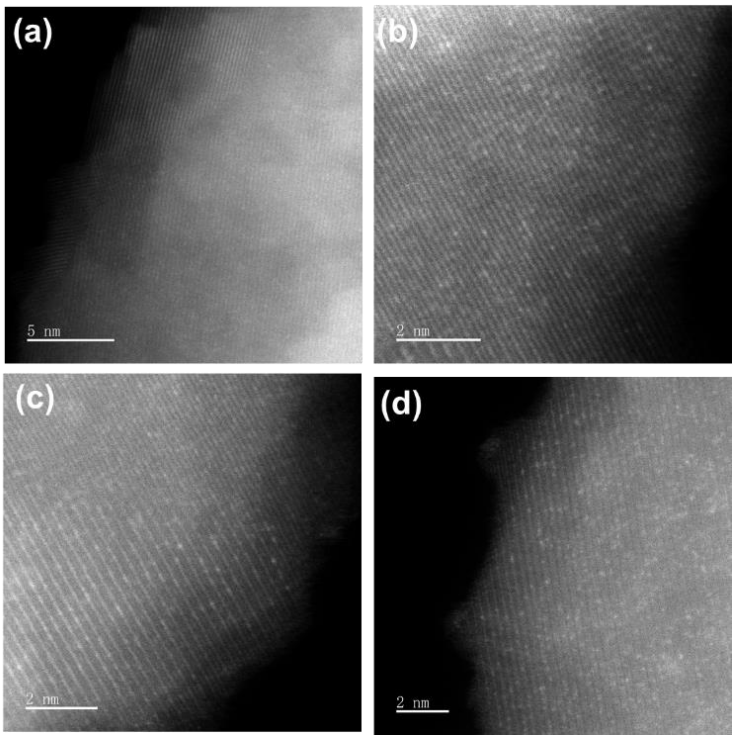

Figure 14. HAADF-STEM images of Fe/Zn-**L1**@MgO-Al_2O_3-70.

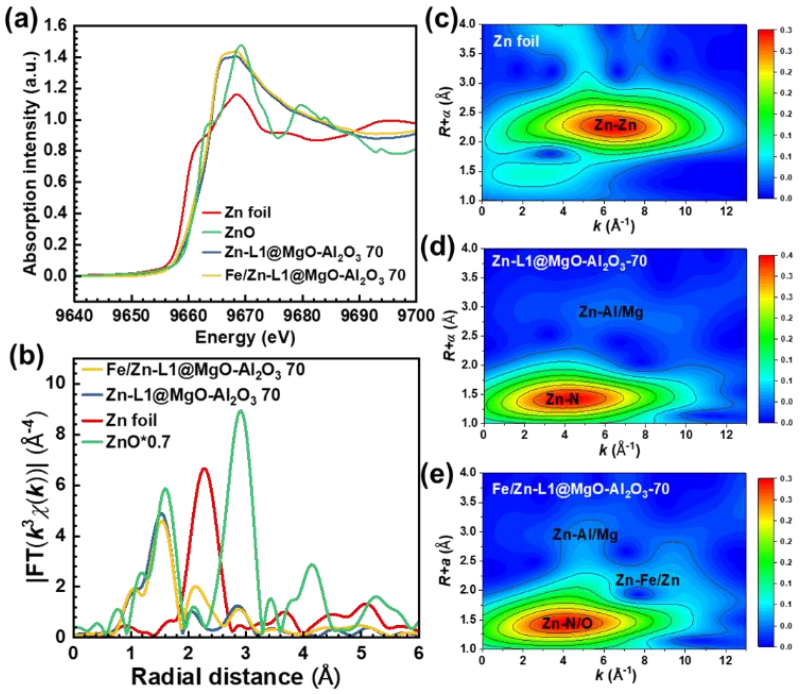

Figure 15. Structural characterizations of catalysts at Zn K-edge. (a) XANES spectra of Zn foil, ZnO, Zn-**L1**@MgO-Al_2O_3-70 and Fe/Zn-**L1**@MgO-Al_2O_3-70. (b) Fourier transformation of k3-weighted EXAFS spectra of Zn foil, ZnO, Zn-**L1**@MgO-Al_2O_3-70 and Fe/Zn-**L1**@MgO-Al_2O_3-70. (c-e) Wavelet transforms (WT) of Zn foil, Zn-**L1**@MgO-Al_2O_3-70 and Fe/Zn-**L1**@MgO-Al_2O_3-70.

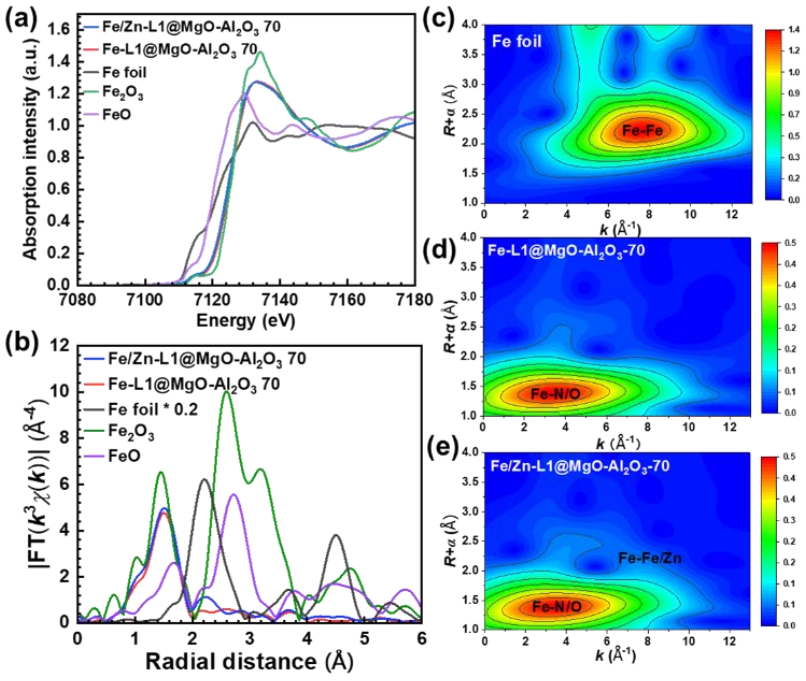

Figure 16. Structural characterizations of catalysts at Fe K-edge. (a) XANES spectra of Fe foil, Fe_2O_3, FeO, Fe-**L1**@MgO-Al_2O_3-70 and Fe/Zn-**L1**@MgO-Al_2O_3-70. (b) Fourier transformation of k3-weighted EXAFS spectra of Fe foil, Fe_2O_3, FeO, Fe-**L1**@MgO-Al_2O_3-70 and Fe/Zn-**L1**@MgO-Al2O3-70. (c-e) Wavelet transforms (WT) of Fe foil, Fe-**L1**@MgO-Al_2O_3-70 and Fe/Zn-**L1**@MgO-Al_2O_3-70.

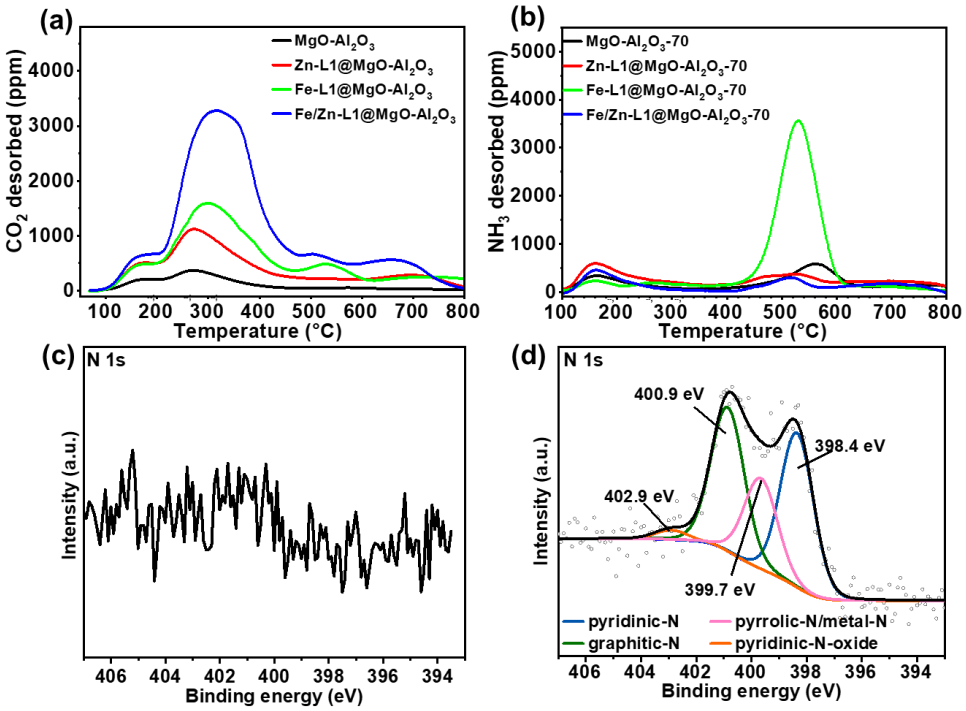

Figure 17. Characterization of catalysts. (a) TPD-CO_2 curves and (b) TPD-NH_3 curves of Fe/Zn-**L1**@MgO-Al_2O_3-70. (c) N 1s spectra of Fe-**L1**@MgO-Al_2O_3-70. (d) N 1s spectra of Fe/Zn-**L1**@MgO-Al_2O_3-70.

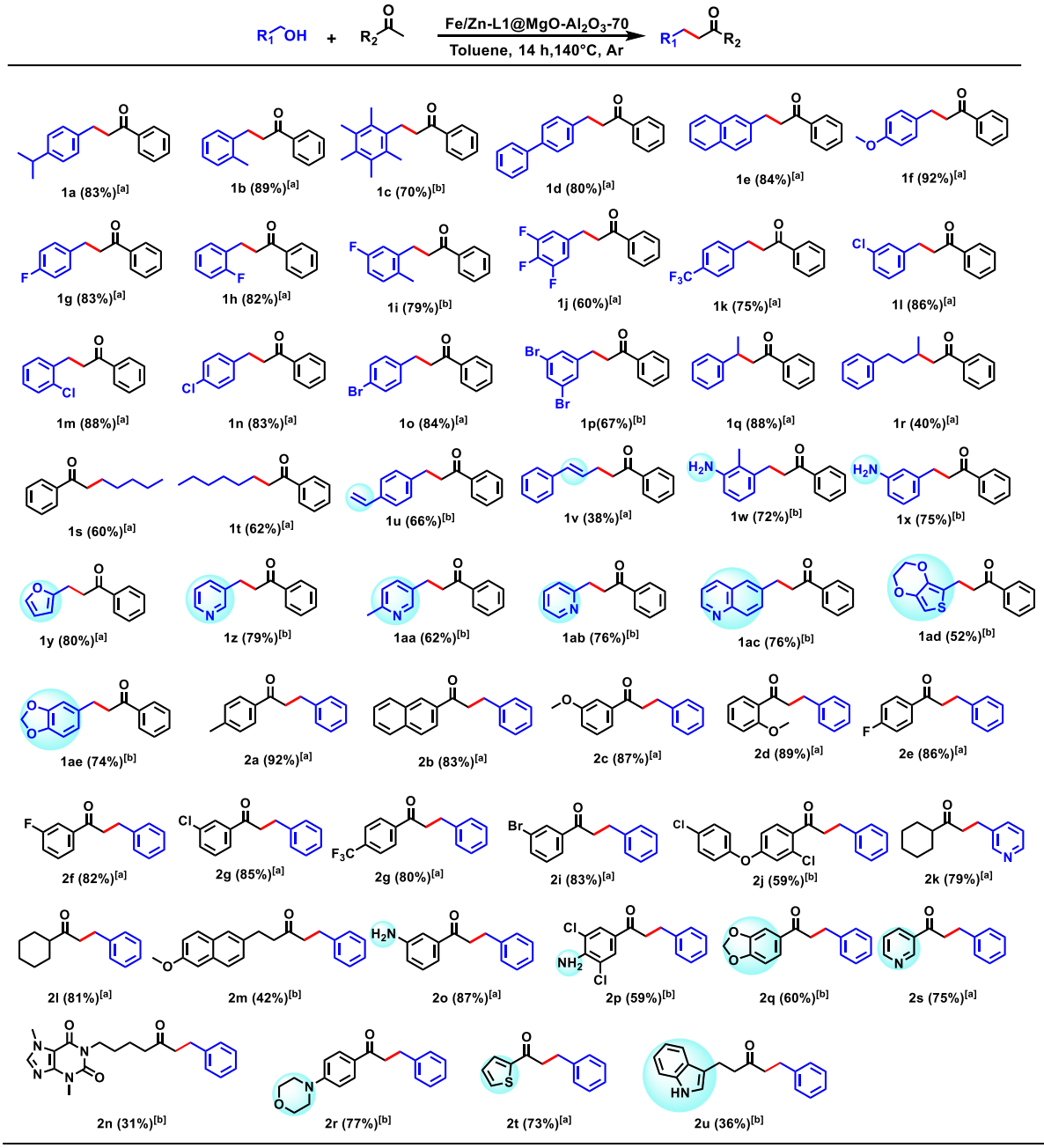

Scheme 5. Substrate scope of Fe/Zn-**L1**@MgO-Al_2O_3-70 in C-alkylation. Reaction conditions: [a] 0.5 mmol ketones, 0.55 mmol alcohol, 60 mg catalyst, 1 atm argon, 3 mL toluene 140 °C,14 h. Isolated yield in parentheses. [b] The same as [a] at 145 °C.

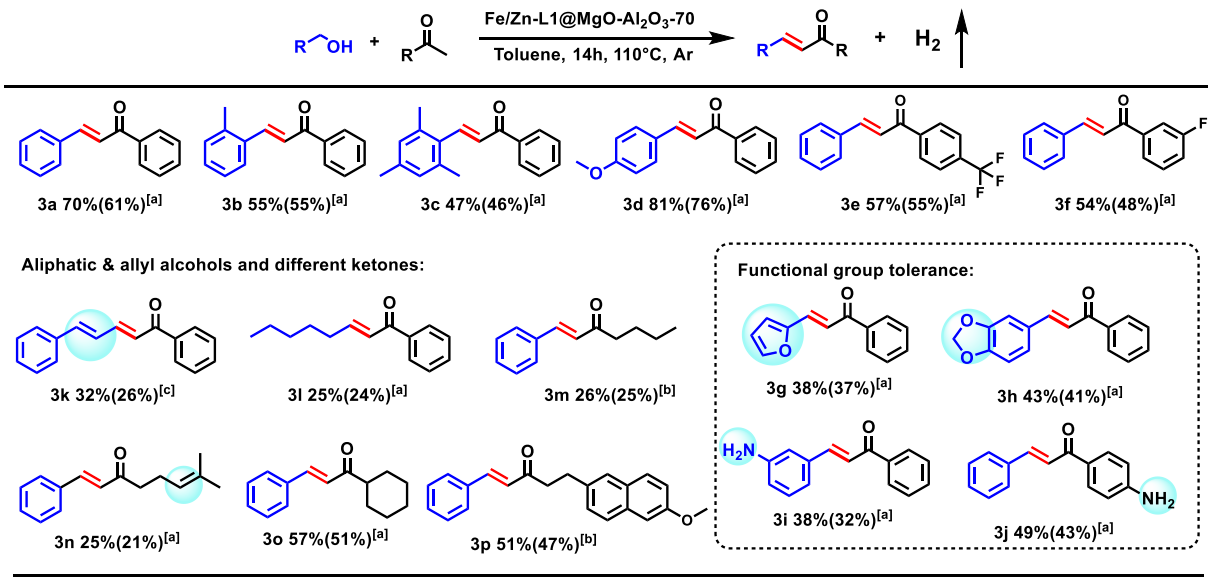

Scheme 6. Fe/Zn-**L1**@ MgO-Al_2O_3-70 catalyzed synthesis of enones from diverse alcohols and ketones. Reaction conditions: [a] 1mmol ketone, 0.5 mmol alcohol, 60 mg catalyst, 1 atm argon, 3 mL toluene 110 °C,14h. Substrate conversion were determined by GC-MS，Isolated yield in parentheses. [b] The same as [a] at 125 °C. [c] The same as [a], GC yield.

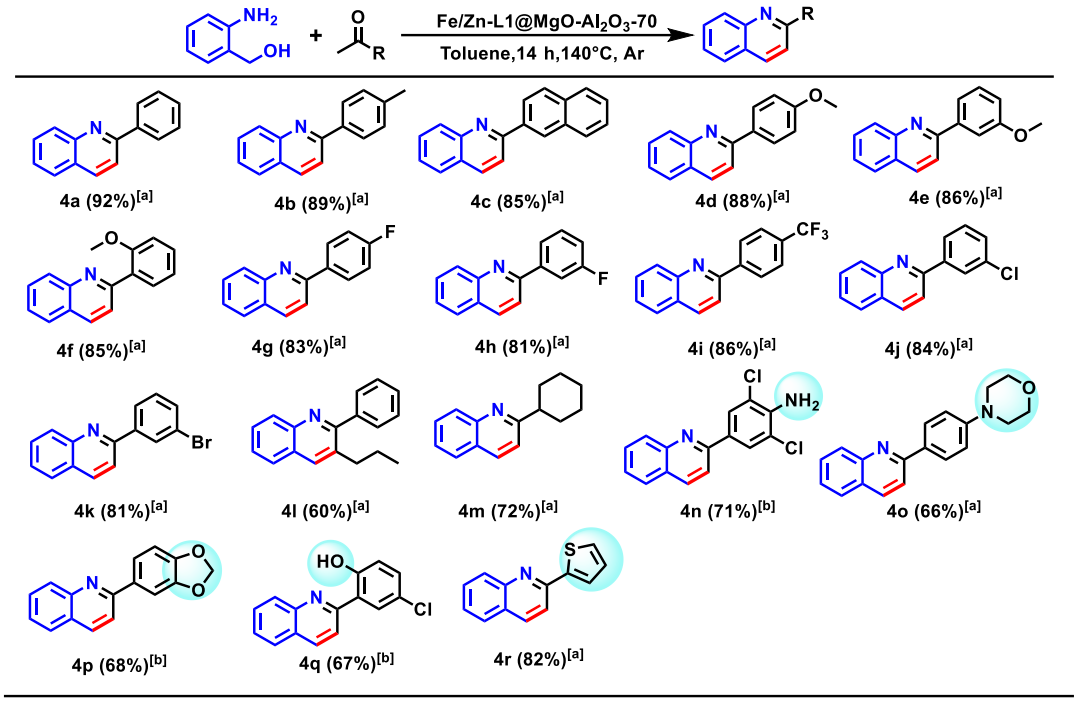

Scheme 7. Fe/Zn-**L1**@MgO-Al_2O_3-70 catalyzed synthesis of quinolines from diverse ketones. Reaction conditions: [a] 0.5 mmol ketone, 0.55 mmol alcohol, 60 mg catalyst, 1 atm argon, 3 mL toluene 140 °C,14h. Isolated yield in parentheses. [b] The same as [a] at 145 °C.

3.3 Co-SACs catalyzed upgrading of levulinic acid [77]

Reductive amination of levulinic acid (LA) is a useful method to produce pyrrolidones and other N-heterocycles. In this work, we immobilized and pyrolyzed cobalt-phenanthroline complex on carbon and then treated with HCl solution to afford Co-SACs. The existing Co single atom (**Figure 18-19**) is the active cite for the reaction (**Scheme 8**). As shown in **Scheme 9**, lactams can also be obtained using keto acids starting material. Following, the synthesis of isoindolinones was conducted **(Scheme 10)**, which is widely used for drugs. Finally, indoprofen drug was synthesized using this catalytic method and its yield is 87%.

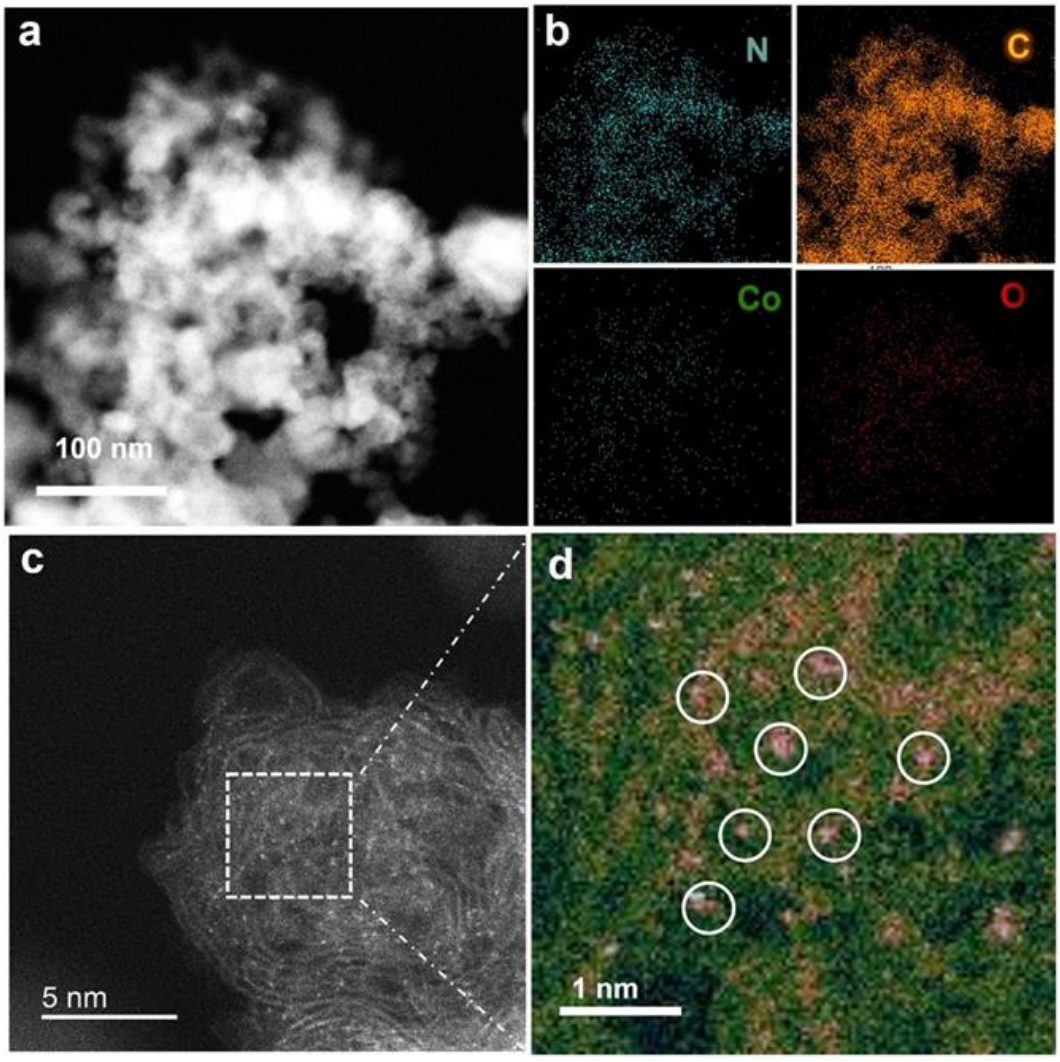

Figure 18. Electron microscope of 0.75Co-phen@C-800-HCl catalyst. (a) HAADF-STEM image and (b) EDS elemental mapping. (c) Atomic-resolution HAADF-STEM image and the(d) magnified HAADF-STEM image reveals highly dispersed Co atoms.[77]

[77]

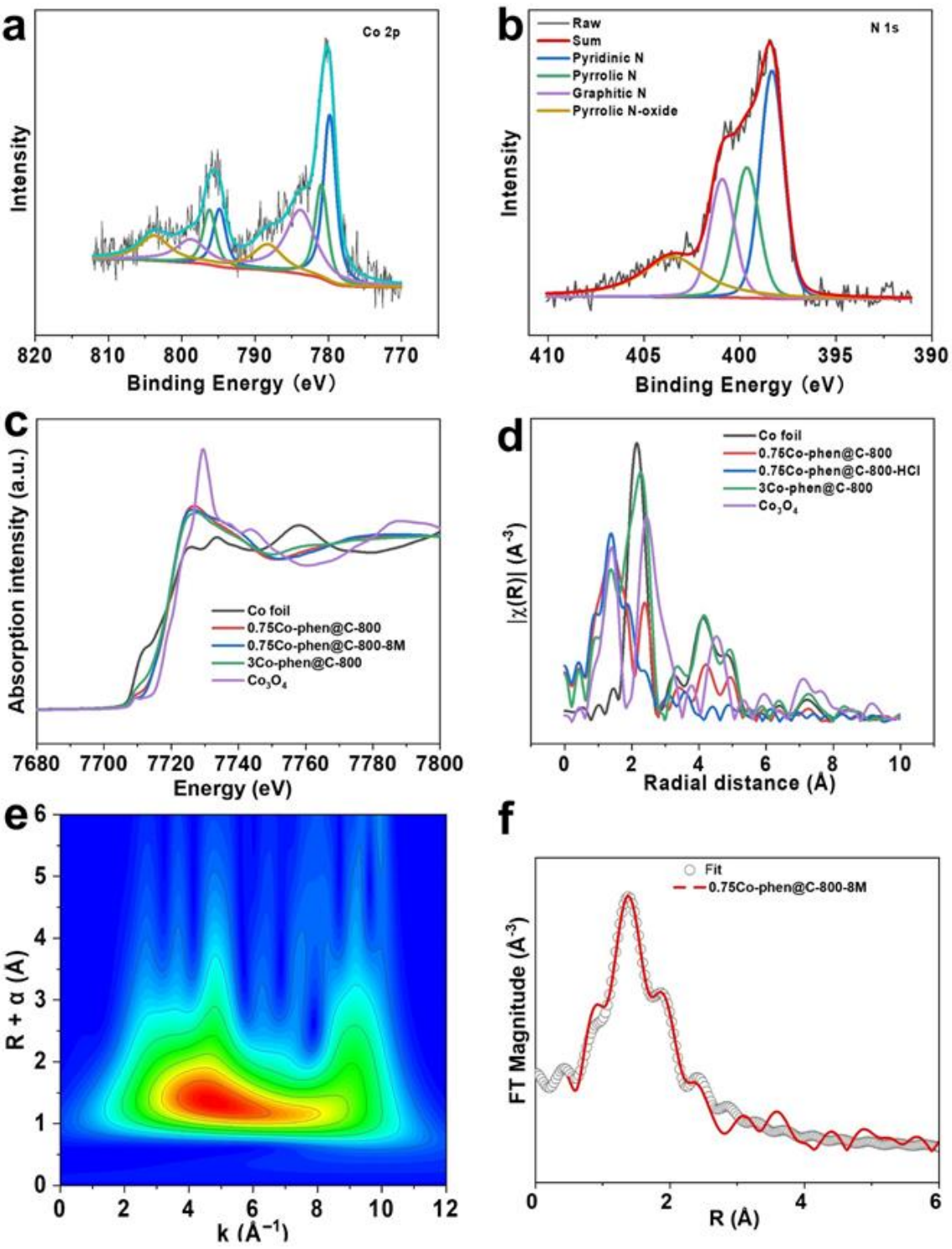

Figure 19. Structure characterization of 0.75Co-phen@C-800-HCl. (a, b) High-resolution Co 2p and N 1s XPS spectra. (c) Normalized X-ray absorption near-edge fine structure (XANES) spectra at the Co K-edge. (d) Fourier transformation of k^2-weighted EXAFS spectra at the K-edge. (e) Wavelet transforms. (f) Fitting results.[77]

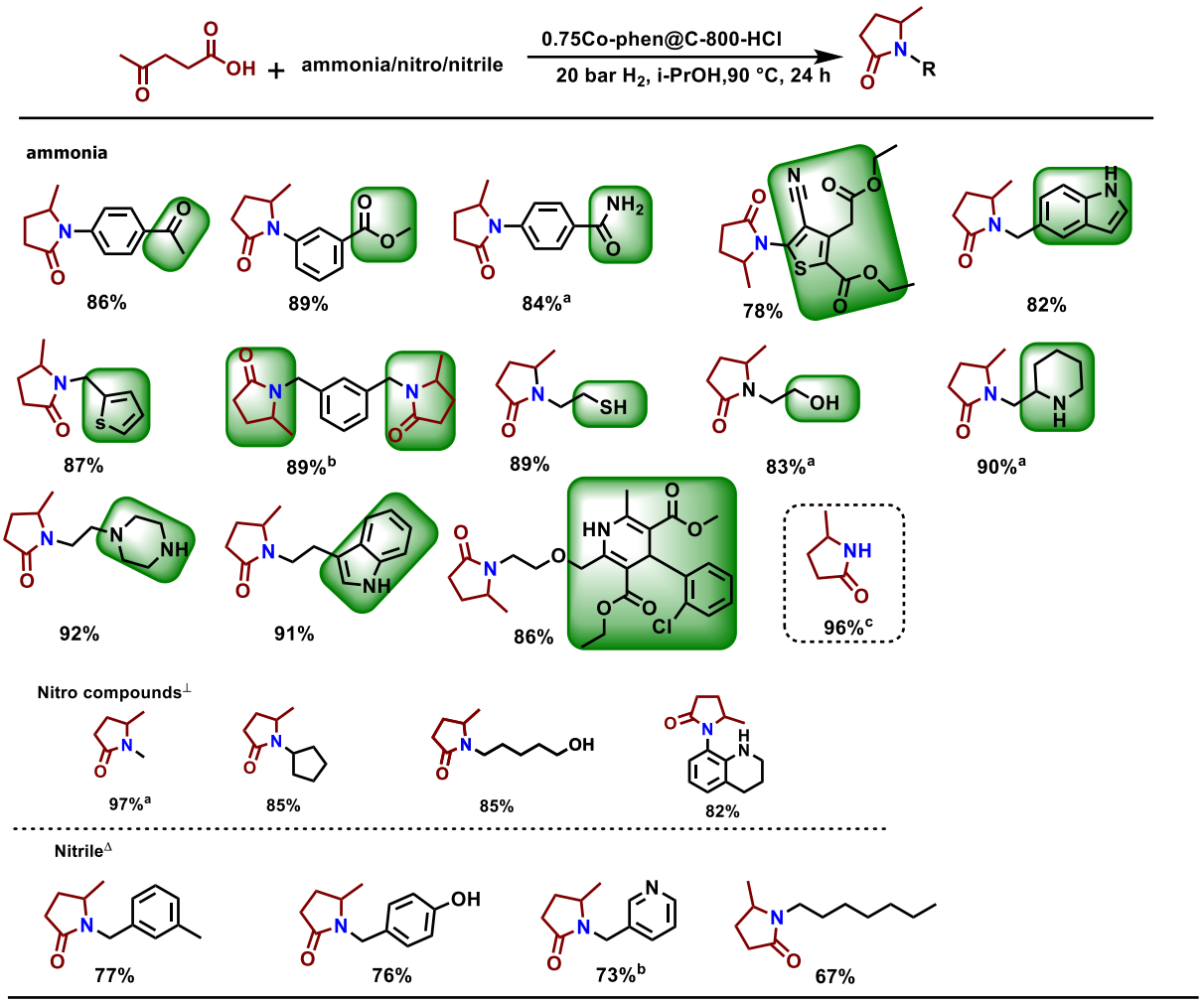

Scheme 8. Reductive amination of LA with aromatic and benzylic amines, nitro and nitrile using 0.75Co-phen@C-800-HCl. Reaction conditions: 0.5 mmol LA, 0.5 mmol amine, 40 mg catalyst (0.64 mmol% cobalt), 20 bar H_2, 90 °C, 24 h. 2 mL i-ProH. Isolated yields based on amine. [a]GC yield based on amine. [b]With 1 mmol LA, 05 mmol diamine,110 °C, 24h. [c]5 bar NH_3, 20 bar H_2, 2-mL i-PrOH, 90 °C, 24 h, GC yield based on LA.[⊥]0.5 mmol LA and 0.5 mmol nitro compounds, 40 mg catalyst (0.64 mmol% cobalt), 110 °C, 20 bar H_2, 24 h. Isolated yield based on nitro. [a]GC yield based on nitro. [△]1 mmol LA and 0.5 mmol nitrile compounds, 40 mg catalyst (0.64 mmol% Cobalt), 125 °C, 20 bar H_2, 5 bar NH_3, 24 h. Isolated yield based on nitrile. [b]GC yield based on nitrile.[77]

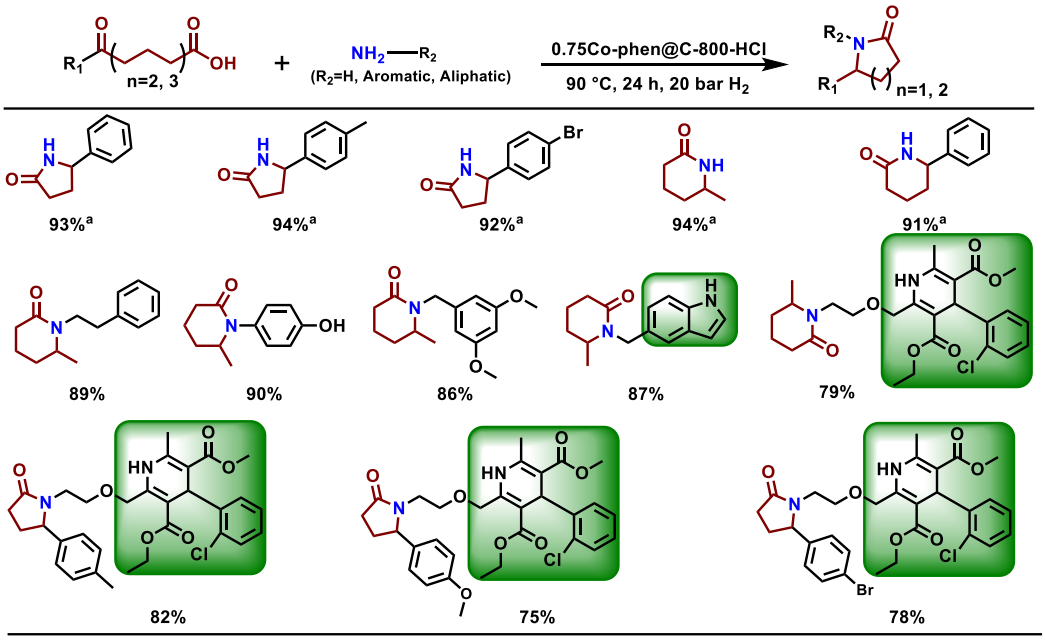

Scheme 9. Synthesis of substituted lactams from different keto acids. Reaction conditions: 0.5 mmol LA and 0.5 mmol nitro compounds, 40 mg catalyst (0.64 mmol% Cobalt), 90 °C, 20 bar H_2, 24 h. Isolated yield based on amine. [a]GC yield based on amine.[77]

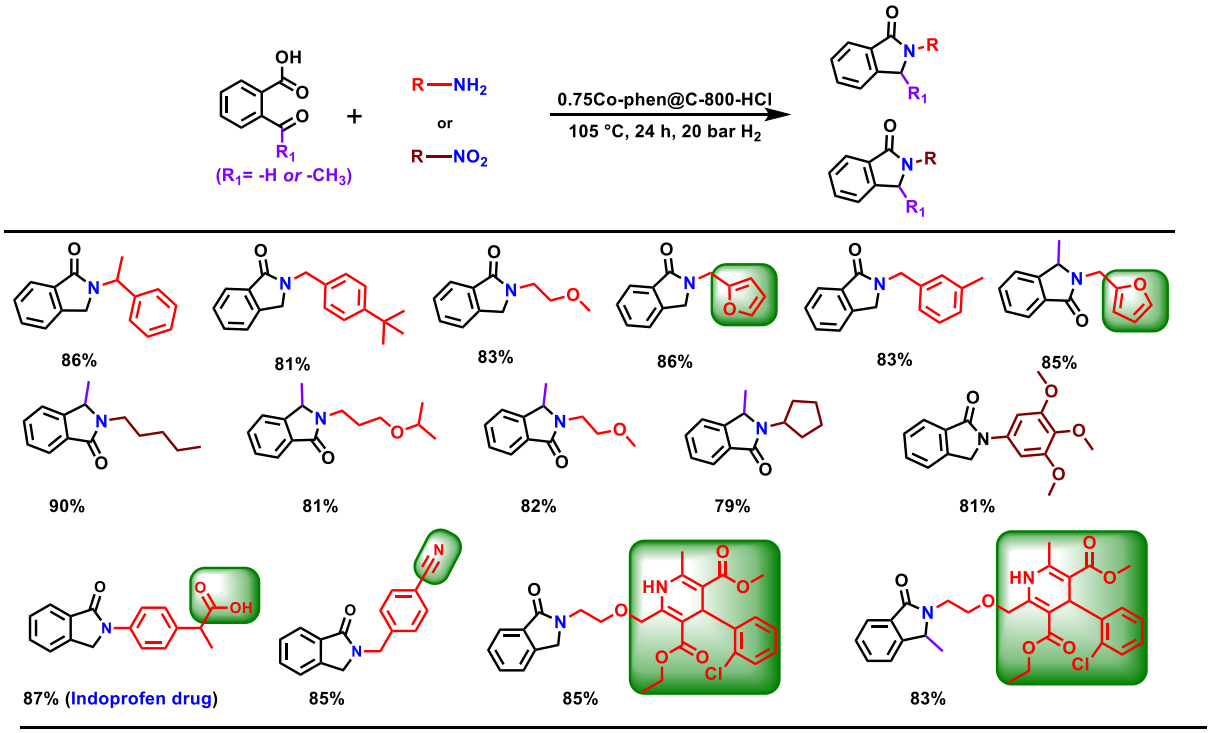

Scheme 10. Synthesis of isoindolinones. Reaction conditions: 0.5 mmol 2-formylbenzoic acid or 2-acetyl-benzoic acid, and 0.5 mmol amines or nitro compounds, 40 mg catalyst (0.64 mmol% Cobalt), 105 °C, 20 bar H_2, 24 h. Isolated yield based on amine or nitro compounds.[77]

3.4 Ni-NPs catalyzed amide synthesis from esters and nitro compounds [78]

Amides are widely used in drugs. The traditional synthesis method is the reaction of carboxylic acid with amine which needs lots of agents. Thus, exploring more sustainable approaches for amides synthesis without using external reagents is very important. In this work, we use esters as reaction partner for the direct amide bond formation in presences of the Ni NPs.

Because of Ni^{2+} is reduced to metallic Ni and more Ti^{2+} and Ti^{3+} species exist in Ni-L1@TiO_2-800 under H_2 at 130 °C (**Figures 20e and g**), which makes it have the highest activity among all tested catalysts. According to the DFT computations (**Figure 21**), we can find that Ti_{5c}^{3+} has lower adsorption energy of aniline molecule and longer bond length of N–H, which makes the low-valent Ti-species play an important role in the second amidation step.

Ni-L1@TiO_2-800 showed a good generality in amide preparation, >54 diverse amides can be obtained in good to excellent yield (**Scheme 13-14**). Finally, we come to test its application (**Scheme 15**), besides some drug molecular are obtained (**Scheme 15** entries 55-58), this catalytic protocol also shows good upscaling ability.

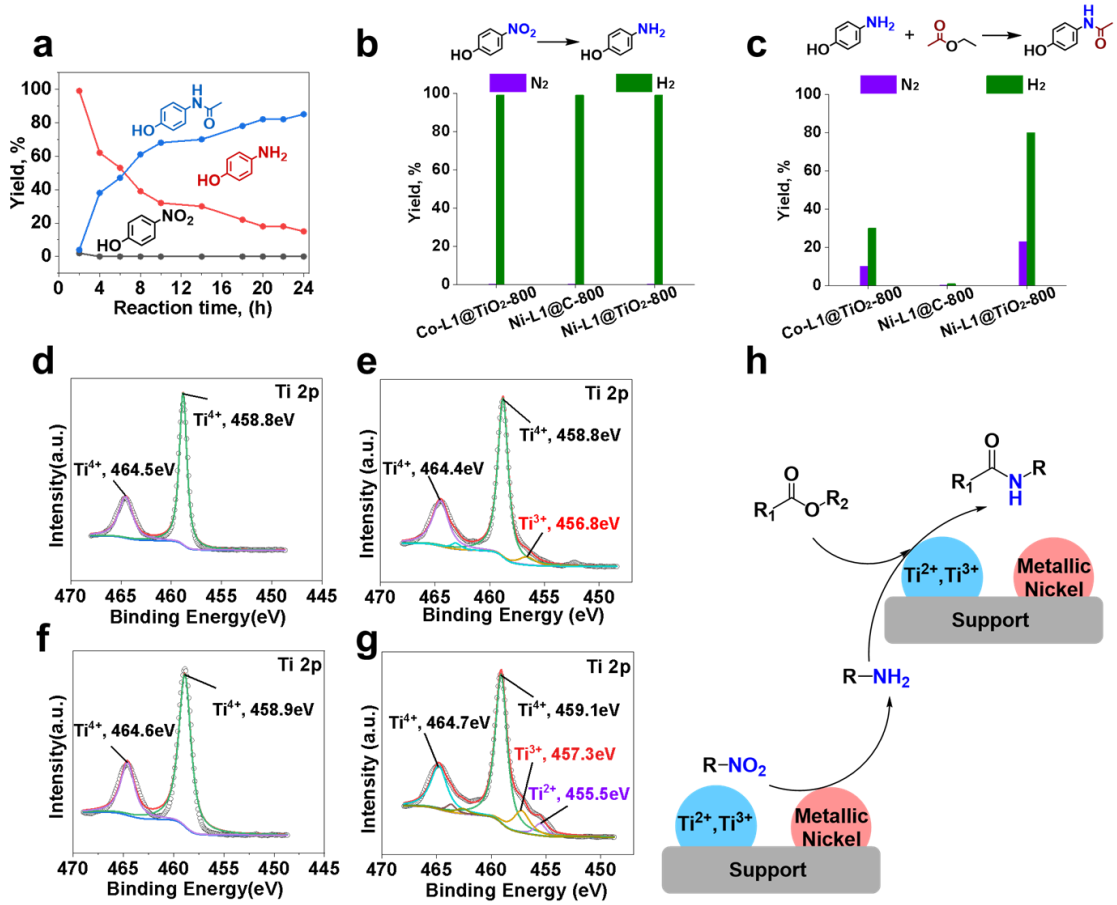

Figure 20. Mechanistic investigations. (a) Kinetic studies. Reaction conditions: 0.5 mmol 4-nitrophenol, 1 mL ethyl acetate, 60 mg Ni-L1@TiO_2-800, 20 bar H_2, 130 °C, 24 h. (b-c) Control experiments.

Reaction conditions: (b) the same as (a) with 0.5 mmol 4-nitrophenol, 1 mL ethanol. (c) the same as (a) with 0.5 mmol 4-aminophenol, 1 mL ethyl acetate, 17 h. In-situ XPS characterization was performed at 130 °C under 1 bar N_2 (d, f) and H_2 (e, g) for 1 h, (d, e) Ti 2p for Co-L1@TiO_2-800, (f, g) Ti 2p for Ni-L1@TiO_2-800. (h) Proposed reaction pathway.[78]

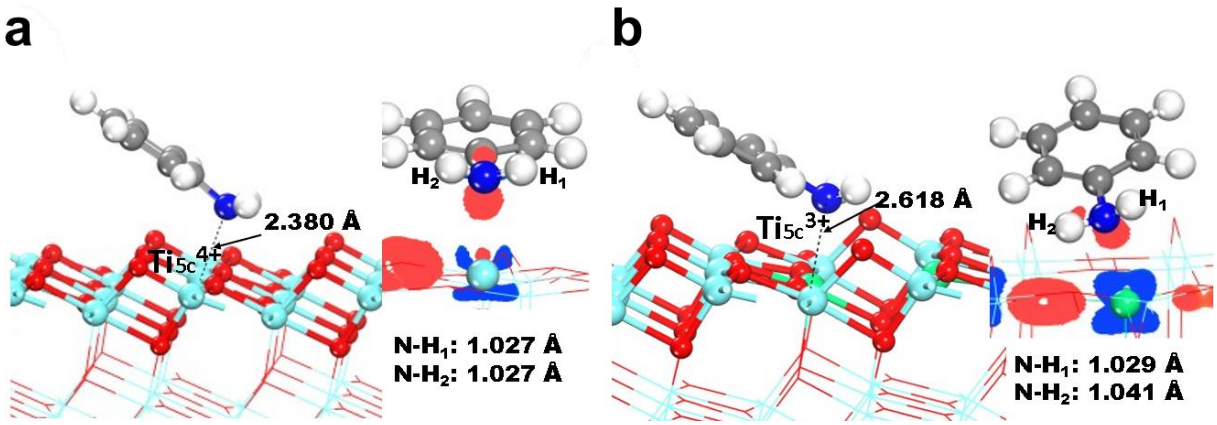

Figure 21. DFT modulation. The most stable configuration of aniline adsorbed on anatase-TiO_2 (101) surface. (a) aniline is interacting with a Ti^{4+} ion, and (b) aniline is interacting with a Ti^{3+} ion in anatase-TiO_2 (101) surfaces. The inset was the different charge density of the complex. Blue areas represent electron depletion and red areas means electron accumulation with an isosurface value of 0.1 electrons/Å.[78]

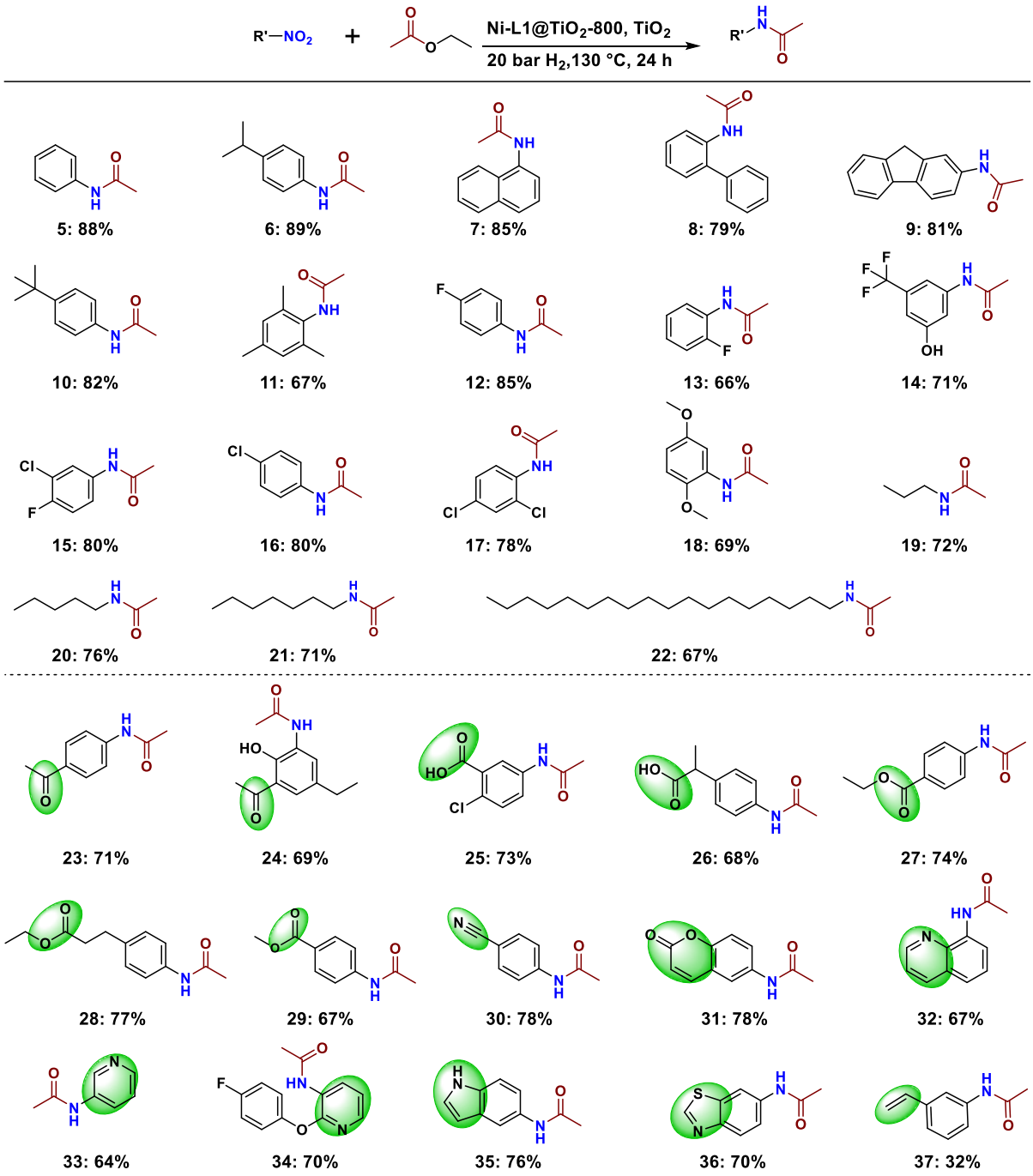

Scheme 11. Scope of nitro compounds. Reaction conditions: 0.5 mmol nitro compound, 1mL ethyl acetate, 30 mg Ni-L1@TiO_2-800, 20 mg TiO_2, 20 bar H_2, 130 °C, 24 h. Isolated yields based on nitro compound.[78]

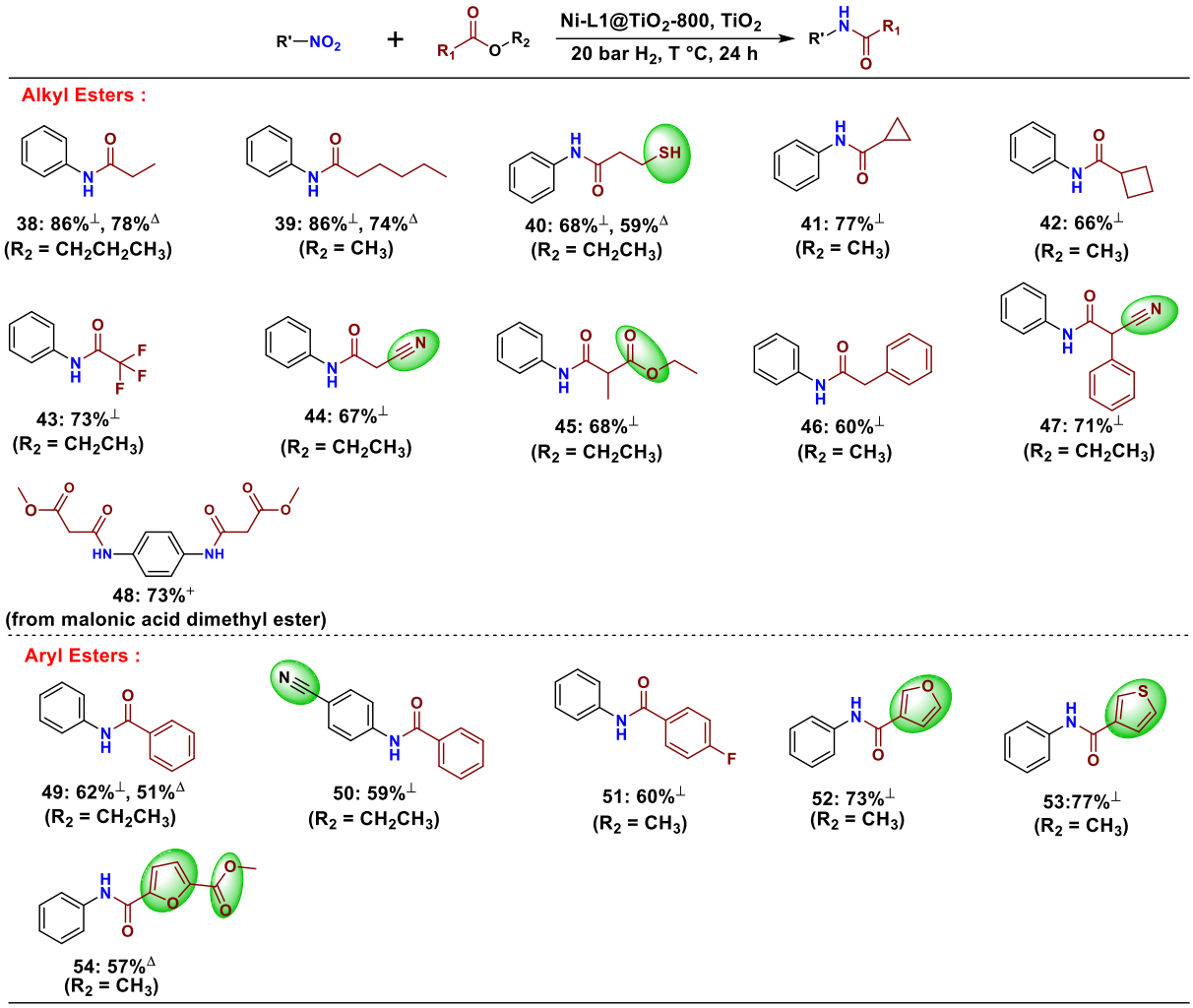

Scheme 12. Scope of esters. ⊥Reaction conditions: 0.5 mmol nitro compound, 1 mL ester, 30 mg Ni-L1@TiO_2-800, 20 mg TiO_2, 20 bar H_2, 130 °C, 24 h. ΔReaction conditions: the same as ⊥ with 0.5 mmol nitro compound, 2 mmol ester, 1 mL toluene, 30 mg catalyst at 140 °C. +Reaction conditions: the same as ⊥ with 0.5 mmol 4-nitroaniline for 48 h. All are isolated yields based on nitro compound.[78]

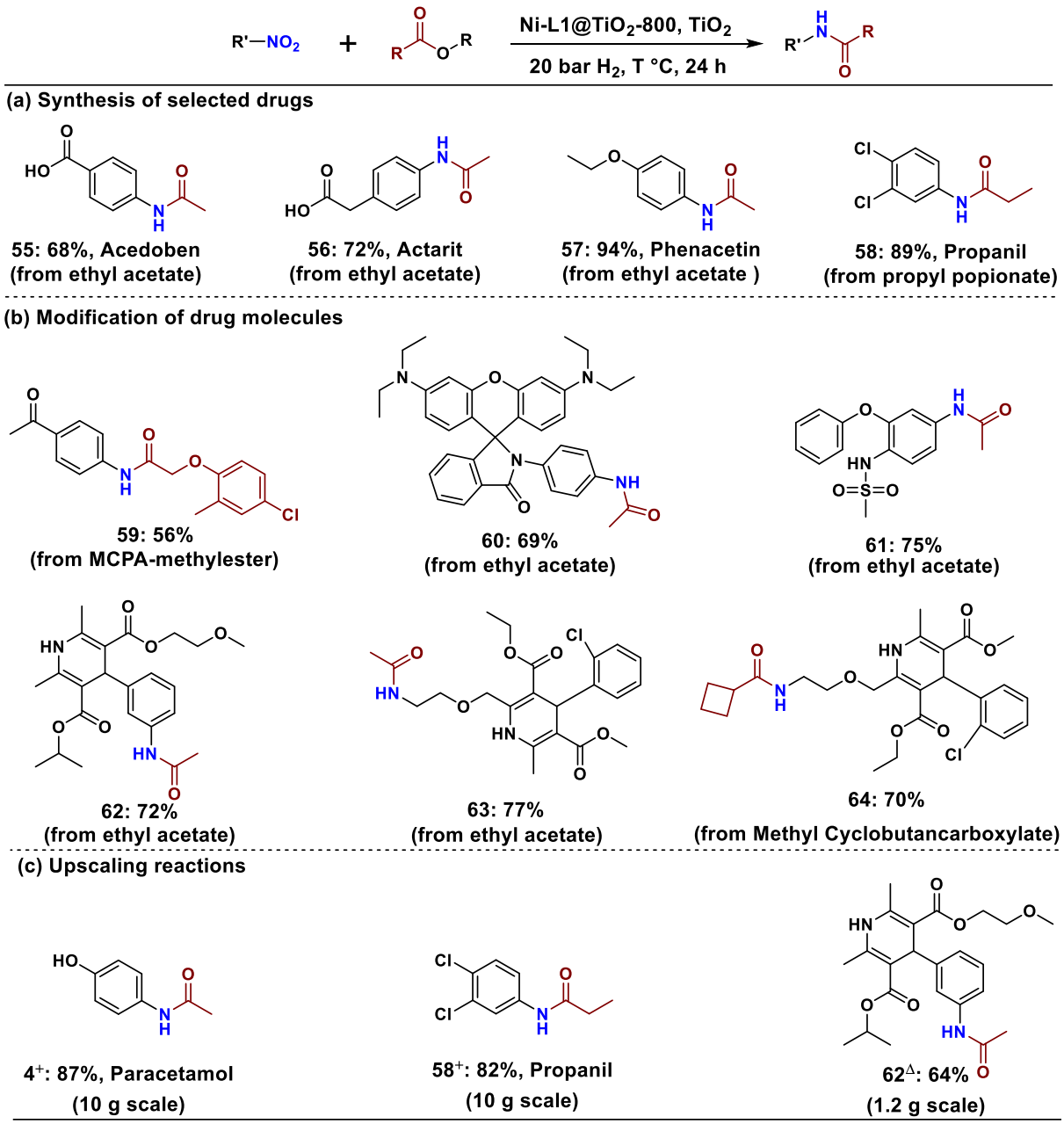

Scheme 13. Applications. (a) Synthesis of selected drugs. Reaction conditions: 0.5 mmol nitro compound, 1 mL ester, 30 mg Ni-L1@TiO_2-800, 20 mg TiO_2, 20 bar H_2, 130 °C, 24 h. Isolated yields based on nitro compound. (b) Amidation of nitro and ester containing drugs. Reaction conditions: the same as (a). Isolated yield based on nitro compound. (c) Scale-up reactions. $^{+}$Reaction conditions: the same as (a) with 10 g nitro compound, 30 mL ethyl acetate, required amount of catalyst and TiO_2 (30 mg of Ni-L1@TiO_2-800 and 20 mg TiO_2 for each 0.5 mmol nitro compound), $^{\Delta}$the same as (a) with 1.2 g nitro compound, 4 mL ethyl acetate, required amount of catalyst and TiO_2 (30 mg of Ni-L1@TiO_2-800 and 20 mg TiO_2 for each 0.5 mmol nitro compound). Isolated yields based on nitro compound.[78]

4. References

1. D. S. Wang, Q. A. Chen, S. M. Lu and Y. G. Zhou, *Chem. Rev.*, 2012, **112**, 2557-2590.
2. M. A. Stoffels, F. J. R. Klauck, T. Hamadi, F. Glorius and J. Leker, *Adv. Synth. Catal.*, 2020, **362**, 1258-1274.
3. G. Vilé, D. Albani, N. Almora-Barrios, N. López and J. Pérez-Ramírez, *ChemCatChem*, 2015, **8**, 21-33.
4. L. Zhang, M. Zhou, A. Wang and T. Zhang, *Chem. Rev.*, 2020, **120**, 683-733.
5. A. Wang, J. Li and T. Zhang, *Nat. Rev. Chem.*, 2018, **2**, 65-81.
6. S. Mitchell and J. Perez-Ramirez, *Nat. Commun.*, 2020, **11**, 4302.
7. Y. Ren, Y. Tang, L. Zhang, X. Liu, L. Li, S. Miao, D. Sheng Su, A. Wang, J. Li and T. Zhang, *Nat. Commun.*, 2019, **10**, 4500.
8. T. Heinze, S. Dorn, M. Schöbitz, T. Liebert, S. Köhler and F. Meister, *Macromol Symp*, 2008, **262**, 8-22.
9. W. Bonrath, J. Medlock, J. Schutz, B. Wustenberg and T. Netscher, *Hydrogenation*, 2012, DOI: 10.5772/48751, ch. Chapter 3.
10. D. Wang and D. Astruc, *Chem Rev*, 2015, **115**, 6621-6686.
11. B. G. Reed-Berendt, D. E. Latham, M. B. Dambatta and L. C. Morrill, *ACS Cent. Sci.*, 2021, **7**, 570-585.
12. M. G. Edwards, R. F. Jazzar, B. M. Paine, D. J. Shermer, M. K. Whittlesey, J. M. Williams and D. D. Edney, *Chem. Commun.*, 2004, DOI: 10.1039/b312162c, 90-91.
13. C. F. A. Winans, H, *J. Am. Chem. Soc.*, 1932, **54**, 306−312.
14. E. F. F. Pratt, E. J, *J. Am. Chem. Soc.*, 1954, **76** 6174−6179.
15. R. M. Grigg, T. R. B.; Sutthivaiyakit, S.; Tongpenyai, N, *Tetrahedron Lett.*, 1981, **22**, 4107−4110.
16. Y. T. Watanabe, Y.; Ohsugi, Y, *Tetrahedron Lett.*, 1981, **22**, 2667−2670.
17. Y. T. Watanabe, Y.; Ige, H.; Ohsugi, Y.; Ohta, T, *J. Org. Chem.*, 1984, **49**, 3359−3363.
18. X. Ma, C. Su and Q. Xu, *Top Curr Chem*, 2016, **374**, 27.
19. X. P. Yin, L. Zhu and J. Zhou, *Adv. Synth. Catal.*, 2018, **360**, 1116-1122.
20. X. Dai and F. Shi, *Org. Biomol. Chem.*, 2019, **17**, 2044-2054.
21. Q. Yang, Q. Wang and Z. Yu, *Chem. Soc. Rev.*, 2015, **44**, 2305-2329.
22. K.-i. Fujita, Z. Li, N. Ozeki and R. Yamaguchi, *Tetrahedron Lett.*, 2003, **44**, 2687-2690.
23. M. H. S. A. A. Hamid, C. L.; Lamb, G. W.; Maxwell, A. C.;Maytum, H. C.; Watson, A. J. A.; Williams, J. M. J, *J. Am. Chem. Soc.*, 2009, **131**, 1766-1774.
24. K. Shimizu, M. Nishimura and A. Satsuma, *ChemCatChem*, 2009, **1**, 497-503.
25. R. Martinez, D. J. Ramon and M. Yus, *Org. Biomol. Chem.*, 2009, **7**, 2176-2181.
26. A. Corma, T. Rodenas and M. J. Sabater, *Chem.-Eur. J.*, 2010, **16**, 254-260.
27. L. He, X. B. Lou, J. Ni, Y. M. Liu, Y. Cao, H. Y. He and K. N. Fan, *Chem.-Eur. J.*, 2010, **16**, 13965-13969.
28. D. Ramón, A. Martínez-Asencio and M. Yus, *Synthesis*, 2011, **2011**, 3730-3740.
29. M. Bertoli, A. Choualeb, A. J. Lough, B. Moore, D. Spasyuk and D. G. Gusev, *Organometallics*, 2011, **30**, 3479-3482.
30. W. He, L. Wang, C. Sun, K. Wu, S. He, J. Chen, P. Wu and Z. Yu, *Chem.-Eur. J.*, 2011, **17**, 13308-13317.
31. P. Satyanarayana, G. M. Reddy, H. Maheswaran and M. L. Kantam, *Adv. Synth. Catal.*, 2013, **355**, 1859-1867.
32. K.-i. Shimizu, N. Imaiida, K. Kon, S. M. A. Hakim Siddiki and A. Satsuma, *ACS Catal.*, 2013, **3**, 998-1005.
33. M. Dixit, M. Mishra, P. A. Joshi and D. O. Shah, *Catal. Commun.*, 2013, **33**, 80-83.
34. A. Abdukader, H. Jin, Y. Cheng and C. Zhu, *Tetrahedron Lett.*, 2014, **55**, 4172-4174.
35. X. Yu, L. Jiang, Q. Li, Y. Xie and Q. Xu, *Chinese J. Chem.*, 2012, **30**, 2322-2332.
36. C. Liu, S. Liao, Q. Li, S. Feng, Q. Sun, X. Yu and Q. Xu, *J. Org. Chem.*, 2011, **76**, 5759-5773.
37. X. Cui, Y. Zhang, F. Shi and Y. Deng, *Chem.-Eur. J.*, 2011, **17**, 1021-1028.
38. S. B. Ankade, A. B. Shabade, V. Soni and B. Punji, *ACS Catal.*, 2021, **11**, 3268-3292.
39. C. S. Cho, B. T. Kim, T.-J. Kim and S. Chul Shim, *Tetrahedron Lett.*, 2002, **43**, 7987-7989.

40. K. N. Taguchi, H.; Hirabayashi, T.; Sakaguchi, S.; Ishii, Y, *J. Am. Chem. Soc.*, 2004, **126** 72–73,.
41. C. S. Cho, *J. Mol. Catal. A: Chem.*, 2005, **240**, 55–60.
42. M. Yus, F. Alonso and P. Riente, *Synlett*, 2007, **2007**, 1877-1880.
43. M. L. Buil, M. A. Esteruelas, J. Herrero, S. Izquierdo, I. M. Pastor and M. Yus, *ACS Catal.*, 2013, **3**, 2072-2075.
44. P. Satyanarayana, G. M. Reddy, H. Maheswaran and M. L. Kantam, *Adv. Synth. Catal.*, 2013, **355**, 1859-1867.
45. X. Yu, Q. Y. Wang, Q. J. Wu and D. W. Wang, *Russ. J. Gen. Chem.*, 2016, **86**, 178-183.
46. S. Elangovan, J. B. Sortais, M. Beller and C. Darcel, *Angew. Chem. Int. Ed.*, 2015, **54**, 14483-14486.
47. M. Pena-Lopez, P. Piehl, S. Elangovan, H. Neumann and M. Beller, *Angew. Chem. Int. Ed.*, 2016, **55**, 14967-14971.
48. P. Piehl, M. Pena-Lopez, A. Frey, H. Neumann and M. Beller, *Chem. Commun.*, 2017, **53**, 3265-3268.
49. G. Zhang, J. Wu, H. Zeng, S. Zhang, Z. Yin and S. Zheng, *Org. Lett.*, 2017, **19**, 1080-1083.
50. J. Das, K. Singh, M. Vellakkaran and D. Banerjee, *Org. Lett.*, 2018, **20**, 5587-5591.
51. V. R. Pattabiraman and J. W. Bode, *Nature*, 2011, **480**, 471-479.
52. M. Todorovic and D. M. Perrin, *Pept. Sci.*, 2020, **112**.
53. X. Wang, *Nat. Catal.*, 2019, **2**, 98-102.
54. M. T. Sabatini, L. T. Boulton, H. F. Sneddon and T. D. Sheppard, *Nat. Catal.*, 2019, **2**, 10-17.
55. F. Zhao, H. J. Ai and X. F. Wu, *Angew. Chem. Int. Ed.*, 2022, DOI: 10.1002/anie.202200062, e202200062.
56. C. W. Cheung, M. L. Ploeger and X. Hu, *Nat. Commun.*, 2017, **8**, 14878.
57. C. W. Cheung, N. Shen, S.-P. Wang, A. Ullah, X. Hu and J.-A. Ma, *Org. Chem. Front.*, 2019, **6**, 756-761.
58. L. Ling, C. Chen, M. Luo and X. Zeng, *Org. Lett.*, 2019, **21**, 1912-1916.
59. S. S. Chen, T. Maneerung, D. C. W. Tsang, Y. S. Ok and C.-H. Wang, *Chem. Eng. J.*, 2017, **328**, 246-273.
60. X. Zhang, K. Wilson and A. F. Lee, *Chem. Rev.*, 2016, **116**, 12328-12368.
61. G. W. Huber and J. A. Dumesic, *Catal. Today*, 2006, **111**, 119-132.
62. J. He, L. Chen, S. Liu, K. Song, S. Yang and A. Riisager, *Green Chem.*, 2020, **22**, 6714-6747.
63. H. Tadesse and R. Luque, *Energy Environ. Sci.*, 2011, **4**.
64. K. C. Badgujar, L. D. Wilson and B. M. Bhanage, *Renew. Sust. Energ. Rev.*, 2019, **102**, 266-284.
65. T. Heinze, S. Dorn, M. Schöbitz, T. Liebert, S. Köhler and F. Meister, *Macromol. Symp.*, 2008, **262**, 8-22.
66. B. Lindman, B. Medronho, L. Alves, C. Costa, H. Edlund and M. Norgren, *Phys. Chem. Chem. Phys.*, 2017, **19**, 23704-23718.
67. A. S. Piskun, J. E. de Haan, E. Wilbers, H. H. van de Bovenkamp, Z. Tang and H. J. Heeres, *ACS Sustain. Chem. Eng.*, 2016, **4**, 2939-2950.
68. S. Dutta, L. Wu and M. Mascal, *Green Chem.*, 2015, **17**, 2335-2338.
69. C. Xie, J. Song, H. Wu, Y. Hu, H. Liu, Z. Zhang, P. Zhang, B. Chen and B. Han, *J. Am. Chem. Soc.*, 2019, **141**, 4002-4009.
70. Z. Xue, D. Yu, X. Zhao and T. Mu, *Green Chem.*, 2019, **21**, 5449-5468.
71. A. S. Touchy, S. M. A. Hakim Siddiki, K. Kon and K.-i. Shimizu, *ACS Catal.*, 2014, **4**, 3045-3050.
72. G. Gao, P. Sun, Y. Li, F. Wang, Z. Zhao, Y. Qin and F. Li, *ACS Catal.*, 2017, **7**, 4927-4935.
73. Y. Wu, Y. Zhao, H. Wang, F. Zhang, R. Li, J. Xiang, Z. Wang, B. Han and Z. Liu, *Green Chem.*, 2020, **22**, 3820-3826.
74. R. Ma, J. Gao, L. Zhang, N. Wang, Y. Hu, S. Bartling, H. Lund, S. Wohlrab, J. Rajenahally and M. Beller, *Green Chem.*, 2023, DOI: 10.1039/d3gc03286h.
75. H. Wu, X. Li, L. Yang, W. Chen, C. Zou, W. Deng, Z. Wang, J. Hu, Y. Li and Y. Huang, *Org. Lett.*, 2022, **24**, 9342-9347.
76. A. Kurose, Y. Ishida, G. Hirata and T. Nishikata, *Angew. Chem. Int. Ed.,* 2021, **60**, 10620-10625.

77. J. Gao, L. Feng, R. Ma, B.-J. Su, A. M. Alenad, Y. Liu, M. Beller and R. V. Jagadeesh, *Chem Catalysis*, 2022, DOI: 10.1016/j.checat.2021.12.009.
78. J. Gao, R. Ma, F. Poovan, L. Zhang, H. Atia, N. V. Kalevaru, W. Sun, S. Wohlrab, D. A. Chusov, N. Wang, R. V. Jagadeesh and M. Beller, *Nat. Commun.*, 2023, **14**, 5013.

5. Contribution to the publications

5.1 Cobalt-nanoparticles catalysed *N*-alkylation of amides with alcohols

Rui Ma, Jie Gao, Lan Zhang, Ning Wang, Yue Hu, Stephan Bartling, Henrik Lund, Sebastian Wohlrab, Rajenahally V. Jagadeesh, and Matthias Beller

Green Chemistry

DOI: 10.1039/D3GC03286H

In this paper, I prepared all the catalysts and performed all the reactions including the isolation and purification of products. The figures and schemes are made by myself. In addition, Matthias Beller, Sebastian Wohlrab and Rajenahally. Jagadeesh give me lots of help and comments in this work and they also corrected this manuscript. My contribution as the first author of this paper is approximately 70%.

5.2 Base-free Selective α-Alkylation and α-Vinylation of Ketones with Alcohols over Fe/Zn Bimetallic Catalysts

Rui Ma, Jie Gao, Lan Zhang, Hanan Atia, Stephan Bartling, Henrik Lund, Ning Wang, Sebastian Wohlrab, Rajenahally V. Jagadeesh, and Matthias Beller

In this paper, I prepared all the catalysts and performed all the reactions including the isolation and purification of products. The figures and schemes are made by myself. In addition, Matthias Beller, Sebastian Wohlrab and Rajenahally. Jagadeesh give me lots of help and comments in this work and they also corrected this manuscript. My contribution as the first author of this paper is approximately 70%.

5.3 Cobalt single-atom catalysts for domino reductive amination and amidation of Levulinic acid and related molecules to N-heterocycles

Jie Gao, Lu Feng, Rui Ma, Bing-Jian Su, Asma M. Alenad, Yuefeng Liu,

Matthias Beller and Rajenahally V. Jagadeesh

Chem Catalysis ***2***, 178–194, 2022

DOI: 10.1016/j.checat.**2021**.12.009

In this work, I prepared the catalysts, carried out the reproducibility of experiments and corrected the manuscript. My contribution as the co-first author of this paper is approximately 30%.

5.4 Practical and general synthesis of amides from nitro compounds and esters using nickel-based nanoparticles

Jie Gao, Rui Ma, Fairoosa Poovan, Lan Zhang, Hanan Atia, Narayana V. Kalevaru, Sebastian Wohlrab, Ning Wang, Denis A. Chusov, Rajenahally V. Jagadeesh, and Matthias Beller

Nature Communications ***14***, Article number: 5013 (2023)

DOI: 10.1038/s41467-023-40614-1

In this work, I prepared the catalysts, carried out the reproducibility of experiments and corrected the manuscript. My contribution as the co-author of this paper is approximately 20%.

Rui Ma

Signature of the student

(Rui Ma)

Signature of the supervisor

(Prof. Dr. Matthias Beller)

Green Chemistry

PAPER

View Article Online
View Journal

Cite this: DOI: 10.1039/d3gc03286h

Cobalt nanoparticle-catalysed *N*-alkylation of amides with alcohols†

Rui Ma,[a] Jie Gao,[a] Lan Zhang,[b] Ning Wang,[b] Yue Hu,[a] Stephan Bartling,[a] Henrik Lund,[a] Sebastian Wohlrab,*[a] Rajenahally V. Jagadeesh*[a,c] and Matthias Beller*[a]

Received 31st August 2023,
Accepted 28th November 2023

DOI: 10.1039/d3gc03286h

rsc.li/greenchem

A protocol for efficient *N*-alkylation of benzamides with alcohols in the presence of cobalt-nanocatalysts is described. Key to the success of this general methodology is the use of highly dispersed cobalt nanoparticles supported on carbon, which are obtained from the pyrolysis of cobalt(II) acetate and *o*-phenylenediamine as a ligand at suitable temperatures. The catalytic material shows a broad substrate scope and good tolerance to functional groups. Apart from the synthesis of a variety of secondary amides (>45 products), the catalyst allows for the conversion of more challenging aliphatic alcohols and amides, including biobased and macromolecular amides. The practical applicability of the catalyst is underlined by the successful recycling and reusability.

Introduction

The amide bond is one of the most fundamental functional groups in organic chemistry. It plays a central role in the formation and preservation of biological systems.[1] Amides are generally synthesized by condensation of carboxylic acids with amines,[2,3] or by the reaction between amides and aryl or aliphatic halides (Fig. 1).[3,4] However, these established methods often exhibit a poor atom economy and inevitably lead to the formation of (stoichiometric amounts of) waste. In contrast to organic halides, alcohols are broadly available raw materials including many renewable resources. Hence, the catalytic *N*-alkylation of primary amides with alcohols attracted significant attention in recent years (Fig. 1).[4–10] From a mechanistic point of view, the method involves an initial dehydrogenation of the alcohol to the corresponding aldehyde, followed by condensation with the amide.[8] Then, the newly formed C=N bond gets hydrogenated by a metal-hydride to give the *N*-alkylated amide, and water is formed as the sole by-product. Unfortunately, most of these transformations require relatively harsh reaction conditions.[5,9]

To date, homogeneous metal complexes based on Ir,[11] Ru,[12] Pd,[13] Ni,[5] and Cu[14] dominate as catalysts for *N*-alkylation of primary amides with alcohols (Fig. 1). Although these homogeneous systems with suitably designed ligands are usually selective and active, their main drawbacks are the costs and the difficulties in separating and recovering the catalysts from the reaction mixture. In contrast, heterogeneous materials are generally more durable and often easier to separate from products. Over the past decades, only a few heterogeneous systems based on Ag,[4] Pd/Au,[15] and Ru[15] were developed, and all of them required high temperatures (Fig. 1). Therefore, the preparation of metal-based nanomaterials that function under milder conditions continues to be a challenge in the catalytic functionalization of amides.

Here, we show that *N*-alkylation of primary amides with alcohols proceeds in the presence of non-noble and reusable cobalt-based nanocatalysts under comparably mild conditions.

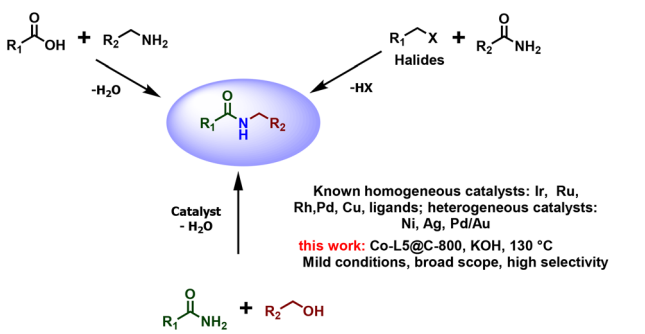

Fig. 1 General methods for amide synthesis and our presented approach.

[a]*Leibniz-Institut für Katalyse e.V., Albert-Einstein-Str. 29a, 18059 Rostock, Germany. E-mail: Sebastian.Wohlrab@catalysis.de, jagadeesh.rajenahally@catalysis.de, matthias.beller@catalysis.de*

[b]*Faculty of Environment and Life, Beijing University of Technology, 100124 Beijing, China*

[c]*Nanotechnology Centre, Centre for Energy and Environmental Technologies, VŠB–Technical University of Ostrava, Ostrava-Poruba, Czech Republic*

†Electronic supplementary information (ESI) available. See DOI: https://doi.org/10.1039/d3gc03286h

Following an operationally simple protocol, a series of functionalized and structurally diverse secondary amides were synthesized.

Results and discussion

Catalyst preparation and evaluation

The general synthesis of cobalt catalysts followed our previously developed protocols[16–20] and was initiated by dissolving cobalt (II) nitrate hexahydrate and different types of nitrogen ligands in methanol solution in the presence of various supports. After stirring overnight and removing the solvent, the obtained metal complexes were directly immobilized on the surface of the respective support (ZSM-5, TiO_2, Al_2O_3, and carbon). The resulting materials were pyrolyzed under argon at different temperatures to obtain potential catalysts (as shown in Table 1). The detailed catalyst preparation procedure is described in the ESI.† The obtained materials are labelled as Co–**L**@support-T, where Co, **L** and T represent the type of metal (cobalt), ligand (**L**), and pyrolysis temperature (T), respectively.

In our initial investigations, we tested the influence of the support on the formation of cobalt nanoparticles for *N*-alkylation of benzamide with benzyl alcohol as a benchmark reaction. After testing different bases (Table S1†), KOH was chosen as the optimal one and it was applied in all further experiments. Compared with methanol, ethanol, THF, and *n*-hexane, toluene gave the best results as the reaction solvent (Table S2†). As shown in Table 1, the native properties of the catalyst could strongly alter the reactivity and selectivity.[21] The influence of the variation in the ligand and cobalt content is shown in Table S3.† Based on these results, carbon powder was selected as the most suitable carrier material among all the supports tested (Table 1, entries 1–5). Afterwards, the influence of the selected organic ligands was tested since ligand-free material, Co@C-800, showed no activity in the model reaction (Table 1, entry 6). Comparison of the catalytic performance of materials generated using diverse ligands (**L1**: phenanthroline, **L2**: aniline, **L3**: phenol, **L4**: urea, and **L5**: *o*-phenylenediamine) showed that Co-**L5**@C-800 gave the highest product yield of 87% (Table 1, entries 5 and 7–10). Next, the effect of the pyrolysis temperature on the catalytic performance was studied. Compared to Co-**L5**@C-800, the materials pyrolyzed at 400, 600 and 1000 °C exhibited low or moderate catalytic activity (Table 1, entries 10–13). Notably, a 99% yield of the desired product was realized by running the model reaction at 130 °C (Table 1, entry 14). As expected, in the absence of a base or catalyst, no product is formed.

To gain a deeper understanding of this transformation, especially the interplay between the catalyst (Co-**L5**@C-800) and the base (KOH), a kinetic profile of the model reaction was obtained. As shown in Fig. 2a, in the first 5 hours, the two

Table 1 *N*-Alkylation of benzamide with benzyl alcohol: evaluation of potential Co-materials

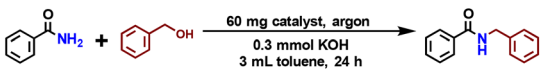

Entry	Catalyst	Metal content (wt%)	Conversion (%)	Yield (%)
1[a]	Co-L1@ZSM-5-800		n.r	n.r
2[a]	Co-L1@TiO_2-800		7	7
3[a]	Co-L1@Al_2O_3-800		40	40
4[a]	Co-L1@MgO–Al_2O_3-800		46	46
5[a]	Co-L1@C-800	0.889	80	80
6[a]	Co@C-800	0.921	n.r	n.r
7[a]	Co-L2@C-800	0.921	49	49
8[a]	Co-L3@C-800	0.892	n.r	n.r
9[a]	Co-L4@C-800	0.876	55	55
10[a]	Co-L5@C-800	0.937	87	87
11[a]	Co-L5@C-400	0.880	53	53
12[a]	Co-L5@C-600	0.880	83	83
13[a]	Co-L5@C-1000	0.896	66	66
14[b]	Co-L5@C-800	0.937	99	99
15[c]	Without catalyst		n.r	n.r
16[d]	Without base		n.r	n.r

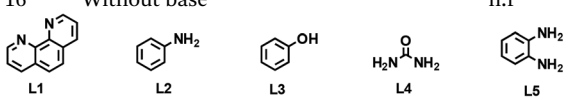

[a] Reaction conditions: 0.5 mmol of benzamide, 0.55 mmol of benzyl alcohol, 60 mg of catalyst, 0.3 mmol of KOH, 1 atm argon, 3 mL of toluene, 115 °C, and 24 h. [b] Same as [a] at 130 °C, 24 h. [c] Same as [b] without a catalyst. [d] Same as [b] without a base. Yields were determined by GC based on benzamide using *n*-hexadecane as the standard. n.r means no reaction. The effect of KOH on the reaction is shown in Fig. S1.†

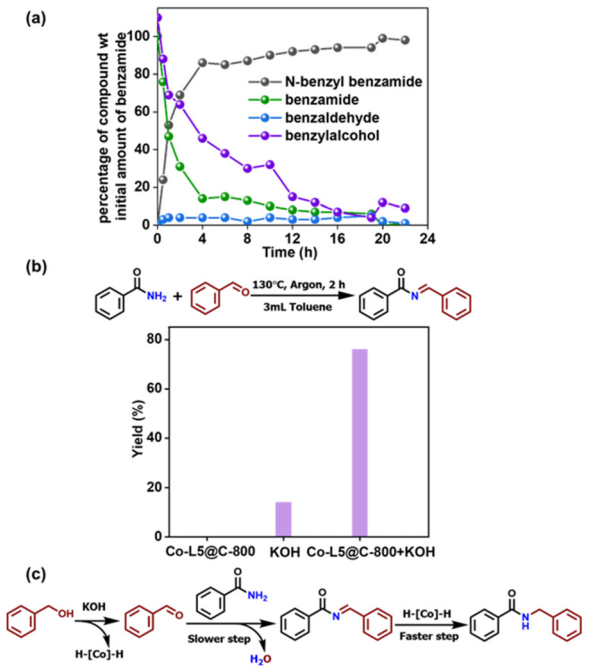

Fig. 2 Kinetic experiment and control reactions. (a) Kinetic profile of the model reaction. Reaction conditions: 0.5 mmol of benzamide, 0.55 mmol of benzyl alcohol, 60 mg of catalyst, 1 atm argon, 3 mL of toluene, 130 °C, and GC yield. (b) Coupling reaction of benzamide and benzaldehyde to form secondary amide. Reaction conditions: same as (a) with 0.5 mmol of benzamide, 0.55 mmol of benzaldehyde, and 2 h. (c) Proposed reaction sequence.

reactants are mainly consumed, and the yield of the desired secondary amide increased to 90%. Then, the reaction rate slows down approaching nearly full conversion of benzyl alcohol after 22 h. Over the course of the reaction, 3–10% of benzaldehyde was observed as an intermediate, which is formed by the dehydration of benzyl alcohol.[22] To understand the effect of Co-**L5**@C-800 and KOH, control reactions were performed (Fig. 2b).

Experiments in the presence of only Co-**L5**@C-800 or KOH showed no/minor reactivity, while the desired product yield increased to 77% when both base and catalyst were used. The kinetic profile and control experiments are in agreement with the previously proposed mechanism (Fig. 2c).[23,24] This *N*-alkylation reaction of benzamide starts with a base-promoted dehydrogenation of benzyl alcohol, which occurs on the catalyst surface, to produce benzaldehyde and H–[Co]–H species on the surface (first reaction step).[25,26] Then, nucleophilic addition of benzamide to benzaldehyde generated the respective *N*-benzoylimine. This second step is likely promoted by a base, too, and represents the rate-determining reaction step due to the poor nucleophilicity of primary amides. Finally, cobalt-catalyzed reduction of this imide occurs (third reaction step).[23]

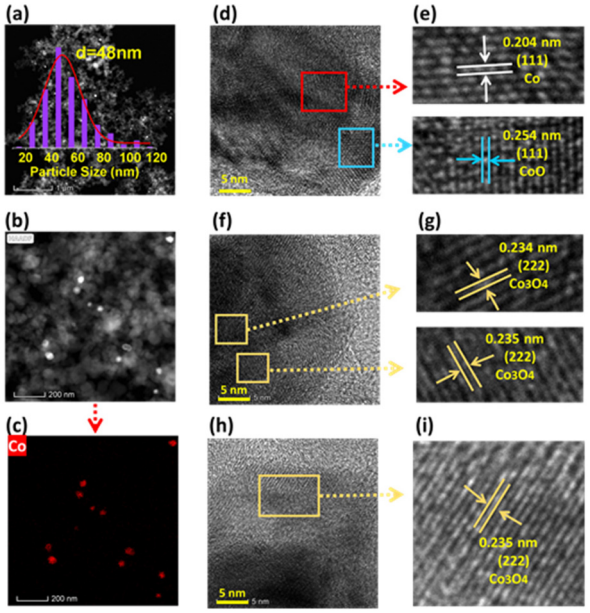

Fig. 3 TEM analysis of Co@C-800. (a and b) TEM-HAADF images, (c) EDX elemental mapping image of Co, and (d–i) identified crystal planes of the Co nanoparticles.

Characterization of selected materials

To elucidate reasons for the markedly different catalytic activities of the prepared Co–**L**@C-T catalysts, the effects of ligand and pyrolysis temperature on the structures of Co@C-800, Co-**L5**@C-400, Co-**L5**@C-600, Co-**L5**@C-800, and Co-**L5**@C-1000 were investigated in detail by transmission electron microscopy (TEM), X-ray powder diffraction (XRD), Brunauer–Emmett–Teller (BET) analysis, and X-ray photoelectron spectroscopy (XPS).

Although the powder X-ray diffraction (XRD) data show broad peaks of the support material[27] (Fig. S2†), Co-containing phases can be suspected by a peak around 37° 2θ, which is assigned to Co-oxide formation.[28–30] However, due to low loading and overlapping peaks, its assignment to different Co-oxides was not successful (Fig. S2†). If the pyrolysis temperature is increased to 800 °C, metallic fcc-Co appeared in the material as seen by its most intense Bragg peaks at 44.2 (111), 51.5 (200) and 75.8° (220).[31] Notably, there are only negligible differences in diffraction data of Co@C-800 and Co-**L5**@C-800 (Fig. S3†).

The presence of organic nitrogen ligands during the thermal catalyst formation induces the formation of some carbon protective layers on the outer surface of metallic Co, which make Co-**L5**@C-800 more stable to oxidation. Although the signal of a metallic Co^0 phase is also observed on Co@C-800, TEM analysis and XPS spectra showed that the surface of these particles is oxidized (Fig. 3d–i and S3†). Consequently, the Co@C-800 material is more sensitive to oxidation.[32]

The HAADF-TEM images of Co@C-800 revealed that cobalt nanoparticles with a size of 45–50 nm are randomly distributed over the surface of the support material (Fig. 3a). EDX mapping images clearly indicate that cobalt nanoparticles are randomly distributed on the surface of the materials (Fig. 3b–c and Table S4†). In the regions at high cobalt magnification (Fig. 3d–i), the nature of the metal nanoparticles is revealed. As shown in the image of Fig. 3d, labeled using red and blue frames, the apparent lattice distance in the red region was found to be 0.204 nm, corresponding to the (111) plane of metallic Co (Fig. 3d and e).[33] Besides, the (111) plane of CoO with a distance of 0.254 nm is also found in the blue region (Fig. 3d and e).[34] Moreover, the (222) plane of Co_3O_4 with a *d*-spacing of 0.235 nm[35] is also found in the yellow region (Fig. 3f–i). These indicate that the surface cobalt particles in Co@C-800 are in the oxidized state, too. Thus, we propose a core–shell structure of the cobalt nanoparticles in Co@C-800, where the core consists of metallic Co with an oxide shell.

High angle annular dark field (HAADF) images of Co-**L5**@C-800 show the Co particles as bright dots with a smaller average diameter of about 9 nm compared to the ligand-free produced pendant (Fig. 4a and b). Obviously, the formation of the Co-**L5** complex prevented the growth of cobalt nanoparticles during the pyrolysis process.[36]

High-magnification TEM images (Fig. 4h and i) show lattice fringes with a *d*-spacing of 0.195 nm, corresponding to the (111) lattice plane of metallic cobalt.[33] Besides, cobalt oxides exist in this sample as indicated by the lattice fringes with a *d*-spacing of 0.186 nm, which correspond to the (331) lattice plane of Co_3O_4 (Fig. 4f and g).[37] Due to the presence of a ligand, some cobalt nanoparticles are encapsulated by few carbon layers (Fig. 4d). The selected area of the nanoparticle core in Fig. 4d shows the lattice fringes with a *d*-spacing of 0.171 nm, corresponding to the (200) lattice plane of metallic

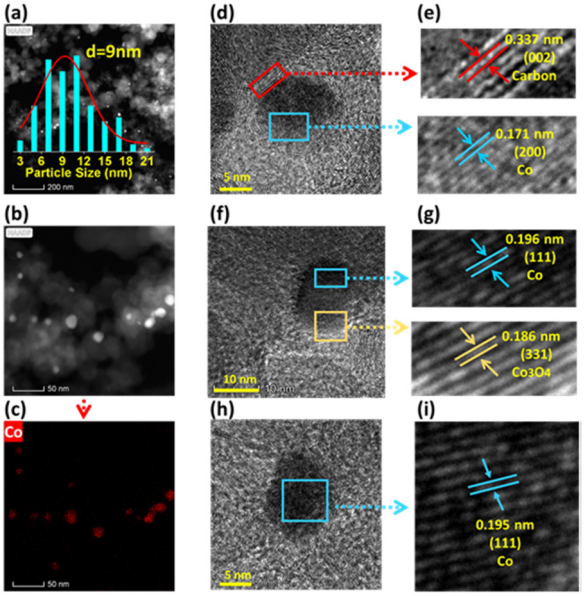

Fig. 4 TEM analysis of Co-**L5**@C-800. (a and b) TEM-HAADF images, (c) EDX elemental mapping image of Co, and (d–i) identified crystal planes of the Co nanoparticles.

cobalt (Fig. 4e).[38] In addition, the shell shown in Fig. 4d possesses lattice fringes with a *d*-spacing of 0.337 nm, corresponding to the (002) lattice plane of carbon (Fig. 4e).[39] Furthermore, the corresponding EDX mapping images of Fig. 4b and c clearly indicate that cobalt nanoparticles are randomly distributed on the surface of the materials, and cobalt species could be clearly detected (Table S5†).

The TEM images of Co-**L5**@C-400, Co-**L5**@C-600 and Co-**L5**@C-1000 are shown in Fig. S5–S7.† Interestingly, the materials prepared at a lower pyrolysis temperature, Co-**L5**@C-400 and Co-**L5**@C-600, show the formation of cobalt nanoparticles, too (Fig. S5 and S6†). It is worth mentioning that compared with Co-**L5**@C-800, the particle size of Co-**L5**@C-1000 is increased to 20.5 nm due to the relatively higher pyrolysis temperature (Fig. S7†).

Next, we performed XPS investigations to obtain further insights into the surface composition and oxidation state of cobalt in these materials. The surface composition of the different catalysts is shown in Table S6† and reveals C, O, Co, and N as the main elements. Small amounts of S and Si can be found as well, which are typical residues in carbon supports. The Co 2p and N 1s spectra of the Co-**L5** temperature series are shown in Fig. S4.† All these materials display the peaks of cobalt oxide (due to the overlap of CoO and Co_3O_4, Co_xO_y is used to represent cobalt oxide) at around 780.4 eV.[40] For Co-**L5**@C-400 (Fig. S4a†), the Co $2p_{3/2}$ peak is shifted to slightly higher binding energies at about 781.2 eV. Together with the pronounced satellite features, this suggests Co^{2+} as the main oxidation state.[40] For higher pyrolysis temperatures, the main Co $2p_{3/2}$ peaks are observed at typical binding energies of oxidized Co at about 780.4 eV.[40] For Co-**L5**@C-600 (Fig. S4a†), the less pronounced satellite features indicate the additional presence of Co_3O_4.[40] For the pyrolysis temperatures 800 and 1000 °C, an additional peak at 778.4 eV appears which is characteristic of metallic cobalt.[41] XPS data indicated that the surface concentration of Co species decreases with increasing pyrolysis temperature from 0.3 to 0.1 at% obviously due to an increased carbon coverage (Table S6†). In addition, the relative concentration of metallic cobalt increases, too (Table S7†). In comparison, the reference sample Co@C-800 shows no metallic Co at the surface (see Fig. S4a,†) even though it could be detected in the bulk material by XRD (see the XRD section Fig. S2-3†). These results underline the importance of the added ligand to form and protect near surface Co species. The nitrogen concentration also decreased with increase in pyrolysis temperature from 1.2 at% for 400 °C to 0.1 at% for 1000 °C (Table S6†). The N 1s XPS spectra shown in Fig. S4b† are deconvoluted showing four N species: pyridinic N (398.5 eV), pyrrolic N (399.8 eV), graphitic N (401.2 eV), and oxidized pyridinic-N (403.4 eV).[42,43] Going from low to higher pyrolysis temperatures, the observed N species change from predominantly pyridinic-N and pyrrolic-N species[44] to graphitic-N, which are incorporated into the support lattice.[44]

Later, the textures of these materials were measured by N_2 physisorption. The specific surface area (S_{BET}) is summarized in Fig. S8.† Among all the samples, Co@C-800 has the largest specific surface area of 201 $m^2\ g^{-1}$. With the increase of pyrol-

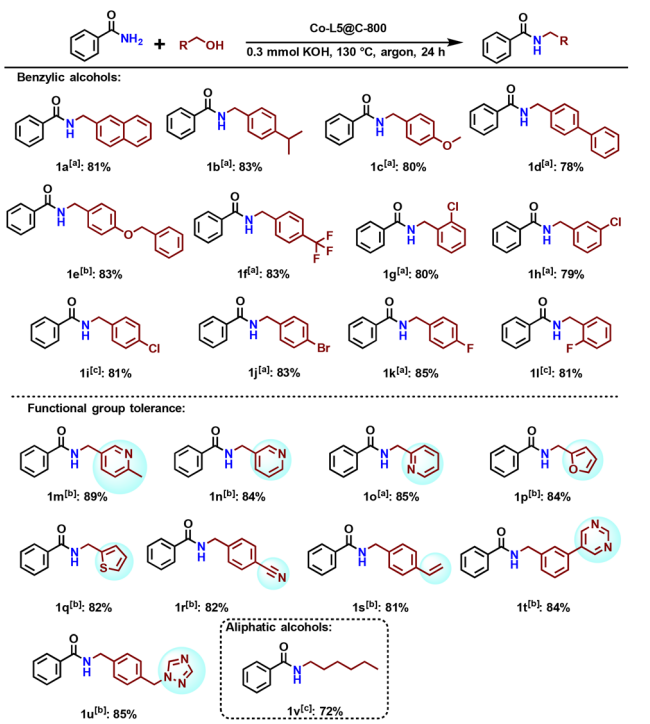

Scheme 1 Co-**L5**@C-800 catalyzed *N*-alkylation of benzamide with different alcohols. Reaction conditions: [a] 0.5 mmol of benzamide, 0.55 mmol of alcohol, 60 mg of Co-**L5**@C-800 (1.9 mol% Co), 0.3 mmol of KOH, 3 mL of toluene, 130 °C, 24 h, and 1 atm argon. Isolated yields. [b] Same as [a] at 140 °C. [c] Same as [a], GC yield.

ysis temperature from 400 to 1000 °C, the surface area of Co-L5@C-T samples increased from 121 $m^2 g^{-1}$ to 164 $m^2 g^{-1}$.

Synthetic applications and substrate scope

Under the optimized reaction conditions, we explored the scope of Co-**L5**@C-800 catalyzed *N*-alkylation of primary amides with alcohols. As shown in Scheme 1, several functionalized and structurally diverse alcohols underwent the desired reactions with benzamide to produce the corresponding products in good to excellent yields.

The substitution on the aryl ring of benzyl alcohol has no noticeable effect on the efficiency of the reaction. With both electron-withdrawing and electron-donating substituents, the *N*-alkylated amides are afforded in 78%–85% yield (Scheme 1, **1a–1l**). For catalyst applications in advanced organic synthesis, achieving a high degree of chemoselectivity is important, yet often challenging. To showcase this aspect, alcohols containing various functional groups were tested in our protocol. Interestingly, the C–C double bond and nitrile are well tolerated (Scheme 1, **1s** and **1r**). Furthermore, heterocyclic benzyl alcohols also reacted well and produced the alkylated amides in 81%–89% yield. 1-Hexanol as an example of aliphatic alcohols led to the corresponding amide in good yield, too (Scheme 1, **1v**).

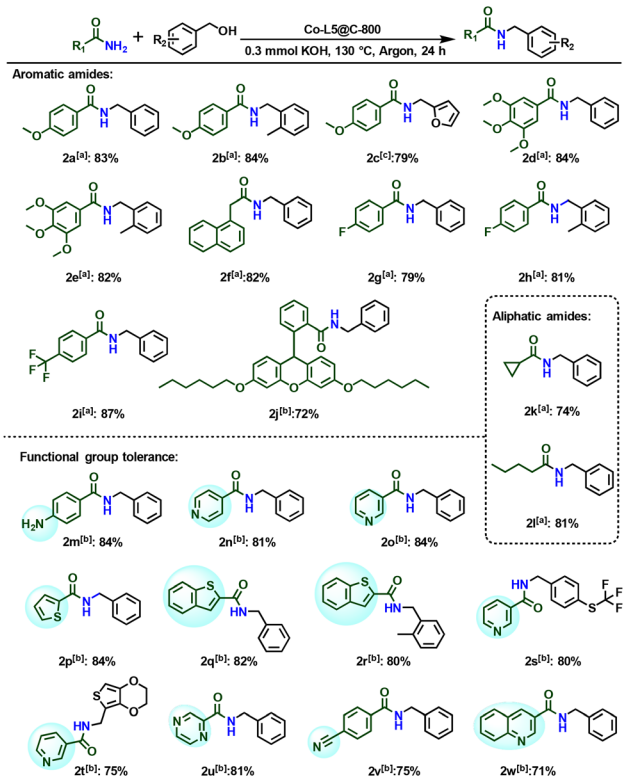

Scheme 2 Co-**L5**@C-800 catalyzed *N*-alkylation of different amides with benzylic alcohol. Conditions: [a] 0.5 mmol of amide, 0.55 mmol of benzyl alcohol, 60 mg of Co-**L5**@C-800 (1.9 mol% Co), 0.3 mmol of KOH, 3 mL of toluene, 130 °C, 24 h, and in 1 atm argon. Isolated yields. [b] Same as [a] at 140 °C. [c] Same as [a], GC yield.

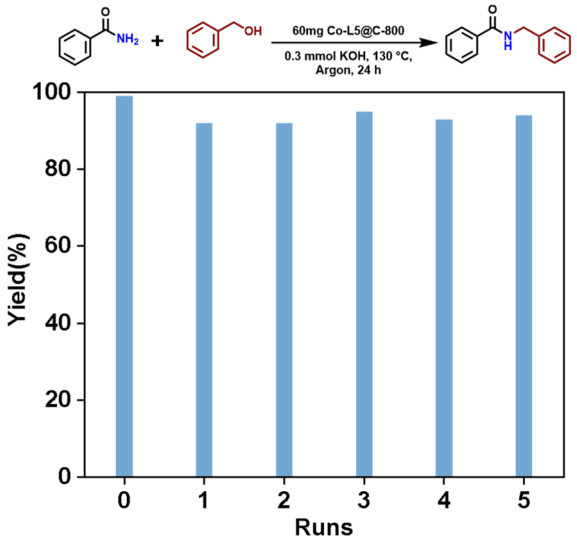

Fig. 5 Reusability of Co-**L5**@C-800 in *N*-alkylation of benzamide with benzyl alcohol. Reaction conditions: 0.5 mmol benzamide, 0.55 mmol benzyl alcohol, 60 mg Co-**L5**@C-800 (1.9 mol% Co), 0.3 mmol KOH, 3 mL toluene, 130 °C, 24 h, in 1 atm argon.

The standard reaction protocol is also applicable using diverse amides. Benzamides with both electron-withdrawing and electron-donating substituents reacted well with benzyl alcohol, and the corresponding secondary amides were obtained in 79%–87% yield (Scheme 2, **2a–2i**). The biological amides can also react well with benzyl alcohol in the presence of this cobalt system to obtain unreported secondary amides in good yields (Scheme 2, **2j**), which provides a method for synthesizing new products. Next, we explored the general applicability for more challenging aliphatic amides. By using this catalytic method, secondary amides could also be produced from less active alkyl amides (Scheme 2, **2k–2l**). Similarly, heterocycles were well tolerated, and this system showed excellent regioselectivity in the substrates containing both amino and nitrile groups (Scheme 2, **2m** and **2v**). Screening of various primary amides and alcohols revealed that the alkylation of amides catalyzed by this cobalt system worked well and provided secondary amides in good to excellent yields (Schemes 1 and 2). To investigate the stability of this novel catalyst, recycling experiments were performed under standard conditions. Indeed, Co-**L5**@C-800 can be reused conveniently and no significant loss of catalytic activity is observed even after five times (Fig. 5). The recycled catalyst was also characterized to explore the structural differences by XRD. Compared with fresh material, no significant structural difference was seen in the XRD pattern (Fig. S9b†).

Conclusions

We reported a novel nano-structured Co-based catalyst for practical and convenient *N*-alkylation of primary amides with alcohols. Introduction of nitrogen ligands and pyrolysis treat-

ment creates a highly stable and reusable Co-nanoparticles, which activates *N*-alkylation of primary amides with alcohols under mild conditions. The optimal catalyst (Co-**L5**@C-800) showed good to excellent activity and selectivity for the synthesis of functionalized and structurally diverse secondary amides.

Author contributions

R. V. J., S. W. and M. B. supervised the project. R. M., R. V. J., S. W. and M. B. planned and developed the project. R. M., S. W. and R. V. J. designed the experiments. R. M. and J. G. prepared catalysts and performed all catalytic experiments. J. G. and Y. H. carried out reproducibility experiments. L. Z. and N. W. performed the TEM measurements and analysis. S. B. and H. L. performed XPS and XRD analysis. R. M., J. G., S. W., R. V. J. and M. B. wrote the paper.

Conflicts of interest

There are no conflicts to declare.

Acknowledgements

We gratefully thank the European Research Council (EU project 670986-NoNaCat) and the State of Mecklenburg-Vorpommern for financial and general support. We thank the analytical team of the Leibniz-Institut für Katalyse e.V. for their excellent service. We thank Mr Reinhard Eckelt for performing BET. Rui Ma, Jie Gao and Yue Hu thank the China Scholarship Council (CSC) for the fellowship.

References

1 M. T. Sabatini, L. T. Boulton, H. F. Sneddon and T. D. Sheppard, *Nat. Catal.*, 2019, **2**, 10–17.
2 C. A. G. N. Montalbetti and V. Falque, *Tetrahedron*, 2005, **61**, 10827–10852.
3 E. Valeur and M. Bradley, *Chem. Soc. Rev.*, 2009, **38**, 606–631.
4 X. Dai and F. Shi, *Org. Biomol. Chem.*, 2019, **17**, 2044–2054.
5 J. Das and D. Banerjee, *J. Org. Chem.*, 2018, **83**, 3378–3384.
6 C. Chen, F. Verpoort and Q. Wu, *RSC Adv.*, 2016, **6**, 55599–55607.
7 X. J. Wu, H. J. Wang, Z. Q. Yang, X. S. Tang, Y. Yuan, W. Su, C. Chen and F. Verpoort, *Org. Chem. Front.*, 2019, **6**, 563–570.
8 C. Gunanathan and D. Milstein, *Science*, 2013, **341**, 1229712.
9 S. Kerdphon, X. Quan, V. S. Parihar and P. G. Andersson, *J. Org. Chem.*, 2015, **80**, 11529–11537.
10 A. Wang, Y. Xie, J. Wang, D. Shi and H. Yu, *Chem. Commun.*, 2022, **58**, 1127–1130.
11 N. Wang, X. Zou, J. Ma and F. Li, *Chem. Commun.*, 2014, **50**, 8303–8305.
12 Y. Watanabe, T. Ohta and Y. Tsuji, *Bull. Chem. Soc. Jpn.*, 1983, **56**, 2647–2651.
13 X. C. Yu, L. Jiang, Q. Li, Y. Y. Xie and Q. Xu, *Chin. J. Chem.*, 2012, **30**, 2322–2332.
14 P. Xu, F.-S. Han and Y.-H. Wang, *Adv. Synth. Catal.*, 2015, **357**, 3441–3446.
15 G. C. Y. Choo, H. Miyamura and S. Kobayashi, *Chem. Sci.*, 2015, **6**, 1719–1727.
16 B. Sardar, R. Jamatia, A. Samanta and D. Srimani, *J. Org. Chem.*, 2022, **87**, 5556–5567.
17 R. V. Jagadeesh, T. Stemmler, A. E. Surkus, H. Junge, K. Junge and M. Beller, *Nat. Protoc.*, 2015, **10**, 548–557.
18 J. Gao, L. Feng, R. Ma, B.-J. Su, A. M. Alenad, Y. Liu, M. Beller and R. V. Jagadeesh, *Chem. Catal.*, 2022, **2**, 178–194.
19 J. Gao, R. Ma, L. Feng, Y. Liu, R. Jackstell, R. V. Jagadeesh and M. Beller, *Angew. Chem., Int. Ed.*, 2021, **60**, 18591–18598.
20 J. Gao, R. Ma, F. Poovan, L. Zhang, H. Atia, N. V. Kalevaru, W. Sun, S. Wohlrab, D. A. Chusov, N. Wang, R. V. Jagadeesh and M. Beller, *Nat. Commun.*, 2023, **14**, 5013.
21 R. V. Jagadeesh, K. Murugesan, A. S. Alshammari, H. Neumann, M. M. Pohl, J. Radnik and M. Beller, *Science*, 2017, **358**, 326–332.
22 P. D. Coan, M. B. Griffin, P. N. Ciesielski and J. W. Medlin, *J. Catal.*, 2019, **372**, 311–320.
23 K. Sun, H. Shan, G. P. Lu, C. Cai and M. Beller, *Angew. Chem., Int. Ed.*, 2021, **60**, 25188–25202.
24 A. J. Watson, A. C. Maxwell and J. M. Williams, *J. Org. Chem.*, 2011, **76**, 2328–2331.
25 K. Lida, T. Miura, J. Ando and S. Saito, *Org. Lett.*, 2013, **15**, 1436–1439.
26 T. Miura, O. Kose, F. Li, S. Kai and S. Saito, *Chem. – Eur. J.*, 2011, **17**, 11146–11151.
27 B. J. Hwang, *J. Phys. Chem. C*, 2007, **111**, 15267–15276.
28 L. Belles, C. Moularas, S. Smykała and Y. Deligiannakis, *Nanomaterials*, 2021, **11**, 925.
29 K. Deori and S. Deka, *CrystEngComm*, 2013, **15**, 8465–8474.
30 T. Rao Penki, D. Shanmughasundara, B. Kishore and N. Munichandraiah, *Adv. Mater. Lett.*, 2014, **5**, 184–190.
31 J. Jansson, A. E. C. Palmqvist, E. Fridell, M. Skoglundh, L. Österlund, P. Thormählen and V. Langer, *J. Catal.*, 2002, **211**, 387–397.
32 A. K. Datye, J. Bravo, T. R. Nelson and L. Pfefferle, *Appl. Catal., A*, 2000, **198**, 179–196.
33 X. Deng, Y. Yang, L. Wang, X. Z. Fu and J. L. Luo, *Adv. Sci.*, 2021, **8**, 1–9.
34 X. Sun, Y. Lu, T. Li, S. Zhao, Z. Gao and Y.-Y. Song, *J. Mater. Chem. A*, 2019, **7**, 372–380.
35 J. Mu, L. Zhang, G. Zhao and Y. Wang, *Phys. Chem. Chem. Phys.*, 2014, **16**, 15709–15716.
36 B. Y. Guan, X. Y. Yu, H. B. Wu and X. W. D. Lou, *Adv. Mater.*, 2017, **29**, 1703614.

37 J. O. D. Malafatti, A. J. Moreira, E. C. Paris, L. J. Cardenas Flechas, O. A. P. Pereira and M. Rincón Joya, *Catalysts*, 2022, **12**, 1199.
38 X. Peng, L. Wang, L. Hu, Y. Li, B. Gao, H. Song, C. Huang, X. Zhang, J. Fu, K. Huo and P. K. Chu, *Nano Energy*, 2017, **34**, 1–7.
39 J. Chen, X. Yuan, F. Lyu, Q. Zhong, H. Hu, Q. Pan and Q. Zhang, *J. Mater. Chem. A*, 2019, **7**, 1281–1286.
40 M. C. Biesinger, B. P. Payne, A. P. Grosvenor, L. W. M. Lau and A. R. Gerson, *Appl. Surf. Sci.*, 2011, **257**, 2717–2730.
41 L. Chen, Y. Zhang, H. Wang, Y. Wang, D. Li and C. Duan, *Nanoscale*, 2018, **10**, 21019–21024.
42 X. Yang, C. Chen, Z. Zhou and S. Sun, *Acta Phys.-Chim. Sin.*, 2019, **35**, 472–485.
43 B. J. Matsoso, K. Ranganathan, B. K. Mutuma, T. Lerotholi, G. Jones and N. J. Coville, *RSC Adv.*, 2016, **6**, 106914–106920.
44 R. V. Jagadeesh, A. E. Surkus, H. Junge, M. Pohl, J. Radnik, J. Rabeah, H. Huan, V. Schünemann, A. Brückner and M. Beller, *Science*, 2013, **342**, 1073–1076.

RESEARCH ARTICLE

Base-free Selective α-Alkylation and α-Vinylation of Ketones with Alcohols over Fe/Zn Bimetallic Catalysts

Rui Ma[a], Jie Gao[a], Lan Zhang[b], Hanan Atia[a], Stephan Bartling[a], Henrik Lund[a], Ning Wang*[b], Sebastian Wohlrab*[a], Rajenahally V. Jagadeesh*[a, c], and Matthias Beller*[a]

[a] R. Ma, Dr. J. Gao, Dr. H. Atia, Dr. S. Wohlrab, Prof. Dr. R. V. Jagadeesh and Prof. Dr. M. Beller
Leibniz-Institut für Katalyse e.V.
Albert-Einstein-Str. 29a, 18059 Rostock, Germany
E-mail: sebastian.wohlrab@catalysis.de; jagadeesh.rajenahally@catalysis.de; matthias.beller@catalysis.de

[b] L. Zhang, Prof. Dr. N. Wang
Faculty of Environment and Life, Beijing University of Technology,
Chaoyang, 100124, Beijing, China
E-mail: ning.wang.1@bjut.edu.cn

[c] Nanotechnology Centre, Centre for Energy and Environmental Technologies, VŠB-Technical University of Ostrava, Ostrava-Poruba, Czech Republic

Abstract: General and benign α-alkylations and α-vinylations of ketones with alcohols proceed in the presence of heterogeneous Fe-Zn catalyst (Fe/Zn-**L1**@MgO-Al_2O_3-70). Applying this catalyst material, the synthesis of a variety of ketones (> 52 products), substituted chalcones (17 products) and quinoline derivatives (>18 products) is carried out with a broad substrate range and good functional group tolerance. In addition to the model substrates, the catalyst also allows for the reaction of more challenging secondary and aliphatic alcohols, which have been selectively converted to the corresponding products in good to high yields. A notable feature of the Fe/Zn catalyst is the ability to selectively perform chemo-divergent alkylation or vinylation reactions by temperature control. Another advantage of the presented methods is the exclusion of (strong) external base, which is a common prerequisite in such transformations.

Introduction

The construction of C-C bonds is of fundamental importance in organic chemistry and a plethora of such synthetic methods are available to academic and industrial chemists. Among these methods, α-functionalization of carbonyl compounds is a highly valuable strategy to synthesize basic organic building blocks as well as heterocycles, pharmaceuticals, and natural product related molecules.[1] Conventionally, the synthesis of α-alkylated ketones is performed using environmentally harmful alkyl halides as alkylating agents in the presence of strong bases (**Scheme 1a**).[2] This leads to the inevitable formation of (over) stoichiometric amounts of waste. In contrast, metal-catalyzed α-functionalization of ketones with alcohols has inherent advantages and has therefore attracted much attention in recent years.[3] More specifically, several research groups have developed different types of homogeneous organometallic complexes for such transformations.[4] Despite these interesting developments, most of the known catalytic systems still have some drawbacks, such as the need for precious metals (Ru, Ir, Pd, etc.)[3b, 5] or sophisticated ligands, as well as the necessity of large amounts of additives and/or bases (**Scheme 1b**).[3c, 6] In addition, homogeneous catalysts are sometimes limited in their applications due to difficult handling and separation. In this respect, heterogeneous materials offer a more practical approach for easy catalyst recycling in the α-alkylation of ketones with alcohols. Although, Pd-[3a, 3d, 7] and Ru-[8] based nanomaterials have been developed for this transformation, these systems generally require a large excess of base, and in some cases additional hydrogen acceptor (**Scheme 1b**).

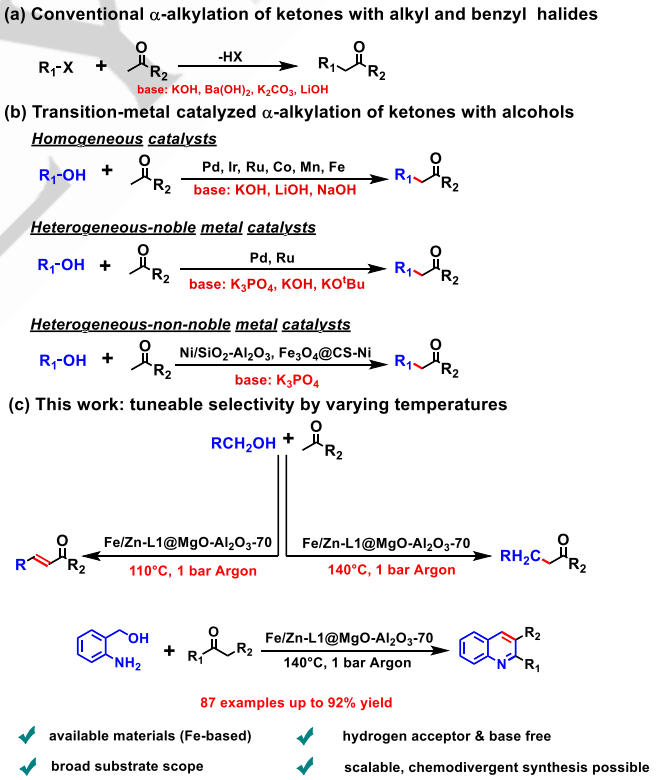

Scheme 1. Transition metal catalyzed α-alkylation of ketones: Comparison between conventional methods and this work.

In addition to the distinct reactivity profiles, the use of non-noble 3d transition metals in catalysis offers significant economic and ecological advantages. A nickel-based heterogeneous catalytic system has been reported to date, which requires 20

mol% Ni of a 65 wt% Ni/SiO_2/Al_2O_3, an additional base (10 mol% K_3PO_4), and high temperature (175 °C).[9] Consequently, the development of a non-noble metal-based heterogeneous catalytic system that enables this transformation to occur smoothly under milder conditions (base-free, hydrogen acceptor-free, lower reaction temperature) remains a significant challenge. In this regard, iron (Fe) is a particularly intriguing candidate due to its abundance (the second-most prevalent metal in the Earth's crust) and its toxicity profile, which differs from that of most other transition metals.[10]

In this study, we present the synthesis and comprehensive characterization of a Fe-Zn based material, which exhibits remarkable activity for the α-alkylation of ketones with alcohols in the absence of a base and a hydrogen acceptor. The catalytic system exhibited a broad substrate scope and allowed for selective switching between alkylation and vinylation of ketones. To the best of our knowledge, this is the first Fe-based heterogeneous catalyst for the direct alkylation and vinylation of ketones without the use of a base or hydrogen acceptor.

Results and Discussion

Preparation of Catalytic Materials and Model Studies

In recent decades, catalytic materials for organic syntheses have been developed through the immobilization of metal complexes, generated in situ, on stable inorganic supports and subsequent pyrolysis. This preparative approach can result in the formation of highly dispersed metal nanoparticles or single atoms, which can be understood as a method for the heterogenization of homogeneous catalysts.[11] For example, in our research group, many Fe-[12], Co-[13], and Ni-[14] based nanostructured catalysts were prepared using this method and applied for different (de)hydrogenation and reductive amination reactions. In the majority of these preceding studies, specific heteroarenes, such as phenanthroline or combinations of diamines and dicarboxylic acids,[13a, 15] were employed as ligands to facilitate the formation of active metal species embedded in a nitrogen-doped carbon matrix. We were curious to ascertain whether the use of the simplest (and least expensive) aromatic di- and monoamines (1,2- and 1,4-diaminobenzene **L1** and **L2**, aniline **L3**) would also permit the creation of active catalyst materials. In order to prepare potential heterogeneous catalysts, $Fe(NO_3)_3{\cdot}9H_2O$ was combined with three ligands (**L1**-**L3**), and the resulting metal complexes were immobilized on the surface of various supports, including ZSM-5 and TiO_2 The resulting materials were pyrolyzed under argon at 800 °C to obtain a small library of potential iron catalysts (**Figure 1**, **Table 1**). The pyrolysis process was conducted on a variety of supports, e.g. ZSM-5, TiO_2, Al_2O_3, carbon, MgO-Al_2O_3-X (X represents the mass ratio of MgO, for example in MgO-Al_2O_3-30: the mass ratio of MgO is 30%). In the following sections, the supported materials will be denoted as M-L@Support, where M and L represent metal and ligand, respectively.

The α-alkylation of acetophenone with benzyl alcohol was selected as the standard reaction. For this widely accepted benchmark reaction, numerous heterogeneous catalysts, particularly those based on precious metals, have been developed in the past (see **Table S1**). In contrast to the majority of previously documented procedures, our approach involved the omission of additional bases and reagents, a strategy that offers significant benefits, including reduced waste generation and lower costs. Initially, the combination of Fe/**L1** on different supports was evaluated for the synthesis of dihydrochalcone **3** under an argon atmosphere in toluene at 130°C for 24 h (**Table 1**).

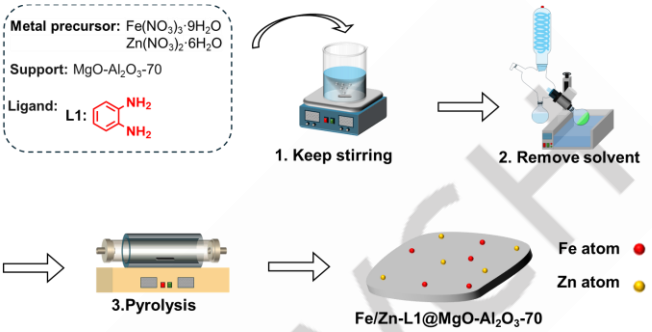

Figure 1. Catalysts preparation: pictorial representation for the synthesis of catalytic materials.

Table 1. α-Alkylation of acetophenone with benzyl alcohol: Catalytic activities and selectivities.

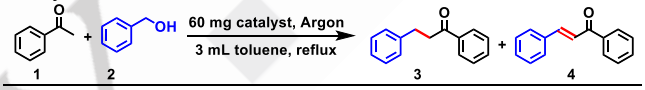

Entry	Catalyst	Metal loading, wt%		Conversion %	Yield, %	
		Fe	Zn		3	4
1[a]	Fe-L1@SiO_2			<1	<1	<1
2[a]	Fe-L1@CaO			<1	<1	<1
3[a]	Fe-L1@TiO_2			12	<1	11
4[a]	Fe-L1@C			10	3	5
5[a]	Fe-L1@Al_2O_3	0.61		36	2	14
6[a]	Fe-L1@MgO	0.63		8	<1	3
7[a]	Fe-L1@MgO-Al_2O_3-30	1.05		76	20	39
8[a]	Fe-L1@MgO-Al_2O_3-50	1.04		93	58	26
9[a]	Fe-L1@MgO-Al_2O_3-70	1.16		87	68	20
10[a]	2Fe-L1@MgO-Al_2O_3-70	2.22		91	50	30
11[a]	Fe/Zn-L1@MgO-Al_2O_3-70	1.15	1.14	96	81	13
12[a]	Fe/Zn-L2@MgO-Al_2O_3-70	1.11	1.12	88	46	29
13[a]	Fe/Zn-L3@MgO-Al_2O_3-70	1.13	1.21	93	73	16
14[a]	Fe/Zn@MgO-Al_2O_3-70	1.13	1.27	89	63	20
15[a]	Fe/3Zn-L1@MgO-Al_2O_3-70	1.11	3.72	96	80	14
16[a]	3Fe/Zn-L1@MgO-Al_2O_3-70	3.24	1.25	85	35	33
17[a]	Zn-L1@MgO-Al_2O_3-70		1.01	86	71	18
18[a]	Fe/Zn-L1@MgO	0.66	0.24	31	<1	19
19[a]	Fe/Zn-L1@Al_2O_3	0.68	0.76	38	<1	19
20[b]	Fe/Zn-L1@MgO-Al_2O_3-70	1.15	1.14	99	94	5
21[b]	MgO-Al_2O_3-70			27	5	18
22[b]	without cat			n.r	n.r	n.r

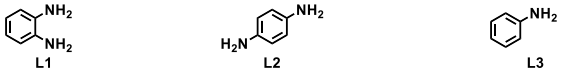

Reaction conditions: [a] 0.50 mmol acetophenone, 0.55 mmol benzyl alcohol, 60 mg catalyst, 1 bar argon, 3 mL toluene, 130°C, 24 h. [b] The same as [a] at 140°C, 14 h. The conversion and yields were determined by GC based on acetophenone using n-hexadecane as the standard.

As shown in **Table 1, entries 1-9**, the yield of **3** is highly dependent on the nature of the support. The activity and

selectivity of the different materials exhibited considerable variation. In addition to the anticipated product **3**, the corresponding dehydrogenated chalcone **4** was also observed in the majority of test reactions. The highest activity and yield of **3** were observed in the presence of Fe-**L1**@MgO-Al_2O_3-70. To enhance the activity of Fe-**L1**@MgO-Al_2O_3-70, we increased the Fe loading; however, no notable advancement was observed (**Table 1, entry 10)**. In light of reports on the alkylation of ketones catalyzed by zinc salts,[16] a certain amount of $Zn(NO_3)_2{\cdot}6H_2O$ was added to the aforementioned catalyst preparation procedure. A comparison of the reactivity of Fe-**L1**@MgO-Al_2O_3-70 and Fe/Zn-**L1**@MgO-Al_2O_3-70 (**Table 1, entries 9 and 11**) revealed that the presence of Zn resulted in an increase in the yield of **3** from 68% to 81%. Further increases in the quantity of Zn did not improve the yield and selectivity of **3** (**Table 1, entry 15**). As with the Fe-only catalyst, the "pure" Zn-based material demonstrated considerable activity (**Table 1,** compare **entries 9 and 17**). However, its performance was inferior to that of the bimetallic material. In contrast, the pure support exhibits minimal activity (**Table 1, entry 21**), suggesting a synergistic reaction involving all components. The use of 1,4-diaminobenzene **L2** and aniline **L3** in place of **L1** also resulted in the formation of active catalysts, although the yields of compounds **3** and **4** were found to be lower. It is noteworthy that the reaction exhibited activity even in the absence of an amine ligand (**Table 1, entry 14**). Ultimately, the optimal yield of the target ketone **3** (94% yield with 99% conversion) was achieved at 140 °C (**Table 1, entry 20**). As anticipated, the reaction did not occur in the absence of a catalyst (**Table 1, entry 22**).

In order to gain a deeper insight into the behaviour of this bimetallic catalyst, a kinetic profile of the model reaction was recorded. As illustrated in **Figure 2a**, the yield of chalcone exhibited a gradual increase, reaching 36% within 2 h, and then underwent consumption, yielding up to 94% of **4** (dihydrochalcone) after 14 h. Throughout the course of the reaction, the formation of 3-5% of benzaldehyde was observed as an additional intermediate, resulting from the dehydration of benzyl alcohol.[17] Based on detailed previous mechanistic investigations of ketone alkylation in the presence of Ni/SiO_2-Al_2O_3[18] and the observed intermediates (**Figure 2a**), a mechanistic proposal is presented in **Figure 2b**. Initially, benzyl alcohol undergoes dehydrogenation, forming benzaldehyde and a corresponding metal hydride. Concurrently, acetophenone is coordinated with the support surface, and ketone-enol tautomerism occurs. Subsequently, the enol nucleophile attacks the ketone, resulting in the elimination of water and the formation of the α,β-unsaturated chalcone **4**. Finally, the metal hydride, which is formed in the initial step, reduces **4**, yielding the chalcone **3**. Notably, the rate-determining step in this process was found to be the final hydrogenation step, which occurs at lower temperatures (<130 C) (**Figure S1**).

Characterizations of the catalysts

To gain insight into the precise composition and structure of the optimal Fe/Zn-**L1**@MgO-Al_2O_3-70 catalyst, detailed characterizations were conducted. A comparison of the X-ray diffraction (XRD) patterns of Fe/Zn-**L1**@MgO-Al_2O_3-70 before and after pyrolysis, reveals that the initial hydrotalcite-like structured support (**Figure S2d**) undergoes a conversion into a mixture of MgO and $MgAl_2O_4$ **(Figure S3**).

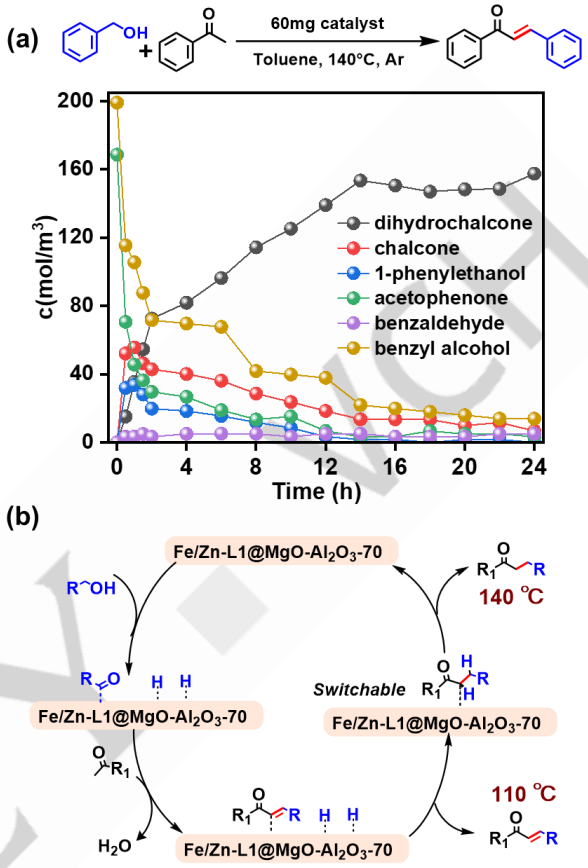

Figure 2. Kinetic profile and reaction mechanism. (a) Kinetic profile of α-alkylation of acetophenone with benzyl alcohol. Reaction conditions: 0.5 mmol acetophenone, 0.55 mmol benzyl alcohol, 60 mg catalyst, and 3 mL toluene were heated at 140 C for different hours in a closed 25 mL pressure tube under 1 bar argon, GC yield. (b) Proposed reaction mechanism.

The XRD patterns of the catalysts Fe-L1@MgO and Fe-L1@Al_2O_3 show the diffraction peaks of the respective supports, MgO and Al_2O_3 (**Figure S4**). As the Mg content of the initially utilized support increases from 30% to 70%, the formation of MgO is observed to a greater extend, as indicated by an intensity increase of peaks assigned to MgO. (**Figure S3**). Due to the low iron loading, the XRD patterns of Fe/Zn-**L1**@MgO-Al_2O_3-70 and 3Fe/Zn-**L1**@MgO-Al_2O_3-70 and Fe/3Zn-**L1**@MgO-Al_2O_3-70 samples did not display the presence of Fe diffraction peaks (**Figures S5**). The atomic resolution HAADF-STEM images of Fe/Zn-**L1**@MgO-Al_2O_3-70 are presented in **Figures 3a-d**. As illustrated in **Figures 3a-d,** the small and bright dots, which correspond to atomically dispersed Fe or Zn are clearly discernible. The EDX mapping images of Fe/Zn-**L1**@MgO-Al_2O_3-70 demonstrates the presence of elements including Mg, Al, C, Fe, Zn, N and O (**Figure S6**). In addition to the isolated metal atoms, particles were observed in the TEM images of Fe/Zn-

L1@MgO-Al_2O_3-70 captured under different resolutions (**Figure S7**). Meanwhile, the TEM images of the catalysts with higher metal content, 3Fe/Zn-**L1**@MgO-Al_2O_3-70 and Fe/3Zn-**L1**@MgO-Al_2O_3-70, clearly show metal nanoparticles (**Figures S8-9)**.

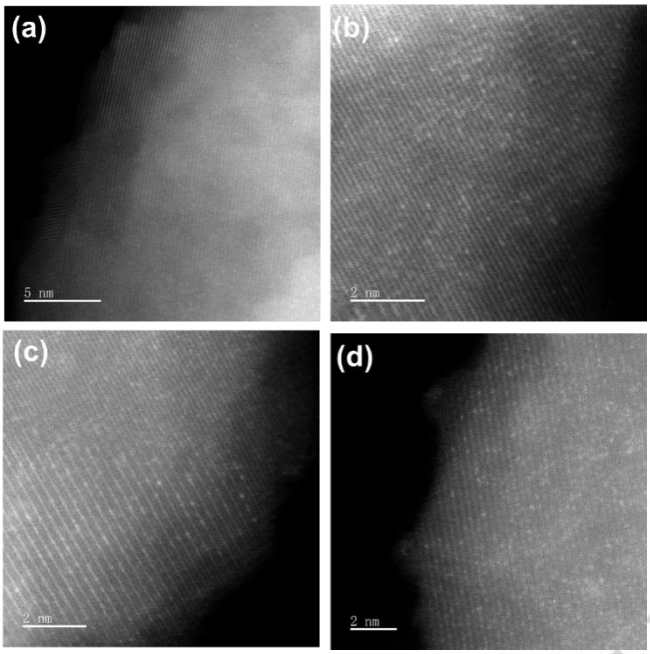

Figure 3. The HAADF-STEM images of Fe/Zn-**L1**@MgO-Al_2O_3-70 material.

Subsequently, CO_2 and NH_3 temperature-programmed desorption (TPD) were conducted to investigate the surface acid-base characteristics of the solid catalysts.[19] Compared to Zn-**L1**@MgO-Al_2O_3-70, the Fe-**L1**@MgO-Al_2O_3-70 material exhibited a greater abundance of basic sites (**Figure 4a**). As evidenced by NH_3-TPD measurements, Fe-**L1**@MgO-Al_2O_3-70 has the largest number of acidic sites among all the samples (**Figures 4b**). It would appear that the addition of Zn has the effect of suppressing Lewis acidic sites on Al_2O_3, which is in accordance with the predictions of Tanabe's model.[20] After introducing Zn, the number of acidic sites on Fe/Zn-**L1**@MgO-Al_2O_3-70 decreases significantly, while the number of basic sites increased dramatically, almost twice as much as before (**Figures 4a-b, Table S2**).

To ascertain the surface chemical and physical information, X-ray photoelectron spectroscopy (XPS) analysis was conducted (see **Figures 4c** and **4d**). It is noteworthy that in the case of the catalyst Fe-**L1**@MgO-Al_2O_3-70, in the absence of added zinc, no nitrogen species are observed on the surface (**Figure 4c**). In contrast, the amount of surface nitrogen species increased to 1.2 at% on Fe/Zn-**L1**@MgO-Al_2O_3-70 (**Figure 4d, Table S3**). The EA analyses also confirmed that the content of nitrogen species in Fe/Zn-**L1**@MgO-Al_2O_3-70 (0.29 wt%) is greater than that of Fe-**L1**@MgO-Al_2O_3-70 (0.17 wt%) (**Table S4**). The N species in Fe/Zn-**L1**@MgO-Al_2O_3-70 were identified as pyridinic-N (398.4 eV), pyrrolic-N (399.7 eV) and/or metal-N_x species, graphitic-N (400.9 eV), and oxidized pyridinic-N (402.9 eV)[21], respectively (**Figure 4d**). With regard to the Fe 2p spectra, the Fe $2p_{3/2}$ peak is located at approximately 710 eV, thus suggesting oxidation states of +2 and/or +3 for Fe in Fe-**L1**@MgO-Al_2O_3-70 and Fe/Zn-**L1**@MgO-Al_2O_3-70 (**Figures S10a-b**).[22] It is worth noting that The introduction of Zn into Fe-**L1**@MgO-Al_2O_3-70 resulted in a notable increase in the specific surface area of the catalyst, from 59.9 m²/g to 175.7 m²/g, representing a threefold enhancement. Additionally, the average pore size was observed to diminish from 10.1 nm to 5.6 nm, indicating a reduction in the pore size distribution (**Table S5, Figure S11**).

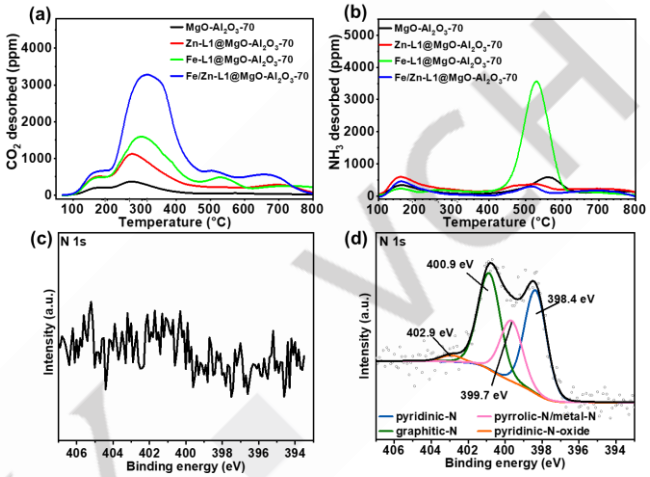

Figure 4. Characterization of catalytic materials: (a) TPD-CO_2 curves and (b) TPD-NH_3 curves of selected materials. N 1s spectra of (c) Fe-**L1**@MgO-Al_2O_3-70 and (d) Fe/Zn-**L1**@MgO-Al_2O_3-70.

To confirm the structural features of the Fe/Zn-**L1**@MgO-Al_2O_3-70 material, an X-ray absorption spectroscopy (XAS) analysis was conducted. The Zn near-edge absorption energy of Zn-**L1**@MgO-Al_2O_3-70 and Fe/Zn-**L1**@MgO-Al_2O_3-70 are situated between those of ZnO and Zn foil, indicating that the Zn species possess positive charges (**Figure 5a**).[23] The Fourier transform (FT) k^3-weighted extended X-ray absorption fine structure (EXAFS) spectrum for Zn-**L1**@MgO-Al_2O_3-70 and Fe/Zn-**L1**@MgO-Al_2O_3-70 (**Figure 5b**) exhibited a main peak at 1.54 Å, which could be attributed to the Zn-(N/O) species.[24] The observed peak at 2.27 Å is caused by the interactions between Zn atoms (Zn-Zn bond) on Zn foil material, which are also observed at Zn-L1@MgO-Al_2O_3-70 and Fe/Zn-L1@MgO-Al_2O_3-70. This indicates the formation of Zn particles in these two materials (**Figure 5b**).To prove the possibilities of the formation of atomically dispersed Zn in Zn-**L1**@MgO-Al_2O_3-70 and Fe/Zn-**L1**@MgO-Al_2O_3-70, wavelet transform (WT) of Zn *k*-edge EXAFS oscillations was carried out owing to its powerful resolutions in both *k* and *R* spaces.[25] From the WT contour plots of Zn foil and Zn-based samples (**Figures 5c-e**), Fe/Zn-**L1**@MgO-Al_2O_3-70 shows an intensity maximum at (x=4.08 $Å^{-1}$, y=1.54 Å) with markedly reduced wave vector *k* and *R* in comparison to that of Zn foil (x=6.57 $Å^{-1}$, y=2.27 Å). As evidenced by TEM images (**Figure 2,** small and bright dots), the FT- and WT-EXAFS analysis (**Figure 5**), it can be concluded that both Zn particles and atomically dispersed Zn atoms were formed in Fe/Zn-**L1**@MgO-Al_2O_3-70.

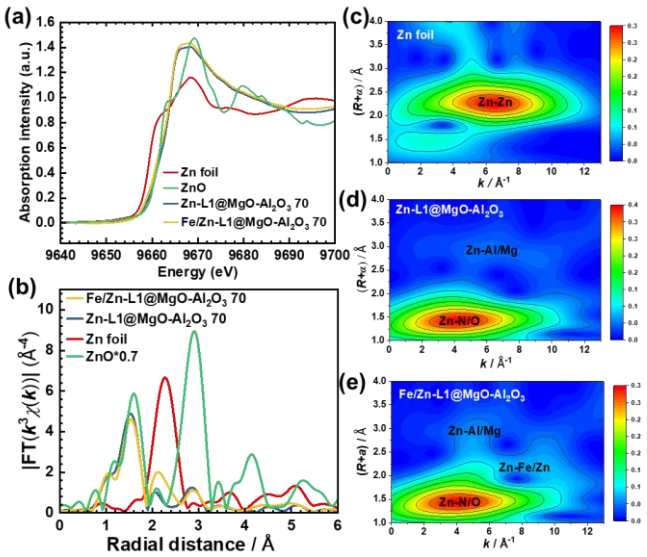

Figure 5. Characterizations of Zn-based materials. (a) Normalized X-ray absorption near-edge fine structure (XANES) spectra at the Zn K-edge of Zn foil, ZnO, Zn-**L1**@MgO-Al_2O_3-70 and Fe/Zn-**L1**@MgO-Al_2O_3-70. (b) Fourier transformation of k3-weighted EXAFS spectra at the K-edge of Zn foil, ZnO (strength is reduced to 0.7 times its original value), Zn-**L1**@MgO-Al_2O_3-70 and Fe/Zn-**L1**@MgO-Al_2O_3-70. (c-e) Wavelet transforms (WT) of Zn foil, Zn-**L1**@MgO-Al_2O_3-70 and Fe/Zn-**L1**@MgO-Al_2O_3-70.

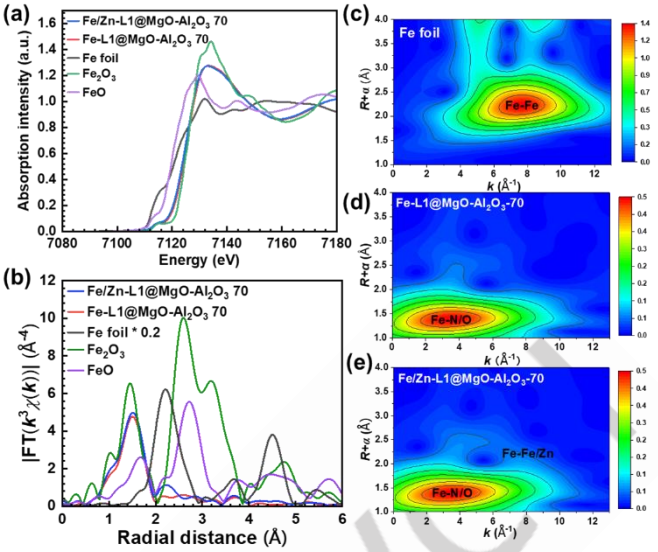

Figure 6. Structural characterizations of Fe-based materials. (a) Normalized X-ray absorption near-edge fine structure (XANES) spectra at the Fe K-edge of Fe foil, Fe_2O_3, FeO, Fe-**L1**@MgO-Al_2O_3-70 and Fe/Zn-**L1**@MgO-Al_2O_3-70. (b) Fourier transformation of k3-weighted EXAFS spectra at the K-edge of Fe foil, Fe_2O_3, FeO, Fe-**L1**@MgO-Al_2O_3-70 and Fe/Zn-**L1**@MgO-Al_2O_3-70. (c-e) Wavelet transforms (WT) of Fe foil, Fe-**L1**@MgO-Al_2O_3-70 and Fe/Zn-**L1**@MgO-Al_2O_3-70.

Similarly, the near-edge Fe feature of Fe-**L1**@MgO-Al_2O_3-70 and Fe/Zn-**L1**@MgO-Al_2O_3-70 are located between the Fe foil and Fe_2O_3 (**Figure 6a**). At the same time, a minor peak at 7114 eV is observed, which is typically attributed to the 1s → 4pz transition and the charge transfer between the ligand and the metal.[26] A representative peak of Fe foil is evident at 2.21 Å, resulting from Fe-Fe interactions within the Fe foil material. Interestingly, Fe/Zn-**L1**@MgO-Al_2O_3-70 exhibits a more pronounced peak at 1.40 Å and a less intense peak at 2.21 Å, indicating that the predominant species in the catalysts are Fe single-atoms (**Figure 6b**). A further wavelet transform (WT) analysis was performed to examine the Fe *K*-edge EXAFS oscillations. As illustrated in **Figures 6c-e**, Fe/Zn-**L1**@MgO-Al_2O_3-70 shows an intensity maximum at (x=3.47 $Å^{-1}$, y=1.38 Å) with considerably smaller wave vector *k* and *R* than Fe foil (x=7.63 $Å^{-1}$, y=2.21 Å), thereby confirming the presence of isolated Fe species in the Fe/Zn catalyst.

Subsequently, least-squares EXAFS fitting was conducted to ascertain the quantitative chemical configuration of Fe/Zn atoms (see **Figures S12-14 and Table S6**). The fitting curves indicate that Zn in Fe/Zn-**L1**@MgO-Al_2O_3-70 is coordinated by three N/O atoms, suggesting that Zn-$(N/O)_3$ is the main species of Zn in Fe/Zn-**L1**@MgO-Al_2O_3-70. The Fourier transformation of the k^3-weighted EXAFS spectra at the *K*-edge of Fe revealed that Fe in Fe/Zn-**L1**@MgO-Al_2O_3-70 is coordinated by six N/O atoms, forming a Fe-$(N/O)_6$ species.

Synthetic Applications and Substrate Scope

To illustrate the general applicability of the optimal iron/zinc-based heterogeneous catalyst (Fe/Zn-**L1**@MgO-Al2O3-70), we investigated the α-alkylation of a range of ketones with diverse alcohols under the optimized reaction conditions. As illustrated in **Scheme 2**, a range of substituted and functionalized alcohols were subjected to reaction with acetophenone, resulting in the formation of the desired products in yields ranging from good to excellent. The substitution on the aryl ring of benzyl alcohols has no discernible impact on the efficiency of the reaction. The use of substrates with both electron-withdrawing and electron-donating substituents resulted in the formation of the corresponding α-alkylated ketones in yields ranging from 60% to 92%. In comparison to the aforementioned reactions of benzylic alcohols, the synthesis of substituted ketones from the corresponding secondary benzylic alcohols, as well as aliphatic ones, is less well-developed.[27] It would appear that the dehydrogenation of the alcohol and the hydrogenation of the α,β-unsaturated ketones are more challenging for such substrates. Nevertheless, the use of such challenging alcohols was also demonstrated, resulting in the corresponding ketones in moderate to good yields through the application of our iron-zinc based catalytic system (**Scheme 2, 1q-1t).**

For any catalyst applicable in advanced chemical synthesis, achieving a high degree of chemo selectivity is of significant importance, yet presents a considerable challenge. To illustrate this point, alcohols containing susceptible functional groups were subjected to testing as substrates. It is encouraging to note that a reactive vinyl group is well tolerated (**Scheme 2, 1u-1v**), which is not the case for most known alkylation catalysts based on precious metals. In addition, our catalyst showed high chemo

selectivity for amino-containing substrates (**Scheme 2, 1w-1x**). It is noteworthy that the N-alkylation of amines with alcohols to yield secondary amines is a well-established reaction. Additionally, alcohols with heterocycles exhibited good reactivity and produced the desired alkylated ketones in 72-75% yield.

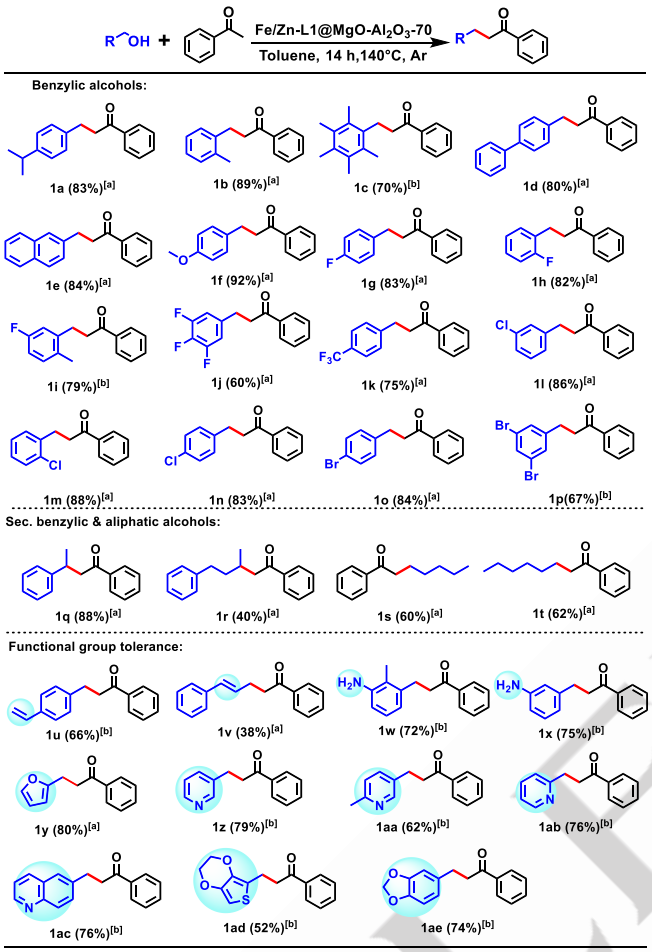

Scheme 2. Fe/Zn-**L1**@MgO-Al_2O_3-70 catalyzed alkylation of acetophenone with diverse alcohols. Reaction conditions: [a] 0.5 mmol acetophenone, 0.55 mmol alcohol, 60 mg catalyst, 1 atm argon, 3 mL toluene 140 ℃,14 h. Isolated yield are mentioned in parentheses. [b] The same as [a] at 145 ℃.

The standard reaction system is also applicable to the coupling reaction of diverse ketones with benzyl alcohol. The reaction proceeded successfully with acetophenones bearing both electron-withdrawing and electron-donating substituents, affording the corresponding ketones in 59-92% yield (**Scheme 3, 2a-2j**). It is noteworthy that aliphatic ketones, which are typically more challenging substrates, also yielded the desired products despite their lower reactivity (**Scheme 3, 2k-2n**). From the perspective of synthetic applications, it is noteworthy that heterocycles are well tolerated, and this system demonstrated excellent chemo selectivity with substrates containing both amino and ketone groups. In conclusion, a variety of ketones and alcohols can be applied in the presence of this material without the need for an external base, and the desired higher ketones were provided in moderate to excellent yield (**Schemes 2** and **3**).

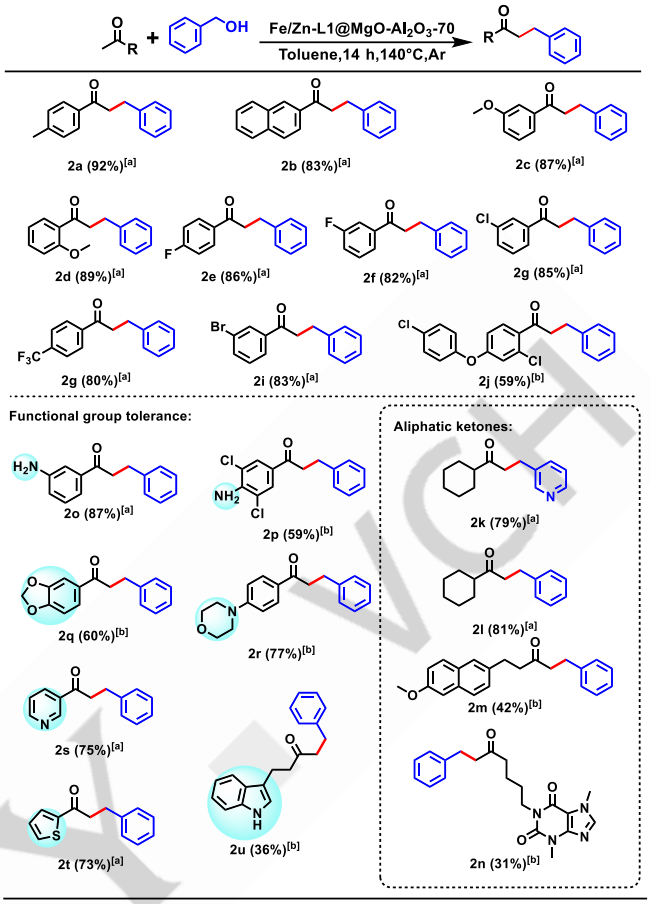

Scheme 3. Fe/Zn-**L1**@ MgO-Al_2O_3-70 catalyzed alkylation of benzyl alcohol with diverse ketones. Reaction conditions: [a] 0.5 mmol ketone, 0.55 mmol alcohol, 60 mg catalyst, 1 atm argon, 3 mL toluene 140 ℃,14 h. Isolated yield are mentioned in parentheses. [b] The same as [a] at 145 ℃.

In the mechanistic investigations of the model reaction, it was observed that the final hydrogenation step was rate-determining at lower temperatures (**Figure S1**). Based on this observation, it should be feasible to develop a selective synthesis of unsaturated ketones through direct C–C bond coupling of ketones with primary alcohols. It is noteworthy that the parent compound, chalcone, serves as the central core of numerous significant biological compounds. Furthermore, chalcones serve as biogenetic precursors for flavonoids and bioflavonoids, which are prevalent in plant-based organisms.[28] Compared to the conventional preparation method involving aldol condensation between ketones and aldehydes, the reaction of ketones and primary alcohols is a promising alternative due to the enhanced accessibility and enhanced stability of the latter substrates. Indeed, the catalyst material (**Figures S1, S15-16**) allows for the straightforward synthesis of different substituted chalcones. As an illustration, benzylic alcohols demonstrated favorable reactivity and yielded the intended α,β-unsaturated ketones in 46-76% yield (**Scheme 4, 3a-3f**). Furfuryl alcohol, which is available from waste biomass such as corncobs or sugar cane bagasse, provided the corresponding chalcone, too (**Scheme 4, 3g**). Interestingly, cinnamyl alcohol can be converted into the sensitive diene ketone **3k** in 32% yield. In a manner similar to the ketone alkylation

protocol, the synthesis of unsaturated ketones tolerates various functional groups and allows for the use of both benzylic and aliphatic alcohols.

The versatility of this iron-zinc catalyst is further highlighted in the synthesis of quinolines by dehydrogenative annulation. In a modified Friedlander synthesis 2-aminobenzyl alcohol and different acetophenones reacted smoothly under the standard conditions, providing the desired products in high yields of up to 92%. Valerophenone, which has a higher steric hindrance, also reacted well with 2-aminobenzyl alcohol, yielding the corresponding product **4l** in 60% yield. As previously observed, the catalyst system exhibited good functional group tolerance (**Scheme 5, 4n-4r**).

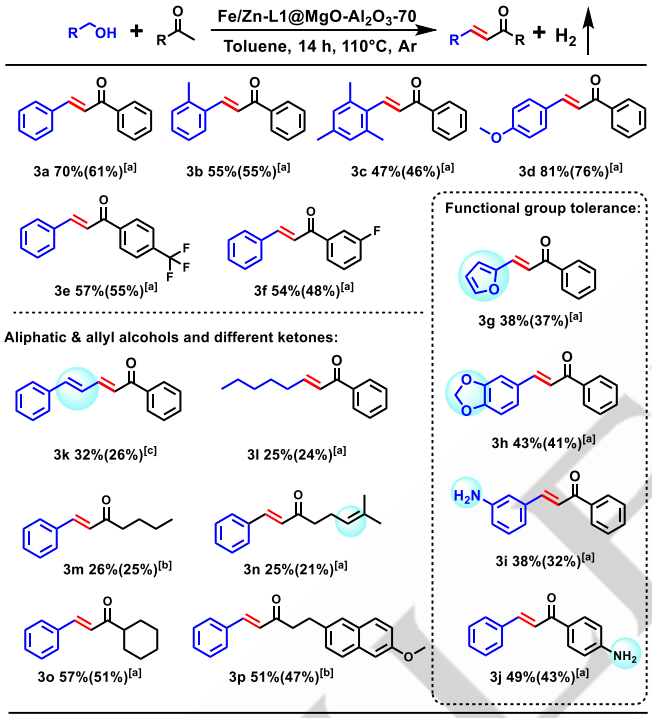

Scheme 4. Fe/Zn-**L1**@ MgO-Al_2O_3-70 catalyzed synthesis of enones from diverse alcohols and ketones. Reaction conditions: [a] 1mmol ketone, 0.5 mmol alcohol, 60 mg catalyst, 1 atm argon, 3 mL toluene 110 ℃,14h. Conversion were determined by GC-MS. Isolated yield are mentioned in parentheses. [b] The same as [a] at 125 ℃. [c] The same as [a], GC yield.

To demonstrate reproducibility and practical utility of this material, we performed the synthesis of dihydrochalcone and 2-phenylquinoline on a gram-scale (**Scheme 6**). The yields obtained for all the tested substrates were comparable to those obtained on a 0.5-mmol scale. Moreover, the alkylation of acetophenone with benzyl alcohol was selected as the model reaction for the recycling experiment (**Figure S17**). Following the second use of the catalyst, the product yield decreased from 94% to 58%. However, no evidence of metal leaching was observed in the reaction solution following each reaction, and the metal loading on the catalyst remained unchanged before and after use. The XPS spectra of Fe 2p, Zn 2p, and N 1s (**Figure S18**) exhibit minimal variation, indicating that the active sites remain stable after multiple uses. X-ray diffraction analysis of the recycled material revealed the absence of Fe and Zn diffraction signals (**Figure S19**). However, a diffraction peak located around 18.2° (attributed to Teflon $(CF_2)_n$) was observed in the XRD patterns of the optimal material before and after the recycling experiment (**Figure S19**). Notably, this diffraction peak (18.2°) disappeared after thermal activation. It is encouraging to note that the regenerated material provided a yield of 90% of the target product, which is similar to that of the fresh material (94%), indicating that this catalyst system is highly durable.

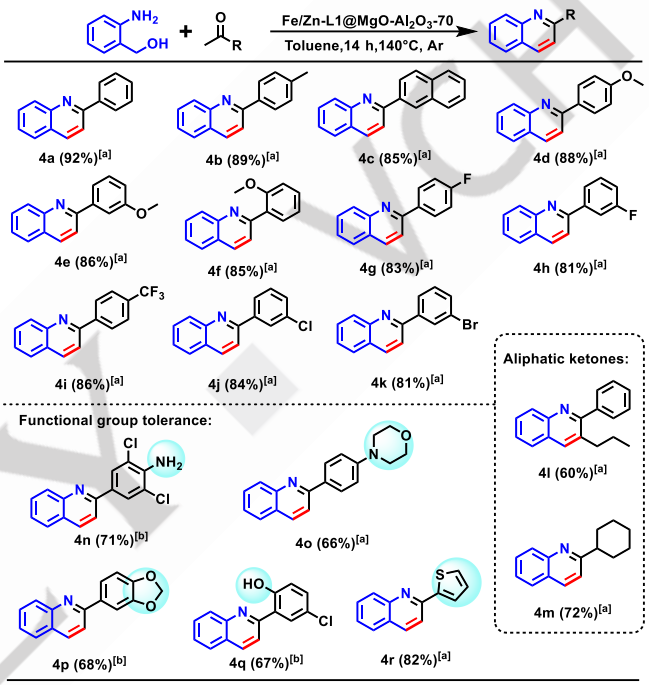

Scheme 5. Fe/Zn-**L1**@MgO-Al_2O_3-70 catalyzed synthesis of quinolines from diverse ketones. Reaction conditions: [a] 0.5 mmol ketone, 0.55 mmol alcohol, 60 mg catalyst, 1 atm argon, 3 mL toluene 140 ℃,14h. Isolated yield are mentioned in parentheses. [b] The same as [a] at 145 ℃.

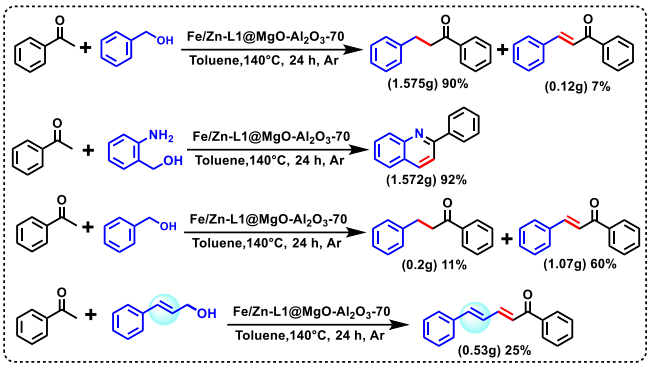

Scheme 6. Upscaling reactions. Reaction conditions: 1g ketones (0.55 mmol alcohols for each 0.5 mmol ketones), Fe/Zn-**L1**@MgO-Al_2O_3-70 catalyst (corresponds to 2 mol% Fe), 110-140 ℃, 1 atm argon, 20 mL Toluene, 24 h,. Isolated yield.

Conclusion

In conclusion, a heterogeneous bimetallic Fe/Zn catalyst has been developed for the waste-free alkylation and alkenylation of ketones. The optimal Fe/Zn-**L1**@MgO-Al_2O_3-70 material enables a range of ketone-alcohol coupling reactions with a diverse substrate scope and the capacity to tolerate sensitive functional groups. It is noteworthy that, in contrast to the majority of known ketone alkylations, the α-alkylation of ketones with alcohols is successfully achieved under base-free conditions. Indeed, this straightforward procedure employs equimolar quantities of substrates and does not necessitate the use of additional reagents or bases. In addition to the synthesis of (unsaturated) ketones, the presented bimetallic catalyst material also enables the preparation of quinoline derivatives. The practical utility is evidenced by gram-scale synthesis and successful recycling. It is our contention that the presented structure-performance relationships illustrate how Fe-based catalytic materials facilitate more efficient, cost-effective, and sustainable organic synthesis.

Supporting Information

The authors have cited additional references within the Supporting Information.

Acknowledgements

We gratefully acknowledge the European Research Council (EU project 670986-NoNaCat), the State of Mecklenburg-Vorpommern for financial and general support, the National Natural Science Foundation of China (22278008), and Beijing Natural Science Foundation (2232001). We thank the analytical team of the Leibniz-Institut für Katalyse e.V. for their excellent service. Rui Ma and Jie Gao thank the China Scholarship Council (CSC) for fellowships.

Keywords: α-Alkylation • α-Vinylation • iron • zinc • waste free• base free

[1] a) A. Messara, A. Panossian, K. Mikami, G. Hanquet, F. R. Leroux, *Angew. Chem. Int. Ed.* **2023**, *62*, e202215899; b) Z. Fan, D. A. Strassfeld, H. S. Park, K. Wu, J. Q. Yu, *Angew. Chem. Int. Ed.* **2023**, *62*, e202303948; c) J. Qiao, R. N. Ci, Q. C. Gan, C. Huang, Z. Liu, H. L. Hu, C. Ye, B. Chen, C. H. Tung, L. Z. Wu, *Angew. Chem. Int. Ed.* **2023**, *62*, e202305679; d) G. M. Kiefl, T. Gulder, *J. Am. Chem. Soc.* **2020**, *142*, 20577-20582; e) S. Guven, G. Kundu, A. Wessels, J. S. Ward, K. Rissanen, F. Schoenebeck, *J. Am. Chem. Soc.* **2021**, *143*, 8375-8380; f) J. Li, C. Y. Huang, C. J. Li, *Angew. Chem. Int. Ed.* **2022**, *61*, e202112770.

[2] a) H. Wu, X. Li, L. Yang, W. Chen, C. Zou, W. Deng, Z. Wang, J. Hu, Y. Li, Y. Huang, *Org. Lett.* **2022**, *24*, 9342-9347; b) A. Kurose, Y. Ishida, G. Hirata, T. Nishikata, *Angew. Chem. Int. Ed.* **2021**, *60*, 10620-10625.

[3] a) D. Yang, H. Wang, C. Liu, C.-R. Chang, *Catal. Sci. Technol.* **2023**, *13*, 3174-3181; b) S. Manojveer, N. K. Garg, Z. Gul, A. Kanwal, Y. Goriya, M. T. Johnson, *ChemistryOpen* **2023**, *12*, e202200245; c) P. Li, G. Xiao, Y. Zhao, H. Su, *ACS Catal.* **2020**, *10*, 3640-3649; d) N. R. Bennedsen, R. L. Mortensen, S. Kramer, S. Kegnæs, *J. Catal.* **2019**, *371*, 153-160; e) B. G. Reed-Berendt, D. E. Latham, M. B. Dambatta, L. C. Morrill, *ACS Cent. Sci.* **2021**, *7*, 570-585.

[4] D. Y. Yang, H. Wang, C. R. Chang, *Adv. Synth. Catal.* **2022**, *364*, 3100-3121.

[5] a) S. Thiyagarajan, R. Vijaya Sankar, C. Gunanathan, *Org. Lett.* **2020**, *22*, 7879-7884; b) S. Yadav, M. Rao Kuram, *Eur. J. Org. Chem.* **2023**, *26*; c) K. Tsuge, S. Kubota, K. Sakamoto, K. Kitayama, T. Nishimura, *Adv. Synth. Catal.* **2023**, *365*, 971-975.

[6] X. B. Lan, Z. Ye, M. Huang, J. Liu, Y. Liu, Z. Ke, *Org. Lett.* **2019**, *21*, 8065-8070.

[7] a) B. W. J. Chen, L. L. Chng, J. Yang, Y. Wei, J. Yang, J. Y. Ying, *ChemCatChem* **2013**, *5*, 277-283; bC. B. Reddy, R. Bharti, S. Kumar, P. Das, *ACS Sustain. Chem. Eng.* **2017**, *5*, 9683-9691.

[8] a) R. Cano, D. J. Ramon, M. Yus, *J. Org. Chem.* **2011**, *76*, 5547-5557; b) C. Chaudhari, K. Sato, Y. Ogura, S. I. Miayahara, K. Nagaoka, *ChemCatChem* **2020**, *12*, 2198-2202.

[9] A. Charvieux, N. Duguet, E. Métay, *Eur. J. Org. Chem.* **2019**, *2019*, 3694-3698.

[10] a) V. G. Chandrashekhar, T. Senthamarai, R. G. Kadam, O. Malina, J. Kašlík, R. Zbořil, M. B. Gawande, R. V. Jagadeesh, M. Beller, *Nat. Catal.* **2021**; b) S. Rana, J. P. Biswas, S. Paul, A. Paik, D. Maiti, *Chem. Soc. Rev.* **2021**, *50*, 243-472; c) X. Tong, Z. P. Yang, C. E. Del Angel Aguilar, G. C. Fu, *Angew. Chem. Int. Ed.* **2023**, *62*, e202306663.

[11] a) B. Wang, C. Cheng, M. Jin, J. He, H. Zhang, W. Ren, J. Li, D. Wang, Y. Li, *Angew. Chem. Int. Ed.* **2022**, *61*, e202207268; b) L. Jiao, H. Yan, Y. Wu, W. Gu, C. Zhu, D. Du, Y. Lin, *Angew. Chem. Int. Ed.* **2020**, *59*, 2565-2576; c) R. Lang, T. Li, D. Matsumura, S. Miao, Y. Ren, Y. T. Cui, Y. Tan, B. Qiao, L. Li, A. Wang, X. Wang, T. Zhang, *Angew. Chem. Int. Ed.* **2016**, *55*, 16054-16058; d) D. T. Genna, A. G. Wong-Foy, A. J. Matzger, M. S. Sanford, *J. Am. Chem. Soc.* **2013**, *135*, 10586-10589.

[12] K. Murugesan, T. Senthamarai, M. Sohail, M. Sharif, N. V. Kalevaru, R. V. Jagadeesh, *Green Chem.* **2018**, *20*, 266-273.

[13] a) J. Gao, L. Feng, R. Ma, B.-J. Su, A. M. Alenad, Y. Liu, M. Beller, R. V. Jagadeesh, *Chem Catalysis.* **2022**; b) K. Murugesan R. V. Jagadeesh A.S. Alshammari, H. Neumann, M. Beller, *Science* **2017**, *358*, 326-332.

[14] J. Gao, R. Ma, L. Feng, Y. Liu, R. Jackstell, R. V. Jagadeesh, M. Beller, *Angew. Chem. Int. Ed.* **2021**, *60*, 18591-18598.

[15] a) T. Senthamarai, V. G. Chandrashekhar, M. B. Gawande, N. V. Kalevaru, R. Zboril, P. C. J. Kamer, R. V. Jagadeesh, M. Beller, *Chem. Sci.* **2020**, *11*, 2973-2981; b) K. Murugesan, M. Beller, R. V. Jagadeesh, *Angew. Chem. Int. Ed.* **2019**, *58*, 5064-5068.

[16] a) G. Zhu, Z.-C. Duan, H. Zhu, D. Ye, D. Wang, *Chin. Chem. Lett.* **2022**, *33*, 266-270; b) E. G. R. de Arruda, B. A. Rocha, M. V. F. Barrionuevo, H. M. Aethalsteinsson, F. E. Galdino, W. Loh, F. A. Lima, C. Abbehausen, *Dalton Trans.* **2019**, *48*, 2900-2916; c) V. Sankar, M. Kathiresan, B. Sivakumar, S. Mannathan, *Adv. Synth. Catal.* **2020**, *362*, 4409-4414.

[17] K. Sun, H. Shan, G. P. Lu, C. Cai, M. Beller, *Angew. Chem. Int. Ed.* **2021**, *60*, 25188-25202.

[18] A. Charvieux, J. B. Giorgi, N. Duguet, E. Métay, *Green Chem.* **2018**, *20*, 4210-4216.

[19] a) Y. L. akano, T.; Hattori, H.; Tanabe, K, *J. Catal.* **1979**, *57*, 1-10; b) B. R.-R. achiller-Baeza, I.; Guerrero-RuizA., *Langmuir* **1998**, *14*, 3556–3564.

[20] a) K. K. Shibata, T.; Kitagawa, J.; Sumiyosh, T.; Tanabe, K., Bull., *Chem. Soc. Jpn.* **1973**, *46*, 2985–2988; b) J. Sun, K. Zhu, F. Gao, C. Wang, J. Liu, C. H. Peden, Y. Wang, *J. Am. Chem. Soc.* **2011**, *133*, 11096-11099.

[21] a) X. Wang, H. Pan, Q. Lin, H. Wu, S. Jia, Y. Shi, *Nanoscale Res. Lett.* **2019**, *14*, 259; b) F. Jaouen, J. Herranz, M. Lefevre, J. P. Dodelet, U. I. Kramm, I. Herrmann, P. Bogdanoff, J. Maruyama, T. Nagaoka, A. Garsuch, J. R. Dahn, T. Olson, S. Pylypenko, P. Atanassov, E. A. Ustinov, *ACS Appl. Mater. Interfaces.* **2009**, *1*, 1623-1639.

[22] T. Yamashita, P. Hayes, *Appl. Surf. Sci.* 2008, 254, 2441-2449.

[23] a) W. Yang, X. Liu, X. Chen, Y. Cao, S. Cui, L. Jiao, C. Wu, C. Chen, D. Fu, I. D. Gates, Z. Gao, H. L. Jiang, *Adv Mater.* **2022**, *34*, e2110123; b) J. Li, S. Chen, N. Yang, M. Deng, S. Ibraheem, J. Deng, J. Li, L. Li, Z. Wei, *Angew. Chem. Int. Ed.* **2019**, 5*8*, 7035-7039; c) L. Han, S. Song, M. Liu, S. Yao, Z. Liang, H. Cheng, Z. Ren, W. Liu, R. Lin, G. Qi, X. Liu, Q. Wu, J. Luo, H. L. Xin, *J. Am. Chem. Soc.* **2020**, *142*, 12563-12567.

[24] S. Li, S. Zhao, X. Lu, M. Ceccato, X. M. Hu, A. Roldan, J. Catalano, M. Liu, T. Skrydstrup, K. Daasbjerg, *Angew. Chem. Int. Ed.* **2021**, *60*, 22826-22832.

[25] H. Fei, J. Dong, M. J. Arellano-Jimenez, G. Ye, N. Dong Kim, E. L. Samuel, Z. Peng, Z. Zhu, F. Qin, J. Bao, M. J. Yacaman, P. M. Ajayan, D. Chen, J. M. Tour, *Nat. Commun.* **2015**, 6, 8668.

[26] K. Sun, H. Shan, H. Neumann, G. P. Lu, M. Beller, *Nat. Commun.* **2022**, *13*, 1848.

[27] X. Q. Li, W. K. Wang, Y. X. Han, C. Zhang, *Adv. Synth. Catal.* **2010**, *352*, 2588-2598.

[28] A. Rammohan, J. S. Reddy, G. Sravya, C. N. Rao, G. V. Zyryanov, *Environ Chem. Lett.* **2020**, *18*, 433-458.

[29] a) R. M. Borade, S. B. Somvanshi, S. B. Kale, R. P. Pawar, K. M. Jadhav, *Mater. Res. Express.* **2020**, *7*; b) D.-G. Crivoi, A. M. Segarra, F. Medina, *J. Catal.* **2016**, *334*, 120-128.

Entry for the Table of Contents

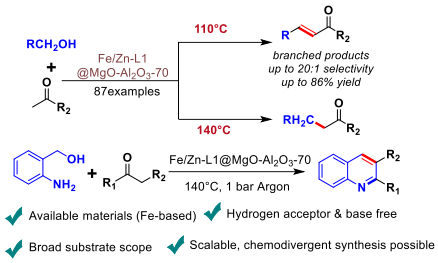

The general and benign α-alkylation and -vinylation of ketones with alcohols proceed in the presence of a heterogeneous Fe/Zn-**L1**@MgO-Al_2O_3-70 catalyst. The synthesis of a variety of ketones (>52 products), substituted chalcones (17 products) and quinoline derivatives (>18 products) is achieved using this material, with a broad substrate scope and good functional group tolerance..

Institute and/or researcher Twitter usernames: @likat_rostock

Chem Catalysis

CellPress

Article

Cobalt single-atom catalysts for domino reductive amination and amidation of levulinic acid and related molecules to N-heterocycles

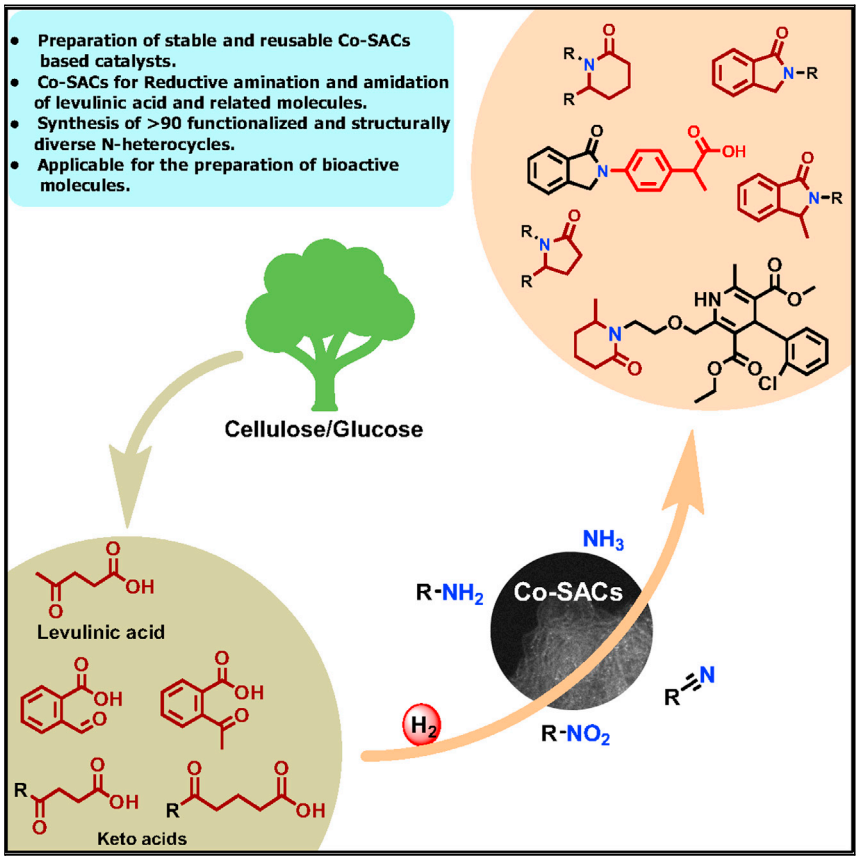

The effective conversion of renewable resources, especially biomass-based feedstocks, to produce chemicals, fuels, and energy is of central importance. To valorize these feedstocks, the development of suitable catalysts, especially single-atom catalysts (SACs), which bridge traditional homogeneous and heterogeneous catalysis, is highly desired. In this respect, we developed Co-based SACs, which allow for the domino reductive amination and amidation of levulinic acid and related molecules to produce functionalized and structurally diverse N-heterocycles including bioactive molecules.

Jie Gao, Lu Feng, Rui Ma, ..., Yuefeng Liu, Matthias Beller, Rajenahally V. Jagadeesh

yuefeng.liu@dicp.ac.cn (Y.L.)
matthias.beller@catalysis.de (M.B.)
jagadeesh.rajenahally@catalysis.de (R.V.J.)

Highlights

Preparation of stable and reusable Co-SACs catalysts

Reductive amination and amidation of levulinic acid and related molecules

Synthesis of >90 functionalized and structurally diverse N-heterocycles

Applicable for the preparation of bioactive molecules

Gao et al., Chem Catalysis *2*, 178–194
January 20, 2022
https://doi.org/10.1016/j.checat.2021.12.009

CellPress

Chem Catalysis

Article

Cobalt single-atom catalysts for domino reductive amination and amidation of levulinic acid and related molecules to N-heterocycles

Jie Gao,[1,5] Lu Feng,[2,5] Rui Ma,[1,5] Bing-Jian Su,[3] Asma M. Alenad,[4] Yuefeng Liu,[2,*] Matthias Beller,[1,6,*] and Rajenahally V. Jagadeesh[1,*]

SUMMARY

The development of single-atom-based catalysts (SACs), which bridge the traditional areas of homogeneous and heterogeneous catalysis, continues to be important for achieving organic synthesis in a more efficient and practical manner. Here, we report reusable cobalt-based SACs for the selective and general reductive amination of levulinic acid and related keto acids, which is of interest in the context of valorization of biomass. The optimal Co-SAC-based catalyst is prepared by pyrolysis (800°C) of cobalt-phenanthroline complexe on carbon and subsequent acid treatment. The resulting Co-SACs showed amazing activity compared with the corresponding Co-nanoparticles and displayed an excellent substrate scope for various reductive domino transformations including reactions of levulinic acid with nitro compounds and nitriles to produce various N-substituted pyrrolidones in good to excellent yields. Further, the synthesis of diverse isoindolinones from aromatic ketoacids and amines/nitro compounds was performed with the optimal catalyst system.

INTRODUCTION

The development of active and selective, but at the same time stable and recyclable catalysts is of central importance for the advancement of more sustainable and cost-effective chemical processes.[1–3] In this respect, catalytic materials with highly distributed metal atoms dispersed on solid supports emerged in the last decade.[4–8] These so-called single-atom-based catalysts (SACs) are considered to bridge both homogeneous and heterogeneous catalysis.[2] Advantageously, SACs minimize the use of metal resources and improve atom-utilization efficiency. The unique electronic structure of single metal centers on the surface and labile coordination environments of the active centers in SACs have been proven to exhibit unique catalytic performance compared with their nanoparticle or nanocluster counterparts.[4–8] In contrast to most molecularly defined homogeneous metal complexes, SACs can be more stable and allow for convenient recyclability.[5–7] For the preparation of SACs, in particular 3d metals are preferred owing to their abundance, low cost, and often low toxicity compared with their noble metal congeners.

Based on their specific properties and advantages, SACs continue to attract significant interest as catalytic materials to perform organic synthesis in a more general, efficient, and practical manner.[9] In addition, the development and applicability of such materials for the effective conversion of renewable resources, especially biomass-based feedstocks, to produce chemicals, fuels, and energy are of actual

The bigger picture

The effective catalytic conversion of biomass-based feedstocks to produce bulk and fine chemicals is a major goal of current chemical research. In this respect, specifically reductive aminations and amidations are interesting, too. To improve the sustainability of such processes, inexpensive, earth-abundant base metals should be employed as catalysts to replace precious metals that currently dominate in this field. Here, we show that cobalt catalysts with isolated metal sites (SACs) enable efficient domino reductive amination and amidation of levulinic acid and related molecules to give a wide array of N-heterocycles. We anticipate that these Co-catalytic systems will create more opportunities for the conversion of biomass-based feedstocks to many value-added compounds.

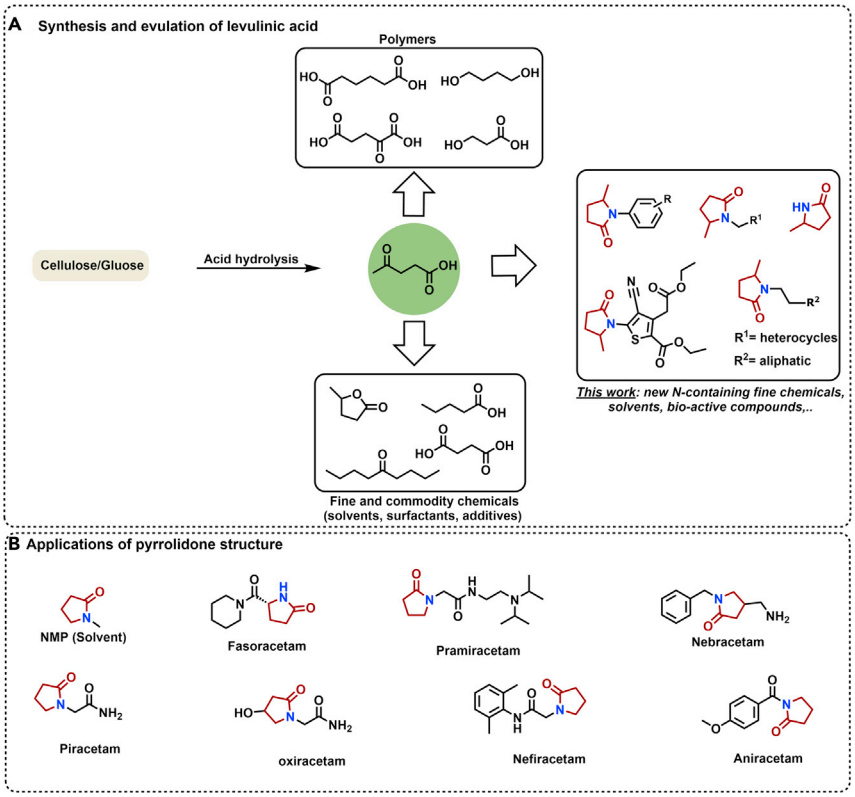

Figure 1. Synthesis and applications of levulinic acid

importance.[10–14] In this context, a variety of different renewable platform chemicals are of interest for both academic and industrial research.[15–18] Among them, levulinic acid (LA) can be simply prepared by acid catalysis from cellulose. Hence, in the past decade it was considered to become one of the top chemical building blocks from biomass.[12] Indeed, LA can be used as a key precursor and intermediate for the synthesis of many value-added chemicals and fuels applying straightforward hydrogenation or oxidation reactions (Figure 1A).

In this respect, reductive amination and subsequent intramolecular amidation of LA represent a straightforward and effective process to produce pyrrolidinones, which represent an important class of five-membered heterocycles finding applications as surfactants, and chelating agents as well as precursors and intermediates for pharmaceuticals and agrochemicals.[18–20] Moreover, the pyrrolidinone structure also could be used to synthesize solvents (N-methyl-2-pyrrolidone [NMP]) as well as drugs (Figure 1B).

Currently, pyrrolidones are mainly produced by the reaction of γ-butyrolactone and amines or the dehydrogenation-amination of 1,4-butanediol with amines under harsh reaction conditions (>200°C).[12] Compared with these existing industrial processes, the synthesis of pyrrolidones starting from LA and amines by a catalytic domino reductive amination-amidation sequence using molecular hydrogen is an attractive and more sustainable approach.[19–24] In general, this transformation involves 3 steps: (1) condensation of the ketone group of LA and amine to form the imine, (2) catalytic hydrogenation of the imine to the corresponding amine, and (3) intramolecular amidation to give C-methyl-and N-substituted pyrrolidones.[19–24] Obviously, performing such cascade reactions in a one-pot manner is more

[1]Leibniz-Institut für Katalyse e.V., 18059 Rostock, Germany

[2]Dalian Institute of Chemical Physics, Chinese Academy of Science, 116023 Dalian, China

[3]Department of Electrophysics, National Chiao Tung University, Hsinchu 30076, Taiwan

[4]Chemistry Department, College of Science, Jouf University, Sakaka, Saudi Arabia

[5]These authors contributed equally

[6]Lead contact

*Correspondence: yuefeng.liu@dicp.ac.cn (Y.L.), matthias.beller@catalysis.de (M.B.), jagadeesh.rajenahally@catalysis.de (R.V.J.)

https://doi.org/10.1016/j.checat.2021.12.009

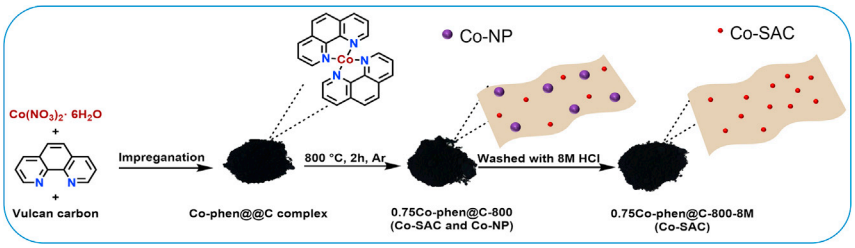

Figure 2. Preparation and pictorial representation of N-doped carbon supported Co-SACs

advantageous because it avoids the separation and purification of intermediates. In the past, mainly precious metal-based nano catalysts such as Pt/P-TiO_2[19] Pt-MoO_X/TiO_2[21], Ir/PVP[22], and Pd/ZrO_2[23] were developed for the preparation of pyrrolidones from LA and amines. Considering the specific properties of SACs, we thought that 3d non-noble-metal-based SACs should work under milder conditions and allow for a general protocol to produce a variety of functionalized pyrrolidines efficiently.

Here, we report the synthesis of atomically dispersed Co-SACs, which enables an efficient domino reductive amination-amidation sequence of LA and other keto acids in a most comprehensive way. Apart from amines, nitroarenes can be also employed in this process, thus avoiding an additional hydrogenation step to make anilines. In addition, the presented catalyst system allows for a methodology to give pyrrolidinones by the reaction of LA and nitriles. In general, using nitroarenes or nitriles instead of anilines or benzylic/aliphatic amines can be advantageous with respect to step economy and saving time and resources.

RESULTS AND DISCUSSION

Preparation of cobalt-based SACs and catalytic activities

In the last decade, we prepared a variety of nanoparticle catalysts (NPCs), especially based on 3d metals for organic synthesis. Specifically, Fe-, Co-, and Ni-based materials showed good to excellent performance in hydrogenation, amination, and oxidation reactions involving diverse functionalized molecules.[25–31] In general, the specific supported NPs were synthesized by immobilization and subsequent pyrolysis of metal complexes or metal organic frameworks on inorganic supports. It is noteworthy that a plethora of inexpensive nitrogen and oxygen ligands are commercially available to prepare metal complexes or metal organic frameworks (MOFs), which serve as potential precursors to create NPs or SACs.[32] Based on our[25–29] and others' precious work,[33–36] we became interested in the reductive amination of LA and related reactions in the presence of SACs.

We started our investigations to prepare cobalt-based SACs using $Co(NO_3)_2{\cdot}6H_2O$ as metal precursor, 1,10-phenanthroline (Phen) as ligand, and Vulcan XC 72R as carbon support. Similar to previous works,[28] we immobilized and pyrolyzed *in situ* generated cobalt-phenanthroline complex (wt% of Co = 3%–0.75%; Co: Phen = 1:2 molar ratio) on Vulcan XC 72R at 800°C for 2 h under argon with a heating rate of 5°C/min. Depending on the wt% of cobalt, these pyrolyzed materials contained cobalt NPs or a mixture of NPs and single atoms *vide infra*. For example, a material with 3 wt% of Co contained predominately NPs, whereas the one with 0.75 wt% of cobalt contains a mixture of NPs and single atoms. Upon washing the latter material with 8M HCl, NPs could be completely removed, and we obtained highly dispersed Co single atoms supported on carbon (Figure 2). In addition, related materials were prepared for comparison by pyrolysis of cobalt nitrate on Vulcan XC 72R. In the

Entry	Catalyst	Cobalt loading[c] (wt%)	Conversion (%)	Yield (%)		
				3	4	5
1[a]	3Co@C-800	2.91	3	<1	0	3
2[a]	1.5Co@C-800	1.44	5	<1	0	5
3[a]	0.75Co@C-800	0.74	9	<1	0	9
4[a]	3Co-phen@C-800	2.93	38	36	0	2
5[a]	1.5Co-phen@C-800	1.52	69	65	0	3
6[a]	0.75Co-phen@C-800	0.74	90	89	0	<1
7[a]	0.75Co-phen@C-400	0.73	11	6	0	2
8[a]	0.75Co-phen@C-600	0.75	58	55	0	2
9[a]	0.75Co-phen@C-1000	0.75	83	77	0	4
10[a]	0.75Co-phen@C-800-HCl (washed with 8M HCl)	0.47	98	97	0	<1
11[a]	0.1Co-phen@C-800	0.08	98	97	0	<1
12[b]	$Co(NO_3)_2$		<1	<1	0	<1
13[b]	$Co(NO_3)_2$ - Phen		<1	<1	0	<1

Figure 3. Screening of different catalysts for LA reductive amination.

Reaction conditions: [a]Heterogeneous catalysis condition: 0.5 mmol LA, 0.5 mmol 2-furanmethanamine, weight of catalyst corresponds to 0.64 mol% Co, 20 bar H_2, 2 mL i-ProH, 90 ℃, 24 h.

[b]Homogeneous catalysis condition: Same as 'a' with 0.64% mol Co-metal salt. Conversions and yields were based on substrate **2** and determined by GC using n-hexadecane as standard.

[c]Cobalt loading was determined by ICP analysis.

following sections, all cobalt materials are represented as xCo-phen@C-y-z, where x, y, and z denote the wt% of cobalt, pyrolysis temperature, and HCl.

To evaluate the catalytic activities, all prepared cobalt materials were tested for the reductive amination of LA **1** with furfuryl amine **2** to synthesize 1-(2-furanylmethyl)-5-methyl-2-pyrrolidinone **3** in the presence of molecular hydrogen as the benchmark reaction (Figure 3). Furfuryl amine **2** was chosen as a coupling partner because it is used for the synthesis of some drugs and can be prepared easily from furfural, another sugar-derived platform chemical. First, we tested Co-based materials prepared by the pyrolysis of cobalt-nitrate (3Co@C-800, 1.5Co@C-800, and 0.75Co@C-800) and observed no activity toward the desired product **3** (Figure 3, entries 1–3). Instead, the formation of small amounts (3%–9%) of γ-valerolactone **5** (GVL) was observed. Interestingly, catalysts prepared by the pyrolysis of Co-phenanthroline complex on carbon (3Co-phen@C-800, 1.5Co-phen@C-800, and 0.75Co-phen@C-800) exhibited significantly improved activities and gave desired product **3** at 38%–90% yield (Figure 3, entries 4–6).

Upon decreasing the cobalt loading from 3 to 0.75 wt%, the catalytic activities of the resulting materials increased (Figure 3, entries 4–6) and 0.75Co-phen@C-800 exhibited improved activity with 90% of conversion and 89% yield of desired product **3** (Figure 3, entry 6). To know the effect of the pyrolysis temperature on the formation of active materials, 0.75Co-phen@C was pyrolyzed at different temperatures (400°C, 600°C, and 1,000°C). In addition, the one pyrolyzed at 1,000°C

(0.75Co-phen@C-1000) also showed good activity and gave 77% yield of **3** (Figure 3, entry 9). However, the samples pyrolyzed at lower temperature (400°C and 600°C) showed no or poor activity (Figure 3, entries 7 and 8). Among these, the material pyrolyzed at 800°C was found to be the best (Figure 3, entry 6). Further washing of this material with HCl solution (8M) to leach out loosely bound NPs resulted in higher activity and gave 98% of desired product **3** in the benchmark reaction (Figure 3, entry 10). The catalytic performance of other HCl-washed catalysts is listed in Table S1. As expected, upon washing, the cobalt content of the materials decreased from 0.76 wt % (0.75Co$(NO_3)_2$@C-800) to 0.47 wt % (0.75Co$(NO_3)_2$@C-800-HCl), which indicates that larger particles were removed from the support whereas the active sites were retained in the material. Consequently, we prepared the 0.1Co-phen@C-800 catalyst and tested its performance using the model reaction. Indeed, this catalyst exhibited performance similar to 0.75Co-phen@C-800-HCl (Figure 3). The X-ray diffraction (XRD), X-ray photoelectron spectroscopy (XPS), and aberration corrected high-angle annular dark-field scanning TEM (HAADF-STEM) analysis of this sample is listed in Figures S4 and S8, respectively. Similarly, the cobalt species were highly dispersed on the catalyst surface. Unpyrolyzed materials and homogeneous complexes were completely inactive (Figure 3, entries 12 and 13).

To understand the optimal activity of the 0.75Co-phen@C-800-HCl catalyst, we compared this material with 0.75Co@C-800 and performed several control experiments (Table S2). In principle, the reactivity difference of the two materials might result from either the reductive amination or amidation step. Interestingly, 0.75Co-phen@C-800-HCl promotes both of these reactions, whereas 0.75Co@C-800 gave only 9% yield of the reductive amination step and less than 1% of the secondary amide (Table S2). Based on previous literature studies[20,21] and these results, we propose first a condensation of the amine and the keto group of LA to generate imine (A). Then, this imine is hydrogenated in the presence of the catalyst to provide the secondary amine (B). Finally, intramolecular amidation takes place to give pyrrolidone (C) (Figure S1). We assume the Co-N interactions of the SAC (0.75Co-phen@C-800-HCl) is mainly responsible for the observed higher activity. Notably, 0.75Co-phen@C-800-HCl gave 36% secondary amine yield and 14% secondary amide yield, indicating that the amidation process (C) is the rate-limiting step.

Characterization of Co-based catalysts

To know the structural features and the reasons for the different catalytic performance, the cobalt materials were characterized by state-of-the-art analytic techniques, such as XRD, HAADF-STEM, XPS, and X-ray absorption spectroscopy (XAS).

The XRD patterns of sample 3Co-phen@C-800 (2.92 wt% by inductively coupled plasma [ICP]) with high cobalt loading showed the presence of mainly metallic Co NPs (diffraction peaks at 36.5°C, 44.3°C, and 51.2°C) (Figure S2). In contrast, the low Co loading samples, such as 0.75Co-phen@C-800 (0.74 wt% from ICP) and 0.75Co-phen@C-800-HCl (0.48 wt% from ICP), did not display the presence of Co diffraction peaks (Figure S4). Atomic resolution HAADF-STEM images of 0.75Co-phen@C-800 confirmed a mixture of highly dispersed cobalt atoms and cobalt NPs (Figure S3). Notably, the material 0.75Co-phen@C-800-HCl, after acid treatment, contained only highly dispersed cobalt species on N-doped carbon (Figure 4).

Next, XPS analysis was conducted for 3Co-phen@C-800, 0.75Co-phen@C-800, and 0.75Co-phen@C-800-HCl, to know the states of cobalt and nitrogen species (Figures S2, S3, 4). The binding energies for the Co2p peak are centered at 779.8, 781.0, 783.9, and 788.3 eV for all three materials. The corresponding satellites of these

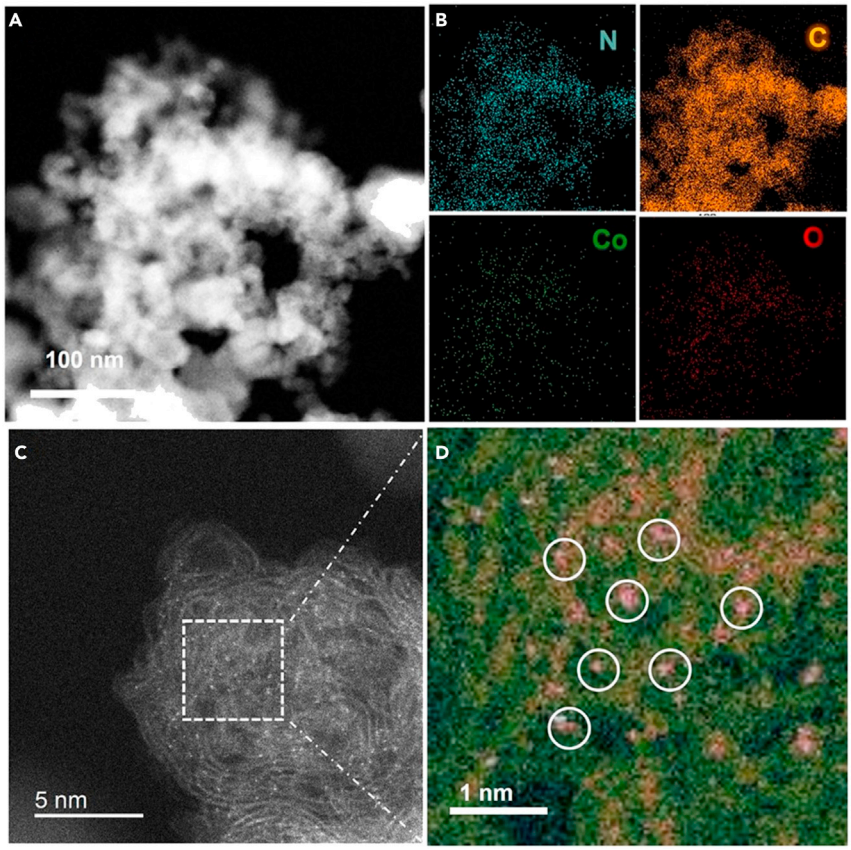

Figure 4. Electron microscope analysis of 0.75Co-phen@C-800-HCl catalyst
(A and B) HAADF-STEM image (A), and the corresponding EDS elemental mapping (B).
(C) Atomic-resolution HAADF-STEM image and the magnified HAADF-STEM image reveals highly dispersed Co atoms (circles in D) on N-doped carbon.

peaks are also observed at 794.9, 796.2, 798.8, and 803.7 eV (Figures S2, S3, and 4). From the N1s spectra, we can see the presence of pyridinic (398.3 eV) and pyrrolic (399.6 eV) N in all three catalysts. In addition, graphitic N and pyrrolic N-oxide species are observed at 400.9 and 403.6 eV in 0.75Co-phen@C-800-HCl. The percent ratio of pyridinic N, pyrrolic N, graphitic N, and pyrrolic N-oxide in 0.75Co-phen@C-800-HCl is 37:22:20:20 (Table S3). The XAS measurements at the Co K-edge were performed to confirm the chemical state and coordination number of the metal. The 3Co-phen@C-800 exhibited similar near-edge adsorption energy to Co_3O_4, indicating the presence of divalent cobalt ions. A well-resolved peak at 7,709 eV can be observed in the pre-edge region of 0.75Co-phen@C-800-HCl, which is ascribed to the electronic transition from the Co core 1s to the unoccupied 3d orbitals.[37] More detailed local coordination information about Co atoms was obtained from the Fourier transform of k2-weighted extended X-ray absorption fine structure (EXAFS) curves at the K-edge in Figure 5D. The 3Co-phen@C-800 showed a peak (2.19 Å) almost completely overlapped with Co foil, demonstrating Co–Co bonds are dominant in this material. Although the 0.75Co-phen@C-800 catalyst has a lower cobalt loading than 3Co-phen@C-800, it still exhibited a peak around 2.19 Å, which proves the existence of Co–Co bonds. After washing with 8M hydrochloric acid, no signal for Co–Co interactions could be observed, which indicates the presence of isolated Co species (e.g. single cobalt atoms in 0.75Co-phen@C-800-HCl). The latter catalyst also displayed a strong peak at 1.41 Å, which is explained

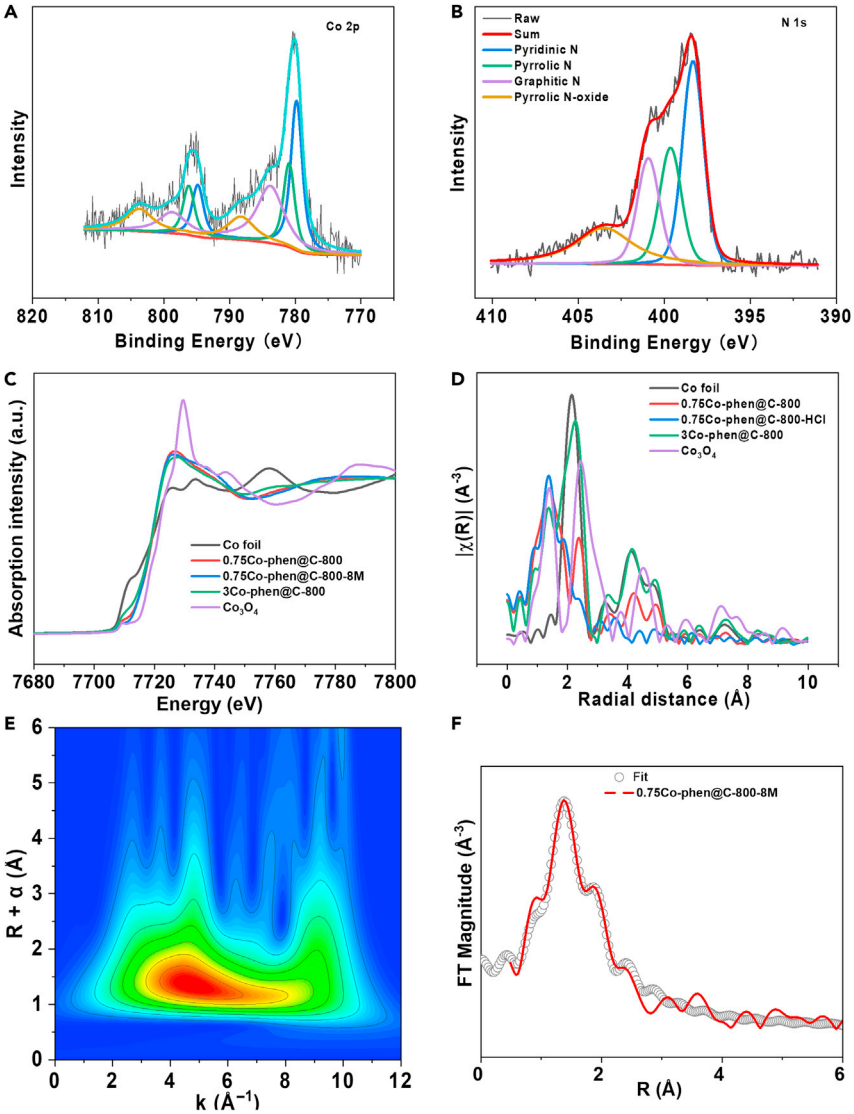

Figure 5. Structure characterization of N-doped carbon supported Co-SACs

(A and B) High-resolution Co 2p and N 1s XPS spectra of 0.75Co-phen@C-800-HCl.

(C) Normalized X-ray absorption near-edge fine structure (XANES) spectra at the Co K-edge of Co foil, Co_3O_4, 0.75Co-phen@C-800, 0.75Co-phen@C-800-HCl, and 3Co-phen@C-800.

(D) Fourier transformation of k2-weighted EXAFS spectra at the K-edge of Co sample, Co foil, and Co_3O_4 samples.

(E) Wavelet transform (WT) of 0.75Co-phen@C-800-HCl.

(F) Fitting results of 0.75Co-phen@C-800-HCl.

by Co–N or Co–O coordination.[37] Only one intensity maximum at around 4.0 $Å^{-1}$ is detected in the Co-SACs, indicating that cobalt species exist as highly dispersed single cobalt atoms in the 0.75Co-phen@C-800-HCl sample (Figure 5E).[7] According to the EXAFS fitting results (Figure 5; Table S3), there is a strong peak at 1.41 Å with a coordination number of six, suggesting that one Co atom is anchored with six other atoms. Our optimal Co-SAC catalyst shows a similar XANES structure coordination number with the reported results, so we assume the coordination structure of our Co-SACs is like CoN_4C_8-1-2O2, which is one example in this literature.[6] Then, we attempted to explore the effect of the pyrolysis temperature on the catalytic

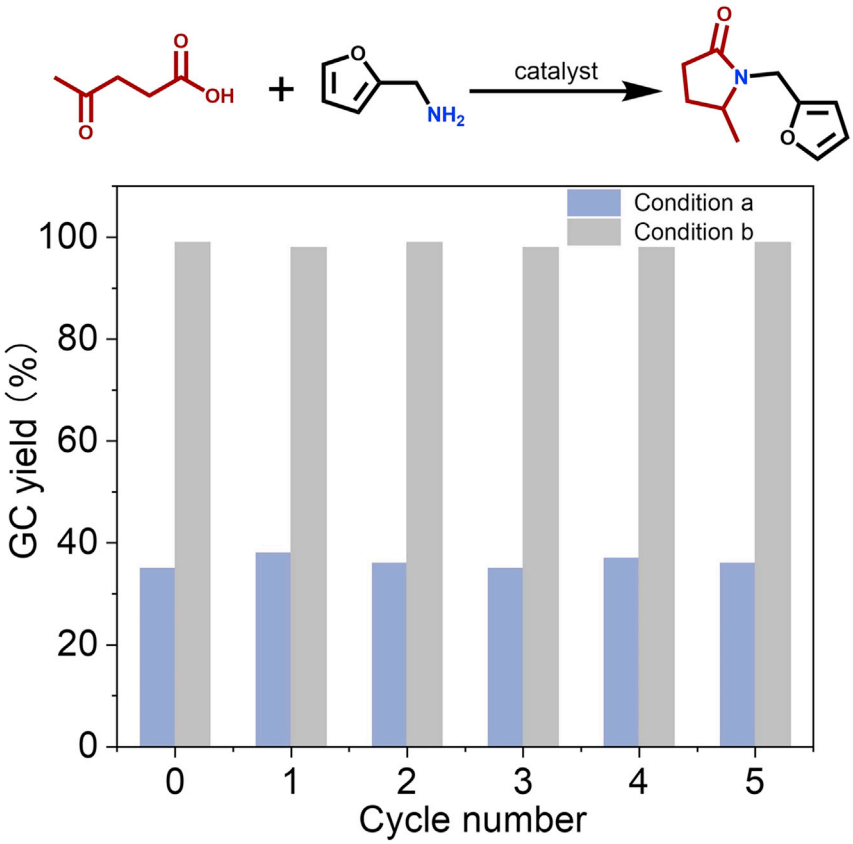

Figure 6. Stability and recycling of 0.75Co-phen@C-800-HCl catalyst for the synthesis of 1-(2-furanylmethyl)-5-methyl-2-pyrrolidinone

(A and B) Reaction conditions: (A) 0.5 mmol LA, 0.5 mmol furfuryl amine, 25 mg catalyst, 90°C, 20 bar H_2, 12 h, 2 mL i-PrOH. GC yield based on amine; (B) 0.5 mmol LA, 0.5 mmol furfuryl amine, 40 mg catalyst, 90°C, 20 bar H_2, 24 h.

performance by using XPS and XRD. A strong diffraction peak of metallic cobalt wass observed for the material 0.75Co-phen@C-1000, indicating the formation of larger cobalt NPs in this sample (Figure S4). In contrast, 0.75Co-phen@C-400, 0.75Co-phen@C-600, and 0.75Co-phen@C-800 showed no diffraction peak of cobalt, which suggests highly dispersed cobalt species in these three samples (Figure S4). The aggregation of cobalt atoms to NPs in the sample pyrolyzed at 1,000°C resulted in fewer active catalytic sites; consequently, its catalytic performance was worse compared with 0.75Co-phen@C-800 (Figure 3). Regarding N doping, in all four samples (0.75Co-phen@C-400, 0.75Co-phen@C-600, 0.75Co-phen@C-800, and 0.75Co-phen@C-1000), pyridinic N species were dominant aside from pyrrolic N, graphitic N, and pyrrolic N^+-O^-, even if the pyrolysis temperature was different. Nevertheless, the relative amount of these four types of nitrogen species varied according to the pyrolysis temperature (Table S3), which also led to different Co-N interactions in these samples.[5,6,8] Hence, diverse peaks were observed in the Co 2p spectra. However, a determination of the Co oxidation state by XPS was difficult because Co–O and Co–N bonds have similar binding energy.[5] In accordance with previously reported results, we assume the presence of Co^{2+} and Co^{3+} but also Co^{2+}-N_x species.[4–6] From these analyses, we conclude that both Co–N interaction and the aggregation of cobalt metal are strongly influenced by the pyrolysis temperature.

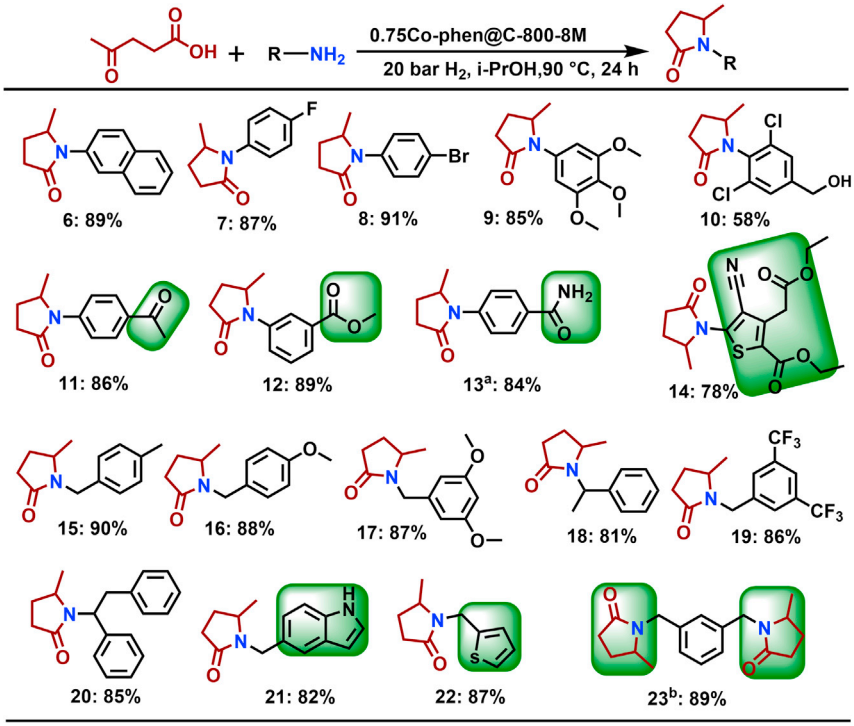

Figure 7. Reductive amination of LA with aromatic and benzylic amines using 0.75Co-phen@C-800-HCl

Reaction conditions: 0.5 mmol LA, 0.5 mmol amine, 40 mg catalyst (0.64 mmol% cobalt), 20 bar H_2, 90°C, 24 h, 2 mL, i-ProH. Isolated yields based on amine.

[a]GC yield based on amine.

[b]With 1 mmol LA, 05 mmol diamine, 110°C, 24 h.

Stability, recycling, and reusability of 0.75Co-phen@C-800-HCl catalyst

After investigating the structure and activity of 0.75Co-phen@C-800-HCl, we examined its stability, recycling, and reusability in the model reaction at two different conditions. As shown in Figure 6, this material can be easily reused up to 5 times without a significant loss of activity or selectivity. ICP analysis of the recycled catalyst and the reaction mixture confirmed that there was no leaching of cobalt species (detection limit: 0.02 wt%). Accordingly, XPS, XRD, and HAADF-STEM analyses of the recycled catalyst were performed to check whether the structure was significantly changed after the additional reactions (Figures S4 and S7). However, no significant alterations from the Co 2p and N 1s XPS spectra could be observed (Figure S7). As shown in Figure S4, the recycled catalyst showed no cobalt diffraction peak in XRD spectra, indicating that cobalt active sites were also highly dispersed in this catalyst. To clarify this assumption, we conducted an HAADF-STEM analysis, which indicated no significant aggregation of cobalt sites (Figure S7).

Synthesis of pyrrolidones from LA and amines

The stable and most active catalyst system, 75Co-phen@C-800-HCl, was used for the preparation of different pyrrolidones to prove its general applicability. Under comparably mild conditions (90°C, 20 bar H2), LA underwent reductive amination with structurally diverse amines as well as ammonia to produce corresponding substituted pyrrolidones in good to excellent yields. As shown in Figure 7, anilines containing both electron-donating and withdrawing groups were successfully reacted and afforded the desired products in general in yields >75%. It is of central importance for advanced organic

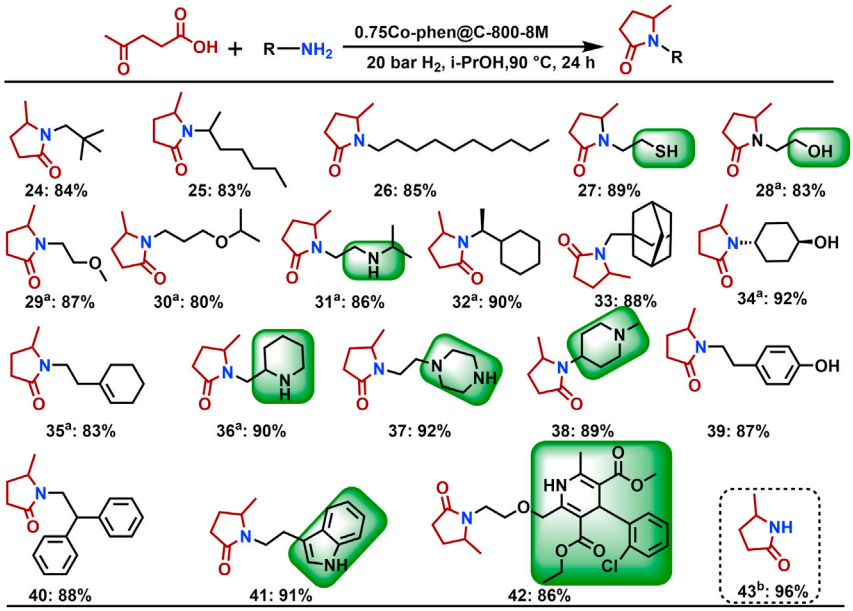

Figure 8. 0.75Co-phen@C-800-HCl catalyzed reductive amination of LA with various aliphatic amines

Reaction conditions: 0.5 mmol LA, 0.5 mmol amine, 40 mg catalyst (0.64 mmol% cobalt), 20 bar H_2, 2-mL i-PrOH, 90°C, 24 h, isolated yield based on amine.

[a]GC yield based on amine.

[b]5 bar NH_3, 20 bar H_2, 2-mL i-PrOH, 90°C, 24 h, GC yield based on LA.

synthesis to achieve chemoselectivity in multifunctional molecules. This is showcased by the selective reductive amination of anilines containing halides, ketone, amide, ester, and nitrile groups (Figure 7, products 11–14). As an example, halogenated amines were converted to their corresponding pyrrolidones without dehalogenation (Figure 7, products 6–8). Apart from (hetero)aromatic amines, LA was also aminated with benzylic amines and provided corresponding products in up to 90% (Figure 7, products 15–23). The reactions of S-containing heterocycles, which are known as catalyst poisons, are notable (Figure 7, product 22). Interestingly, di-pyrrolidones (Figure 7, product 23) from LA and 1,3-phenylenedimethanamine can be also synthesized in excellent yield (89%) using our SAC. At this point, it should be mentioned that in none of the examples was hydrogenation of the (hetero)arene, which is typical for noble-metal-based NPs, observed.

Afterward, aliphatic amines with either a linear or cyclic structure were employed under standard conditions and offered the desired pyrrolidones in high yields (Figure 8). The functional group tolerance of the catalyst was demonstrated by reaction with 2-aminoethyl thiol, which gave the corresponding pyrrolidone in 89% yield (Figure 8, product 27). This also indicates the strong resistance of the catalyst material against sulfur poisoning. Similarly, aliphatic amines containing hydroxyl, C–C double bond and ester groups smoothly reacted with LA and gave 80%–92% yield of the desired products (Figure 8, products 28–30, 34–35, 39, and 42). Substrates containing both primary and secondary amine moieties (Figure 8, products 31, 36, and 37) reacted with LA selectively at the primary amino group without touching the secondary amine, indicating that such Co-SACs catalysts can be used for the selective amination of primary amines in the presence of secondary amines. As another example, tryptamine selectively reacted with LA and furnished 1-(2-(1H-indol-3-yl)ethyl)-5-methylpyrrolidin-2-one in 91% yield (Figure 8, product 41). To highlight the applications of this catalyst in medicinal

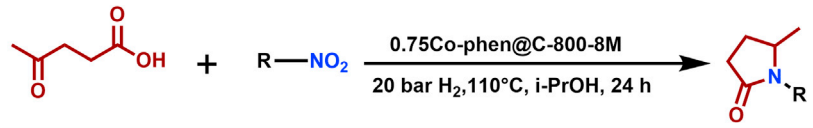

Entry	Nitro	Product	Yield (%)
1			44: 97%[a]
2	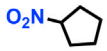	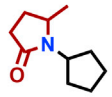	45: 85%
3	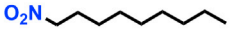	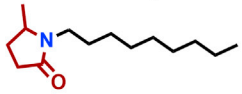	46: 87%
4		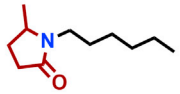	47: 56%[a,b]
5		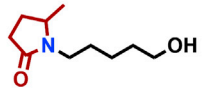	48: 85%
6	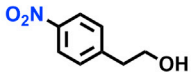	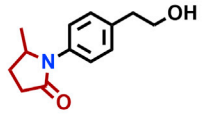	49: 84%
7	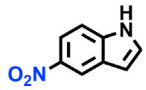	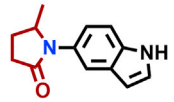	50: 86%
8	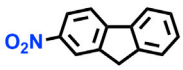	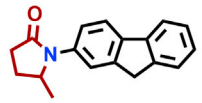	51: 87%
9			52: 82%

Figure 9. Synthesis of pyrrolidones from nitro compounds and LA

Reaction conditions: 0.5 mmol LA and 0.5 mmol nitro compound, 40 mg catalyst (0.64 mmol% cobalt), 110°C, 20 bar H_2, 24 h. Isolated yield based on nitro compound.

[a]GC yield based on nitro compound.

[b]Crude LA is used in this case, which is obtained by acid hydrolysis of glucose.

chemistry, amlodipine, a drug used to treat high blood pressure and coronary artery disease, was selectively reacted with LA and gave the corresponding pyrrolidone derivative in 86% yield (Figure 8, product 42). Finally, the parent compound of all amines, ammonia, was applied and afforded a 96% gas chromatography (GC) yield of 5-methyl-N-pyrrolidone (Figure 8, product 43).

Reductive amination of LA with nitro compounds and nitriles

Compared with the previously discussed reductive aminations *vide supra*, the use of easily available nitroarenes or nitriles has been much less studied.[38,39] The direct use of these substrates can be more attractive with respect to the step economy

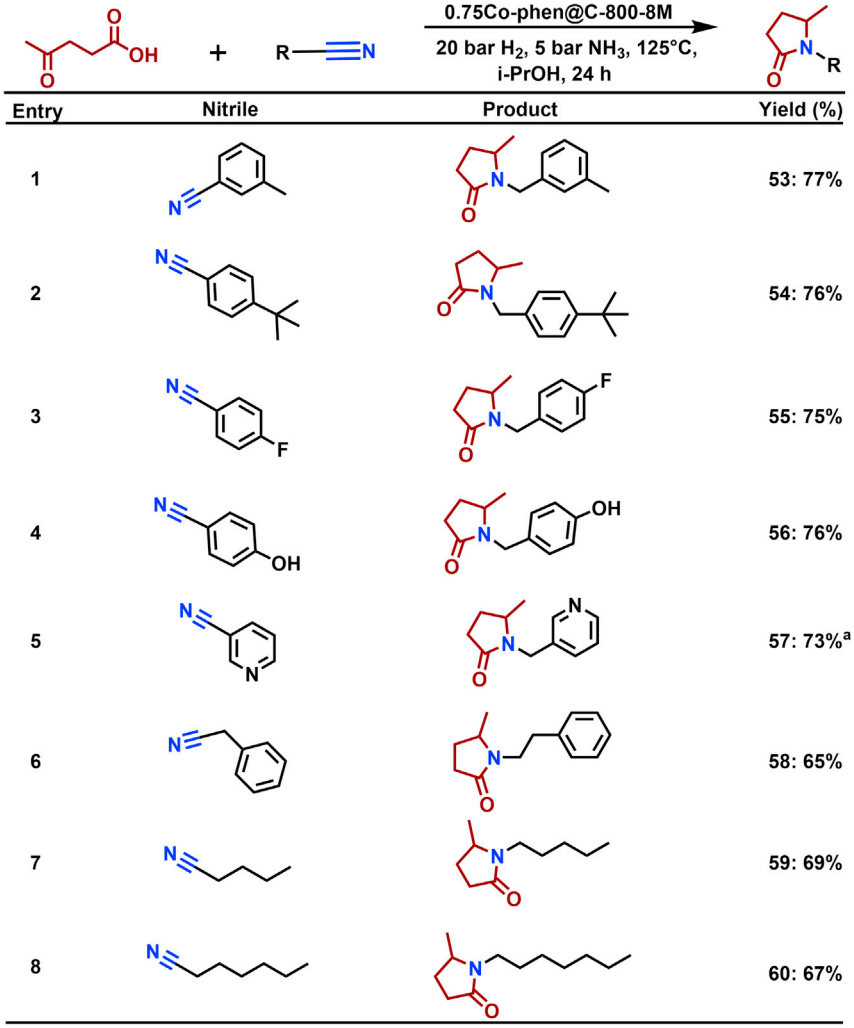

Figure 10. Synthesis of pyrrolidones from nitrile compounds and LA

Reaction conditions: 1 mmol LA and 0.5 mmol nitrile compound, 40 mg catalyst (0.64 mmol% cobalt), 125°C, 20 bar H_2, 5 bar NH_3, 24 h, 2 mL i-PrOH. Isolated yield based on nitrile.

[a]GC yield based on nitrile.

and cost reduction of the starting materials. For example, most anilines are produced by the reduction of the corresponding nitro compounds. Hence, several aliphatic, aromatic, and heterocyclic nitro compounds selectively underwent one-pot reductive amination of LA and were converted into the desired pyrrolidones in 80%–97% yield (Figure 9). Compared with aromatic nitro compounds, the reduction of aliphatic nitro compounds is more demanding, and only two noble catalysts (Ir-PVP[38] and Pt-MoOx/TiO2[39]) are known for this transformation. Nevertheless, these substrates are smoothly hydrogenated in the presence of 0.75Co-phen@C-800-HCl to provide *in situ* the corresponding amines, which subsequently underwent reductive amination with LA to provide the desired N-alkylated pyrrolidones (Figure 9, entries 1–5). As an example, N-methyl 2-methylpyrrolidone, a potential green replacement for NMP, can be directly afforded from nitromethane and LA in 97% GC yield. Furthermore, crude LA directly prepared by the acid hydrolysis of glucose gave the desired product without further purification, albeit in 56% yield (Figure 9, entry 4).

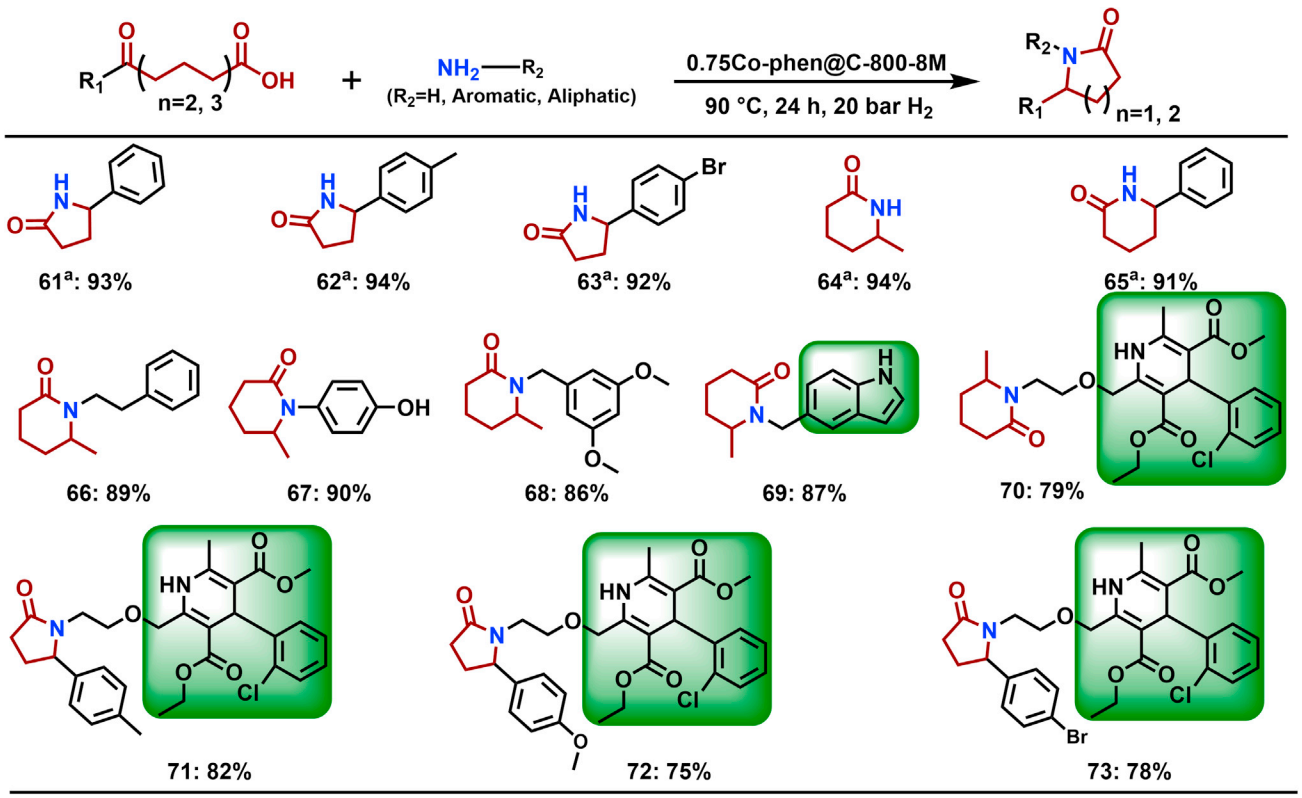

Figure 11. Applications in the synthesis of substituted lactams from different keto acids

Reaction conditions: 0.5 mmol LA and 0.5 mmol nitro compound, 40 mg catalyst (0.64 mmol% cobalt), 90°C, 20 bar H_2, 24 h, 2 mL i-PrOH. Isolated yield based on amine.

[a]GC yield based on amine.

Next, several nitriles were tested in this transformation and provided N-benzylated and alkylated pyrrolidones in up to 77% yield (Figure 10). It is noteworthy that aliphatic and heterocyclic nitriles were easily converted to the corresponding pyrrolidones with 65%–73% yield (Figure 10, entries 5–8).

Synthesis of different lactams from keto acids and amines

Applying our catalyst, the reductive amination of LA with amines, nitro compounds, as well as nitriles and ammonia proceeds smoothly and enables the preparation of a plethora of bio-based pyrrolidines for diverse application. However, the presented protocol is not limited to LA, and many other lactams can be accessed from different keto acids. As shown in Figure 11, several substituted δ-valerolactams and pyrrolidones could be produced under similar conditions with ammonia or amines in high yields (Figure 11, products 61–69). To showcase the potential of this methodology for late-stage drug modification, amlodipine was selectively reacted with 4 different keto acids and gave the corresponding pyrrolidone derivatives in up to 82% yield (Figure 11, products 70–73).

Next, we attempted the synthesis of isoindolinones, which serve as a valuable motif for drugs,[40] following our reductive amination process (Figure 12). Various amines and nitro compounds reacted easily with 2-formylbenzoic acid to give the corresponding isoindolinones (Figure 12, products 74–79, 88–90, 92, 95, 97, 98, and 100). Compared with 2-formylbenzoic acid, amination of 2-acetyl-benzoic acid is

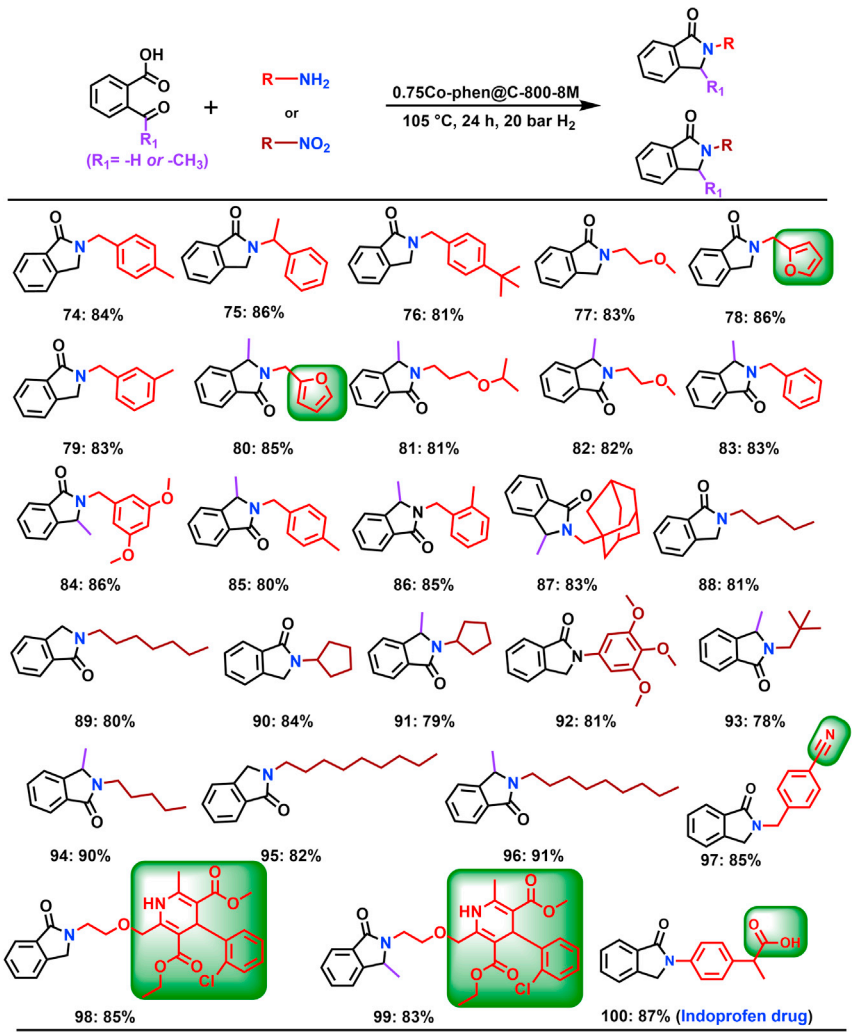

Figure 12. Synthesis of isoindolinones using 0.75Co-phen@C-800-HCl

Reaction conditions: 0.5 mmol 2-formylbenzoic acid or 2-acetyl-benzoic acid, 0.5 mmol amine or nitro compound, 40 mg catalyst (0.64 mmol% cobalt), 105°C, 20 bar H_2, 24 h, 2 mL i-PrOH. Isolated yields based on amine or nitro compound.

more challenging, because hydrogenation of the corresponding ketoimine is more difficult.[41] Nevertheless, both linear and branched amines as well as nitro compounds led to the corresponding isoindolinones with high yields. Again, chemoselectivity of the Co-SAC system was demonstrated in the hydrogenation of nitrile- and ester-containing substrates (Figure 12, products 97–99). Finally, indoprofen, a drug with analgesic, anti-inflammatory, and antipyretic properties, could be synthesized in 87% yield (Figure 12, product 100).

Conclusions

We describe the preparation of highly stable and reusable, dispersed cobalt single atoms supported on carbon. These Co-SCAs have been conveniently synthesized by the impregnation and pyrolysis of an *in situ* generated Co-phenanthroline complex on carbon and subsequent washing with acid. The materials prepared using lower cobalt loading (<0.75 wt%) contained predominately single metal sites,

whereas the ones with higher cobalt loading (>1 wt%) displayed the presence of predominately NPs. This Co-SAC (0.75Co-phen@C-800-HCl) showed excellent activity and selectivity for the domino reductive amination-amidation of the platform chemical LA with amines, nitro compounds, and nitriles as well as ammonia to give a variety of bio-based pyrrolidones. In addition, the presented synthetic methodologies can be applied for the synthesis of diverse other lactams (e.g. pharmaceutically relevant isoindolinones in good to excellent yields). In general, we believe this work provides other opportunities for the development of SACs and their application in organic synthesis, specifically for the future valorization of biomass-derived feedstocks.

EXPERIMENTAL PROCEDURES

Resource availability

Lead contact

Further information and requests for resources should be directed to and will be fulfilled by the lead contact, Prof. Matthias Beller (matthias.beller@catalysis.de).

Materials availability

All materials generated in this study are available from the lead contact without restriction.

Data and code availability

Full experimental procedures are provided in the supplemental information.

SUPPLEMENTAL INFORMATION

Supplemental information can be found online at https://doi.org/10.1016/j.checat.2021.12.009.

ACKNOWLEDGMENTS

We acknowledge the European Research Council (EU project 670986-NoNaCat) and the State of Mecklenburg-Vorpommern for financial and general support. We are grateful to the Deputyship for Research & Innovation, Ministry of Education in Saudi Arabia for financial support through project number 375213500. The DICP team acknowledges financial support from the National Natural Science Foundation of China (21872144 and 21972140), LiaoNing Revitalization Talents Program (XLYC1907053), and CAS Youth Innovation Promotion Association (2018220). J.G. and R.M. thank the China Scholarship Council (CSC) for financial support. We thank the analytical staff of Leibniz-Institut für Katalyse e.V., Germany, and Dalian Institute of Chemical Physics, China, for their excellent service. The BL17C1 beamline at National Synchrotron Radiation Research Center (NSRRC) at Hsinchu, Taiwan is also acknowledged for the XAS results acquirement.

AUTHOR CONTRIBUTIONS

R.V.J. and M.B. supervised the project, J.G., R.V.J., and M.B. planned and developed the project. J.G. R.V.J. and M.B. designed the experiments. J.G. and R.M. prepared catalysts and performed catalytic experiments. R.M. carried out the reproducibility of experiments. L.F. and Y.L. performed the HAADF-STEM measurements. B.-J.S. conducted the XAS measurements. A.M.A. participated in discussions and development of this project. J.G., R.V.J., and M.B. wrote the paper. J.G., L.F., and R.M. contributed equally to this work.

DECLARATION OF INTERESTS

The authors declare no competing interests.

Received: August 16, 2021
Revised: November 4, 2021
Accepted: December 14, 2021
Published: January 6, 2022

REFERENCES

1. Liu, L., and Corma, A. (2018). Metal catalysts for heterogeneous catalysis: from single atoms to nanoclusters and nanoparticles. Chem. Rev. *10*, 4981–5079. https://doi.org/10.1021/acs.chemrev.7b00776.

2. Cui, X., Li, W., Ryabchuk, P., Junge, K., and Beller, M. (2018). Bridging homogeneous and heterogeneous catalysis by heterogeneous single-metal-site catalysts. Nat. Catal. *6*, 385–397. https://doi.org/10.1038/s41929-018-0090-9.

3. Zhang, J., Wang, Z., Chen, W., Xiong, Y., Cheong, W.C., Zheng, L., Yan, W., Gu, L., Chen, C., Peng, Q., et al. (2020). Tuning polarity of Cu-O bondin heterogeneous Cu catalyst to promoteadditive-free hydroboration of alkynes. Chem *6*, 725–737. https://doi.org/10.1016/j.chempr.2019.12.021.

4. Han, Y., Wang, Z., Xu, R., Zhang, W., Chen, W., Zheng, L., Zhang, J., Luo, J., Wu, K., Zhu, Y., et al. (2018). Ordered porous nitrogen-doped carbon matrix with atomically dispersed cobalt sites as an efficient catalyst for dehydrogenation and transfer hydrogenation of N-heterocycles. Angew. Chem. Int. Ed. Engl. *35*, 11262–11267. https://doi.org/10.1002/anie.201805467.

5. Tang, C., Surkus, A.E., Chen, F., Pohl, M.M., Agostini, G., Schneider, M., Junge, H., and Beller, M. (2017). A stable nanocobalt catalyst with highly dispersed CoNx active sites for the selective dehydrogenation of formic acid. Angew. Chem. Int. Ed. Engl. *52*, 16843–16847. https://doi.org/10.1002/ange.201710766.

6. Liu, W., Zhang, L., Yan, W., Liu, X., Yang, X., Miao, S., Wang, W., Wang, A., and Zhang, T. (2016). Single-atom dispersed Co–N–C catalyst: structure identification and performance for hydrogenative coupling of nitroarenes. Chem. Sci. *7*, 5758–5764. https://doi.org/10.1039/C6SC02105K.

7. Xiong, Y., Sun, W., Han, Y., Xin, P., Zheng, X., Yan, W., Dong, J., Zhang, J., Wang, D., and Li, Y. (2021). Cobalt single atom site catalysts with ultrahigh metal loading for enhanced aerobic oxidation of ethylbenzene. Nano Res. *14*, 2418–2423. https://doi.org/10.1002/smll.202006473.

8. He, L., Weniger, F., Neumann, H., and Beller, M. (2016). Synthesis, characterization, and application of metal nanoparticles supported on nitrogen-doped carbon: catalysis beyond electrochemistry. Angew. Chem. Int. Ed. Engl. *55*, 12582–12594. https://doi.org/10.1002/ange.201603198.

9. Zhang, L., Ren, Y., Liu, W., Wang, A., and Zhang, T. (2018). Single-atom catalyst: a rising star for green synthesis of fine chemicals. Natl. Sci. Rev. *5*, 653–672. https://doi.org/10.1093/nsr/nwy077.

10. Bulushev, D.A., and Ross, J.R.H. (2011). Catalysis for conversion of biomass to fuels via pyrolysis and gasification: a review. Catal. Today *1*, 1–13. https://doi.org/10.1016/j.cattod.2011.02.005.

11. Feng, Y., Long, S., Tang, X., Sun, Y., Luque, R., Zeng, X., and Lin, L. (2021). Earth-abundant 3d-transition-metal catalysts for lignocellulosic biomass conversion. Chem. Soc. Rev. *10*, 6042–6093. https://doi.org/10.1039/d0cs01601b.

12. Xue, Z., Yu, D., Zhao, X., and Mu, T. (2019). Upgrading of levulinic acid into diverse N-containing functional chemicals. Green. Chem. *20*, 5449–5468. https://doi.org/10.1039/c9gc02415h.

13. Li, C., Zhao, X., Wang, A., Huber, G.W., and Zhang, T. (2015). Catalytic transformation of lignin for the production of chemicals and fuels. Chem. Rev. *21*, 11559–11624. https://doi.org/10.1021/acs.chemrev.5b00155.

14. Huber, G.W., Iborra, S., and Corma, A. (2006). Synthesis of transportation fuels from biomass chemistry, catalysts, and engineering. Chem. Rev. *9*, 4044–4098. https://doi.org/10.1021/cr068360d.

15. Sun, Z., Fridrich, B., de Santi, A., Elangovan, S., and Barta, K. (2018). Bright side of lignin depolymerization: toward new platform chemicals. Chem. Rev. *2*, 614–678. https://doi.org/10.1021/acs.chemrev.7b00588.

16. De Santi, A., Galkin, M.V., Lahive, C.W., Deuss, P.J., and Barta, K. (2020). Lignin-first fractionation of softwood lignocellulose using a mild dimethyl carbonate and ethylene glycol organosolv process. ChemSusChem *17*, 4468–4477. https://doi.org/10.1002/cssc.201903526.

17. Galebach, P.H., Beussman, M., Johnson, J., Fredriksen, T., Wang, C., Lanci, M.P., and Huber, G.W. (2021). Catalytic conversion of pyrolysis oil to alcohols and alkanes in supercritical methanol over the CuMgAlOx catalyst. ACS Sustainable Chem. Eng. *5*, 2067–2079. https://doi.org/10.1021/acssuschemeng.0c07020.

18. Bomon, J., Van Den Broeck, E., Bal, M., Liao, Y., Sergeyev, S., Van Speybroeck, V., Sels, B.F., and Maes, B.U.W. (2020). Bronsted acid catalyzed tandem defunctionalization of biorenewable ferulic acid and derivates into bio-catechol. Angew. Chem. Int. Ed. Engl. *8*, 3063–3068. https://doi.org/10.1002/ange.201913023.

19. Xie, C., Song, J., Wu, H., Hu, Y., Liu, H., Zhang, Z., Zhang, P., Chen, B., and Han, B. (2019). Ambient reductive amination of levulinic acid to pyrrolidones over pt nanocatalysts on porous TiO2 nanosheets. J. Am. Chem. Soc. *9*, 4002–4009. https://doi.org/10.1021/jacs.8b13024.

20. Louven, Y., Haus, M.O., Konrad, M., Hofmann, J.P., and Palkovits, R. (2020). Efficient palladium catalysis for the upgrading of itaconic and levulinic acid to 2-pyrrolidones followed by their vinylation into value-added monomers. Green. Chem. *14*, 4532–4540. https://doi.org/10.1039/d0gc01043j.

21. Touchy, A.S., Hakim Siddiki, S.M.A., Kon, K., and Shimizu, K.-i. (2014). Heterogeneous Pt catalysts for reductive amination of levulinic acid to pyrrolidones. ACS Catal. *9*, 3045–3050. https://doi.org/10.1021/cs500757k.

22. Wei, Y., Wang, C., Jiang, X., Xue, D., Li, J., and Xiao, J. (2013). Highly efficient transformation of levulinic acid into pyrrolidinones by iridium catalysed transfer hydrogenation. Chem. Commun. (Camb) *47*, 5408–5410. https://doi.org/10.1039/c3cc41661e.

23. Zhang, J., Xie, B., Wang, L., Yi, X., Wang, C., Wang, G., Dai, Z., Zheng, A., and Xiao, F. (2016). Zirconium oxide supported palladium nanoparticles as a highly efficient catalyst in the hydrogenation–amination of levulinic acid to pyrrolidones. ChemCatChem *9*, 2661–2667. https://doi.org/10.1002/cctc.201600739.

24. Wang, S., Huang, H., Bruneau, C., and Fischmeister, C. (2017). Selective and efficient iridium catalyst for the reductive amination of levulinic acid into pyrrolidones. ChemSusChem *21*, 4150–4154. https://doi.org/10.1002/cssc.201701299.

25. Jagadeesh, R.V., Surkus, A.E., Junge, H., Pohl, M.M., Radnik, J., Radesh, J., Huan, H., Schünemann, V., Brückner, A., and Beller, M. (2013). Nanoscale Fe2O3-based catalysts for selective hydrogenation of nitroarenes to anilines. Science *342*, 1073–1076. https://doi.org/10.1126/science.1242005.

26. Jagadeesh, R.V., Murugesan, K., Alshammari, A.S., Neumann, H., Pohl, M.M., Radnik, J., and Beller, M. (2017). MOF-derived cobalt nanoparticles catalyze a general synthesis of amines. Science *358*, 326–332. https://doi.org/10.1126/science.aan6245.

27. Natte, K., Neumann, H., Jagadeesh, R.V., and Beller, M. (2017). Convenient iron-catalyzed reductive aminations without hydrogen for selective synthesis of N-methylamines. Nat. Commun. *1*, 1344. https://doi.org/10.1038/s41467-017-01428-0.

28. Jagadeesh, R.V., Junge, H., and Beller, M. (2014). Green synthesis of nitriles using non-

noble metal oxides-based nanocatalysts. Nat. Commun. *5*, 4123. https://doi.org/10.1038/ncomms5123.

29. Jagadeesh, R.V., Stemmler, T., Surkus, A.E., Bauer, M., Pohl, M.M., Radnik, J., Junge, K., Junge, H., Brückner, A., and Beller, M. (2015). Nat. Protoc. *10*, 916–926. https://doi.org/10.1038/nprot.2015.049.

30. Gao, J., Ma, R., Feng, L., Liu, Y., Jackstell, R., Jagadeesh, R.V., and Beller, M. (2021). Ambient hydrogenation and deuteration of alkenes using a nanostructured ni-core-shell catalyst. Angew. Chem. Int. Ed. Engl. *133*, 2–9. https://doi.org/10.1002/anie.202105492.

31. Gao, J., Jiang, Q., Liu, Y., Liu, W., Chu, W., and Su, D.S. (2018). Probing the enhanced catalytic activity of carbon nanotube supported Ni-LaOx hybrids for the CO2 reduction reaction. Nanoscale *29*, 14207–14219. https://doi.org/10.1039/c8nr03882a.

32. Han, A., Wang, B., Kumar, A., Qin, Y., Jin, J., Wang, X., Yang, C., Dong, B., Jia, Y., Liu, J., and Sun, X. (2019). Recent advances for MOF-derived carbon-supported single-atom catalysts. Small Methods *9*, 1800471. https://doi.org/10.1002/smtd.201800471.

33. Eklfinger, M., Schönauer, T., Thomä, S.L.J., Stäglich, R., Drechsle, M., Zobel, M., Senker, J., and Kempe, R. (2021). Co-catalyzed synthesis of primary amines via reductive amination employing hydrogen under very mild conditions. ChemSusChem *14*, 2360–2366. https://doi.org/10.1002/cssc.202100553.

34. Hahn, G., Kunnas, P., de Jonge, N., and Kempe, R. (2019). General synthesis of primary amines via reductive amination employing a reusable nickel catalyst. Nat. Catal. *2*, 71–77. https://doi.org/10.1038/s41929-018-0202-6.

35. Chen, Z., Liu, C., Liu, J., Li, J., Xi, S., Chi, X., Xu, H., Park, I.H., Peng, X., Li, X., et al. (2020). Cobalt single-atom-intercalated molybdenum disulfide for sulfide oxidation with exceptional chemoselectivity. Adv. Mater. *4*, e1906437. https://doi.org/10.1002/adma.201906437.

36. Pan, Y., Lin, R., Chen, Y., Liu, S., Zhu, W., Cao, X., Chen, W., Wu, K., Cheong, W.C., Wang, Y., et al. (2018). Design of single-atom Co-N5 catalytic site: a robust electrocatalyst for CO2 reduction with nearly 100% co selectivity and remarkable stability. J. Am. Chem. Soc. *12*, 4218–4221. https://doi.org/10.1021/jacs.8b00814.

37. Wang, H., Wang, Y., Li, Y., Lan, X., Ali, B., and Wang, T. (2020). Highly efficient hydrogenation of nitroarenes by n-doped carbon-supported cobalt single-atom catalyst in ethanol/water mixed solvent. ACS Appl. Mater. Inter. *30*, 34021–34031. https://doi.org/10.1021/acsami.0c06632.

38. Chaudhari, C., Shiraishi, M., Nishida, Y., Sato, K., and Nagaoka, K. (2020). One-pot synthesis of pyrrolidones from levulinic acid and amines/nitroarenes/nitriles over the Ir-PVP catalyst. Green. Chem. *22*, 7760–7764. https://doi.org/10.1039/D0GC01725F.

39. Siddiki, S.M.A.H., Touchy, A.S., Bhosale, A., Toyao, T., Mahara, Y., Ohyama, J., Satsuma, A., and Shimizu, K.-i. (2018). Direct synthesis of lactams from keto acids, nitriles, and H2 by heterogeneous Pt catalysts. ChemCatChem *4*, 789–795. https://doi.org/10.1002/cctc.201701355.

40. Enders, D., Narine, A.A., Toulgoat, F., and Bisschops, T. (2008). Asymmetric Bronsted acid catalyzed isoindoline synthesis: enhancement of enantiomeric ratio by stereoablative kinetic resolution. Angew. Chem. Int. Ed. Engl. *30*, 5661–5665. https://doi.org/10.1002/anie.200801354.

41. Murugesan, K., Wei, Z., Chandrashekhar, V.G., Neumann, H., Spannenberg, A., Jiao, H., Beller, M., and Jagadeesh, R.V. (2019). Homogeneous cobalt-catalyzed reductive amination for synthesis of functionalized primary amines. Nat. Commun. *10*, 5443. https://doi.org/10.1038/s41467-019-13351-7.

nature communications

Article

https://doi.org/10.1038/s41467-023-40614-1

Streamlining the synthesis of amides using Nickel-based nanocatalysts

Received: 23 September 2022

Accepted: 3 August 2023

Published online: 17 August 2023

Check for updates

Jie Gao[1], Rui Ma[1], Fairoosa Poovan[1], Lan Zhang[2], Hanan Atia[1], Narayana V. Kalevaru[1], Wenjing Sun[3], Sebastian Wohlrab[1], Denis A. Chusov[4] ✉, Ning Wang[2] ✉, Rajenahally V. Jagadeesh[1,5] ✉ & Matthias Beller[1] ✉

The synthesis of amides is a key technology for the preparation of fine and bulk chemicals in industry, as well as the manufacture of a plethora of daily life products. Furthermore, it constitutes a central bond-forming methodology for organic synthesis and provides the basis for the preparation of numerous biomolecules. Here, we present a robust methodology for amide synthesis compared to traditional amidation reactions: the reductive amidation of esters with nitro compounds under additives-free conditions. In the presence of a specific heterogeneous nickel-based catalyst a wide range of amides bearing different functional groups can be selectively prepared in a more step-economy way compared to previous syntheses. The potential value of this protocol is highlighted by the synthesis of drugs, as well as late-stage modifications of bioactive compounds. Based on control experiments, material characterizations, and DFT computations, we suggest metallic nickel and low-valent Ti-species to be crucial factors that makes this direct amide synthesis possible.

Amides are of fundamental importance in chemistry and find a plethora of applications in organic synthesis, medicine, biology as well as material sciences (Fig. 1a)[1,2]. A characteristic feature of many amides is their strong hydrogen bonding ability which determines the structure of biomolecules, especially proteins, but also numerous pharmaceuticals. In fact, 73 of the top 200 selling drugs of the year 2020 in the US are amide derivatives, mainly aromatic ones[3]. Moreover, essential chemicals, building blocks, and advanced materials such as nylon and aramides are aromatic amides[4–6]. Thus, the creation of amide bonds continues to be a highly relevant task in organic and biochemistry and a toolbox of methodologies exist for their preparation[7].

In general, amide bonds are created through condensation of a carboxylic acid (derivative) and an amine with the release of one equivalent of water[8,9]. To facilitate this process, functionalized amides are typically produced by the reaction of activated carboxylic acid derivatives such as acyl chlorides and anhydrides with amines or direct reaction of carboxylic acids with amines in presence of stoichiometric amounts of coupling reagents (Fig. 1b)[2,10–13]. These classic methods employ stoichiometric quantities of activating reagents, e.g. carbodiimides such as dicyclohexylcarbodiimide (DCC) or (1-ethyl-3-(3-dimethylaminopropyl)carbodiimide (EDC), ammonium or phosphonium salts such as (1-[bis(dimethyllamino)methylene]−1*H*−1,2,3-triazolo[4,5b] pyridinium hexafluorophosphate-3-oxide (HATU), thionyl chloride or *n*-propylphosphonic acid anhydride, which results in the generation of significant amounts of waste[14]. In addition to the cost and toxicity of the activation reagents itself, product purification from the reaction mixture is also a tedious and expensive process[2]. Due to these problems, as well as the importance of the amide bond, the ACS Green Chemistry Institute and members of leading pharmaceutical companies recognized 'the synthesis of amides by avoiding poor atom economy reagents' as one of the major challenges in process chemistry of the pharmaceutical industry[15]. Hence, the development of more

[1]Leibniz-Institut für Katalyse e.V., Albert-Einstein-Street 29a, 18059 Rostock, Germany. [2]Faculty of Environment and Life, Beijing University of Technology, 100124 Beijing, China. [3]Guang-dong Medical University, 523808 Dongguan, China. [4]A. N. Nesmeyanov Institute of Organoelement Compounds, 119991 Moscow, Russia. [5]Nanotechnology Centre, Centre of Energy and Environmental Technologies, VŠB-Technical University of Ostrava, Ostrava-Poruba, Czech Republic. ✉e-mail: denis.chusov@gmail.com; ning.wang.1@bjut.edu.cn; jagadeesh.rajenahally@catalysis.de; matthias.beller@catalysis.de

https://doi.org/10.1038/s41467-023-40614-1

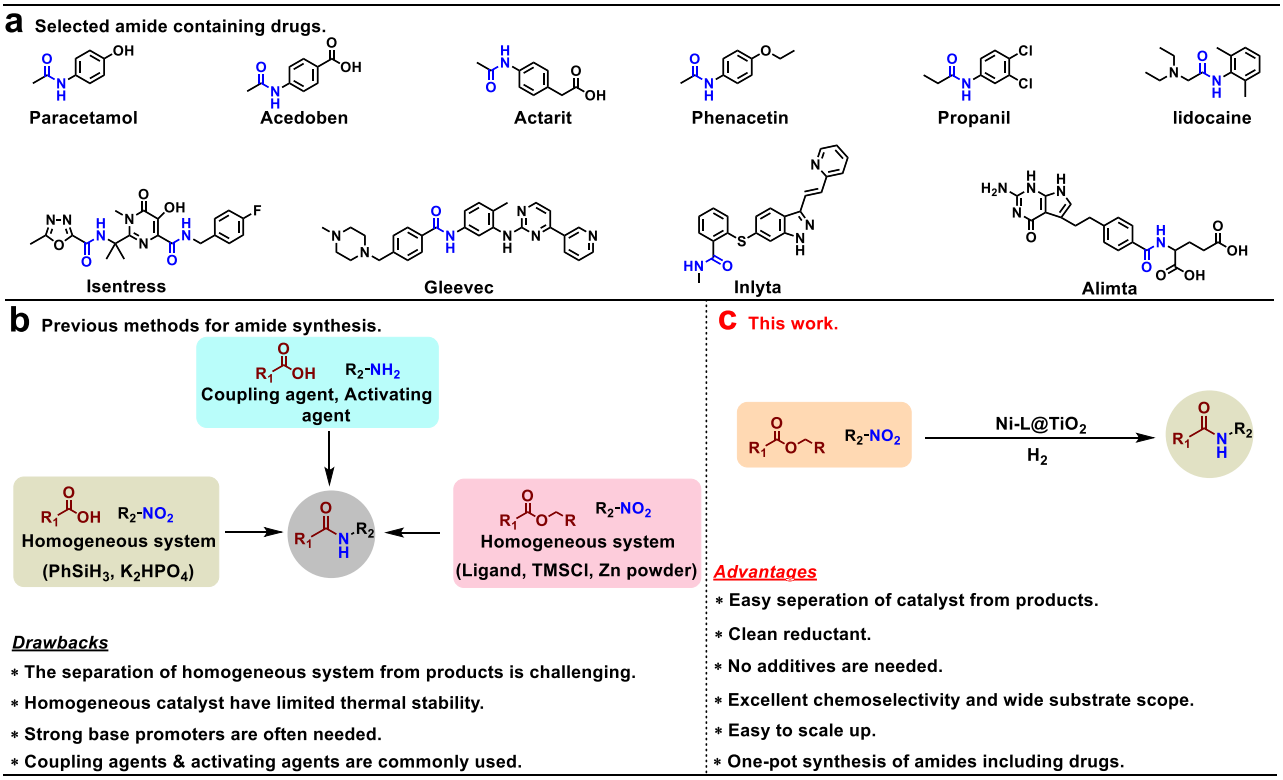

Fig. 1 | Examples of pharmaceuticals containing amide bonds and selected methodologies for amide synthesis. Selected amide containing drugs (**a**) and methods for the synthesis of amides (**b** and **c**).

sustainable methodologies for the synthesis of amides by avoiding stochiometric reagents or activated compounds continues to be important topic both in academia and industry[1]. In this respect, carboxylic esters constitute a promising alternative to the corresponding acids as reaction partner for amide bond formation (Fig. 1b, c)[16].

Considering that anilines are mainly derived by reduction of nitroarenes, the direct use of nitroarenes for amide synthesis features a clear step-economic advantage. So far, nitroarenes have been rarely used for a direct catalytic synthesis of amides[7,17,18]. As one of the few examples, a homogeneous Ni catalyst has been applied in the presence of stochiometric amounts of Zn/TMSCl. Furthermore, an Ir-Fe-homogeneous photocatalyst system was employed using expensive $PhSiH_3$ as reducing agent[19,20]. Considering the current limitations of the desired cascade hydrogenation-amidation reaction, the application of a heterogeneous catalyst would be especially desired[21,22]. Such a methodology has obvious benefits with respect to availability of substrates, cost- and step-economy as well as practicability. Despite the potential advantages, such transformation in the presence of molecular hydrogen remained to the best of our knowledge unexplored[19,20,23,24].

In the past decade, we prepared a variety of nanostructured 3d metal catalysts supported on carbon[25,26] or SiO_2[27,28] as well as other inorganic oxides. These materials showed excellent performances in various redox transformations. In this context, we became interested to prepare such nanoparticles on TiO_2, which should result in interesting catalyst materials[29,30], particularly for valorization of esters[31]. Based on this concept, here, we report a general synthesis protocol for the reductive amidation of nitro compounds and esters using an inexpensive heterogeneous catalyst in the presence of hydrogen. Key for this transformation is the synergistic effect between metallic nickel and low-valent Ti-species, which allows for the preparation of functionalized fine chemicals and structurally complex amides including important drug molecules.

Results

Catalyst synthesis

To realize the reductive amidation of nitro compounds with esters in a straightforward manner, we planned to use a suitable multifunctional catalyst[32]. In this transformation, the initial hydrogenation steps as well as the subsequent amide formation should proceed efficiently to avoid unwanted side reactions[33]. Ideally, the catalyst material should be based on inexpensive and stable supports as well as 3d-metals, due to their inherent advantages (availability, toxicity, price, robustness, recyclability)[34–36]. In the past decade, some of us developed a general approach for the synthesis of such nanoparticles on inert supports and stable supported single atom catalysts[25,26,37–39]. Based on these previous works, we prepared Fe-, Co-, and Ni-nanoparticles in the presence of inexpensive aniline ligands (o-phenylenediamine L1, p-phenylenediamine L2, aniline L3), which were supported on TiO_2, γ-Al_2O_3, SiO_2 and Vulcan carbon. In a typical procedure, the respective metal nitrates were mixed in situ with the ligand in methanol and then immobilized on a given heterogeneous support. Finally, the immobilized materials were pyrolyzed at given temperatures under argon atmosphere to obtain supported nanoparticles-based catalysts (Fig. 2). The obtained materials are labelled as M-L@Suppport-T, where M, L, T denotes metal, ligand, and pyrolysis temperature.

Reaction design and catalyst evaluation

All the catalytic materials were tested for the reductive amidation of 4-nitrophenol in ethyl acetate to give 4-acetaminophen (paracetamol). The target product is one of the most common medications against fever and mild to moderate pain. Thus, it is an active ingredient of a wide range of cold and flu remedies. The currently used processes for paracetamol preparation are shown in Supplementary Fig. 1. As shown in Table 1, a selection of Fe-, Ni-, and Co-based nanoparticles on different supports were prepared in the presence of L1. The performance of all these materials was compared in the model reaction under

https://doi.org/10.1038/s41467-023-40614-1

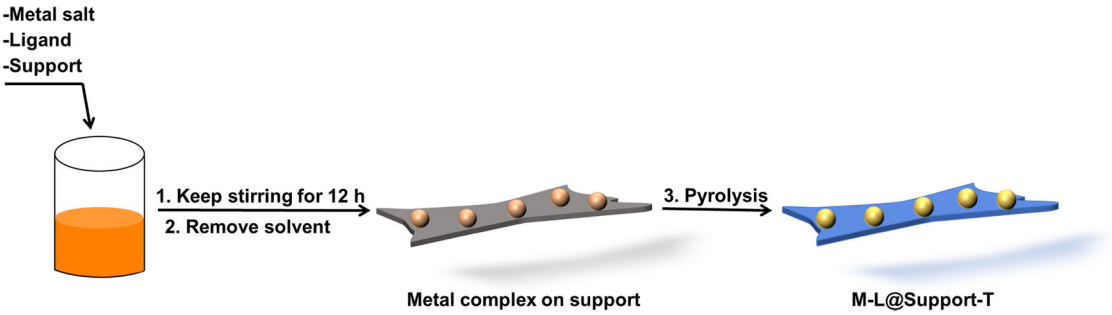

Fig. 2 | Catalysts preparation. Pictorial representation for the synthesis of catalytic materials.

Table 1 | Synthesis of 4-acetaminophen (paracetamol) from nitrophenol and ethyl acetate: Catalytic activities and selectivities

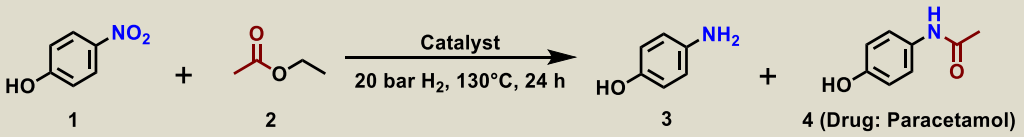

1 2 3 4 (Drug: Paracetamol)

Entry	Catalyst	Metal loading[a] (wt %)	Conversion (%)	Yield (%)	
				3	4
1	Ni-L1@Carbon-800	4.76	>99	97	<1
2	Ni-L1@SiO_2-800	4.68	>99	33	65
3	Ni-L1@g-Al_2O_3-800	4.85	>99	48	50
4	Ni-L1@TiO_2-800	4.78	>99	13	85
5	Fe-L1@TiO_2-800	4.83	17	4	12
6	Co-L1@TiO_2–800	4.62	>99	45	53
7	Ni-L2@TiO_2-800	4.81	>99	21	77
8	Ni-L3@TiO_2-800	4.65	>99	19	79
9	Ni@TiO_2-800	4.66	<1	<1	<1
10	$Ni(NO_3)_2{\cdot}6H_2O$@TiO_2	4.80	<1	<1	<1
11	$Ni(NO_3)_2{\cdot}6H_2O$ + L1	4.80	<1	<1	<1
12	Ni-L1@TiO_2–1000	4.81	30	14	15
13	Ni-L1@TiO_2-600	4.79	>99	21	76
14	Ni-L1@TiO_2–400	4.83	63	46	16
15[b]	Ni-L1@TiO_2-800	4.78	>99	10	88
16[c]	Ni-L1@TiO_2-800	4.78	>99	<1	52
17[d]	Ni_3S_2		<1	<1	<1

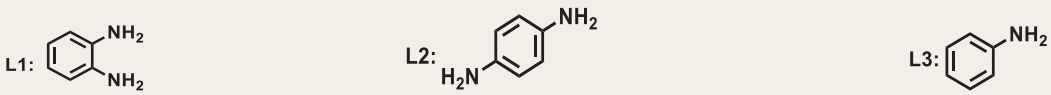

Reaction conditions: 0.5 mmol 4-nitrophenol, 1 mL ethyl acetate, 60 mg catalyst (10 mol% Ni), 20 bar H_2, 130 °C, 24 h. Yields were determined by GC using *n*-hexadecane as the standard.
[a]Metal loading is determined by ICP-OES analysis.
[b]Reaction conditions: 0.5 mmol 4-nitrophenol, 1 mL ethyl acetate, 0.5 mL H_2O, 60 mg catalyst, 20 bar CO, 130 °C, 24 h.
[c]Reaction conditions: 0.5 mmol 4-nitrophenol, 0.3 mL formic acid, 1 mL ethyl acetate, 60 mg catalyst, 20 bar N_2, 130 °C, 24 h.
[d]0.5 mmol 4-nitrophenol, 1 mL ethyl acetate, 4 mg Ni_3S_2 (10 mol% Ni), 20 bar H_2, 130 °C, 24 h.

industrially relevant conditions (20 bar H_2, 130 °C). Noteworthy, no additional solvent or sophisticated activation reagents, etc. were included in this reaction system. In the presence of most catalytic materials, mixtures of **3** and **4** were obtained (Table 1, entries 1–17). Nevertheless, depending on the support and the metal source the individual reaction steps can be controlled. For example, the carbon supported material only promoted hydrogenation of the nitroarene to 4-hydroxyaniline **3** (Table 1, entry 1).

Comparing the activity of the different supports for the desired tandem transformation, SiO_2- and γ-Al_2O_3-supported nickel catalysts were less selective than Ni-L1@TiO_2–800 (Table 1, entries 2–4), which provided the best result towards paracetamol **4**. Among the tested supported metals, Fe-L1@TiO_2–800 showed little activity (Table 1, entry 5), while Co-L1@TiO_2–800 and Ni-L1@TiO_2–800 gave the desired product 4 in 53% and 85% yield, respectively (Table 1, entry 6 vs 4). Interestingly, using other simple anilines (L2, L3) as modifiers for

the preparation of the corresponding materials also produced active catalysts, while the material prepared in the absence of the ligand (Ni@TiO_2–800) and the non-pyrolyzed materials were completely inactive for the benchmark reaction (Table 1, entries 9–11). Optimization of the temperature (400–1000 °C) of the pyrolysis process also revealed a strong influence of this parameter (Table 1, entries 4, 12–14)[40].

The optimal supported nickel catalyst system not only allows to perform the reductive amidation of **1** in the presence of hydrogen, but also permits the desired reaction under transfer hydrogenation conditions in the presence of formic acid (FA)[41] or applying CO as reductant in presence of water[42] (Water-Gas Shift reaction), which shows the tolerance (robustness) of this system against acid, CO, and H_2O. Thus, paracetamol **4** is obtained in 52% and 88% yield, respectively (Table 1, entries 15–16). However, in the presence of FA, the N-formylation product of 4-nitrophenol was formed as a side-product in 48% yield[41].

Next, we examined the stability and recycling of the optimal catalyst in the benchmark reaction. As shown in Supplementary Fig. 2, the material is stable for 7th reaction cycles and only after that a significant decrease of activity was observed. For comparison, the remaining mass of catalyst after each cycle is shown in Supplementary Table 1. ICP-OES analysis of the reaction mixture confirmed no significant leaching of nickel species (detection limit: 0.03 wt%). Consequently, the observed productivity loss cannot be an effect of nickel leaching. TEM characterization of the recycled catalyst (after 8th run) shows that the average size of nickel nanoparticles is significantly increased to 24.2 nm (Supplementary Fig. 3a). Hence, we attribute the productivity loss to the aggregation of nickel nanoparticles.

Catalyst characterization

To understand the structure differences of Ni-L@TiO_2-T samples, synthesized materials have been characterized by the means of TEM, XRD, XPS, TPD and BET. According to the TEM images, nickel particles were uniformly distributed on the titania surface (Fig. 3a and Supplementary Figs. 4–9). Ni particle size distributions are displayed in Fig. 3a (average size of 11.7 nm). The lattice spacings of 0.35 nm were assigned to (101) plane of anatase TiO_2 (Fig. 3b)[43]. In this case EDS mapping images showed an element distribution of N, Ni, C, S, O, and Ti (Fig. 3c–i). Notably, the TiO_2 support was prepared via sulphate process. Hence, the sulphur content is 2.3 wt%, and Ni_3S_2 was detected by XRD in all these samples, too (Supplementary Figs. 10a, 11). TEM images confirmed this observation (Fig. 3e, g). Interestingly, commercially available Ni_3S_2 is inactive for the model reaction (Table 1, entry 17), implying a synergistic effect of all constituents in the as-prepared material.

In XRD measurements, the metallic nickel diffraction peak is observed at 44°, 52° and 76° in Ni-L1@TiO_2-800 and Ni-L1@TiO_2-1000, while Ni-L1@TiO_2-400 and Ni-L1@TiO_2-600 did not show this pattern (Supplementary Fig. 10a)[44]. In Ni-L1@TiO_2-400, Ni-L1@TiO_2-600, and Ni-L1@TiO_2-800, the original titania anatase phase prevailed, while phases including rutile TiO_2, Ti_4O_7 and Ti_6O_{11} are found in Ni-L1@TiO_2-1000 (Supplementary Fig. 10a)[45,46]. Further, we performed XRD characterizations of Ni@TiO_2-800, Ni-L1@TiO_2-800, Ni-L2@TiO_2-800, and Ni-L3@TiO_2-800. The XRD results of these samples demonstrated that pyrolysis of the ligated nickel species promoted formation of metallic nickel, while nickel exists mainly as Ni_3S_2 and $NiTiO_3$ in Ni@TiO_2-800 (Supplementary Fig. 11). Materials prepared in the presence of ligands are more active compared with Ni@TiO_2-800. XRD of the recycled catalyst (after the 8th run) proved the aggregation of nickel nanoparticles as the peak intensity of nickel is relatively increased (Supplementary Fig. 3b). Next, XPS characterizations were conducted to understand the surface properties of these materials. The sample surface mainly consists of C, N, O, Ni, Ti, and S which confirms the STEM results (Supplementary Table 6) and the surface area of the studied materials is in the range of 25–160 m^2/g (Supplementary Fig. 15a). It is worth mentioning that the surface concentration of Ni decreases with pyrolysis temperature from 2.7 to 1.1 at.% from Ni-L1@TiO_2-400 to Ni-L1@TiO_2-1000 (Supplementary Table 6). Figure 4 shows the Ni 2p spectra of the Ni-L1@TiO_2 samples with pyrolysis temperatures 400, 600, 800, and 1000 C. The Ni 2p spectra of Ni-L1@TiO_2-400 in Fig. 4a shows the main Ni $2p_{3/2}$ peak at 855.5 eV and strong satellite features at higher binding energies, thus suggesting an oxidation state of +2 for Ni, probably as $Ni(OH)_2$ or NiOOH[47,48]. At higher pyrolysis temperatures a rather sharp peak at lower binding energies around 852.7 eV appears which can be identified as metallic Ni[48]. Assuming a combination of Ni^0 and Ni^{2+} species for deconvolution, the relative Ni^0 concentration at the surface can be calculated and reaches its maximum with about 43% for Ni-L1@TiO_2-800 (Supplementary Fig. 12). Note that different satellite peak hights might reflect different Ni^{2+} species possibly present at the surface but cannot be distinguished here. Furthermore, all tested materials showed very similar Ti 2p spectra (Supplementary Fig. 13) typical for Ti^{4+}[49]. The N 1 s spectra in Supplementary Fig. 14 is deconvoluted with four peaks indicating the presence of pyridinic N (398.8 eV), pyrrolic N (400.5 eV), graphitic N (401.4 eV), and pyridinic N-oxide (403.3 eV) on all samples[50,51]. However, the ratio of the different nitrogen species changes significantly with the pyrolysis temperature. In detail, the maximum pyrrolic N content (77%) is observed in Ni-L1@TiO_2-400, while for Ni-L1@TiO_2-600 the highest pyridinic N content (56%) is observed.

To address the effect of metallic nickel on the hydrogenation activity of the identified catalyst systems, we also performed the reduction of 4-nitrophenol. The best yield of 4-aminophenol is observed in the presence of Ni-L1@TiO_2-800 (Supplementary Table 2). Further, we conducted CO_2-TPD and NH_3-TPD of the respective catalysts to identify the distributions of basic and acidic sites necessary for the second amidation reaction step (Supplementary Fig. 16). Notably, for Ni-L1@TiO_2-800 more (weak) acidic sites (Supplementary Fig. 16a, NH_3 desorbed between 50–100 °C) were identified compared to Ni-L1@TiO_2-600. To proof whether the identified acidic sites facilitate the formation of paracetamol, we further conducted the reaction of 4-aminophenol with ethyl acetate (Supplementary Table 3). As shown in Supplementary Table 3, Ni-L1@TiO_2-800 afforded a 47% yield of paracetamol, while Ni-L1@TiO_2-600 only gave 34%. Thus, both Ni^0 and weak acidic sites on the support material are advantageous for the overall catalyst activity.

Mechanistic investigations

Apparently, the direct synthesis of paracetamol proceeds first by hydrogenation of **1** to give **3** and subsequent formation of amide **4**. Indeed, as shown in the kinetic profile in Fig. 5a, the hydrogenation step in the presence of the optimal catalyst is finished within 4 h (99% conversion). Amide formation is slower, starts only after 5 h and needs >20 h to be completed. To understand the influence of the catalyst material on both reaction steps, several control experiments were performed (Fig. 5b, c). As shown below the hydrogenation of 4-nitrophenol to 4-aminophenol proceeds under the standard conditions with nearly quantitative yield in the presence of Co-L1@TiO_2-800, Ni-L1@C-800 and Ni-L1@TiO_2-800 (Fig. 5b). Obviously, such hydrogenations easily take place with different types of supported 3d metal nanoparticles[52]. More interestingly, the amidation of 4-aminophenol with ethyl acetate only occurred with Co-L1@TiO_2-800 and Ni-L1@TiO_2-800, while Ni-L1@C-800 did not show any reactivity (Fig. 5c). Using the titania supported nickel catalyst several observations are interesting: under nitrogen atmosphere the target product is afforded in 23% yield (Fig. 5c), while surprisingly the paracetamol yield is increased to 80% under H_2 atmosphere. A similar behaviour is observed for the reaction of nitrobenzene to give acetanilide (Supplementary Fig. 17). Compared with Co-L1@TiO_2-800, Ni-L1@TiO_2-800 is more active in the amidation reaction of ethyl acetate with

https://doi.org/10.1038/s41467-023-40614-1

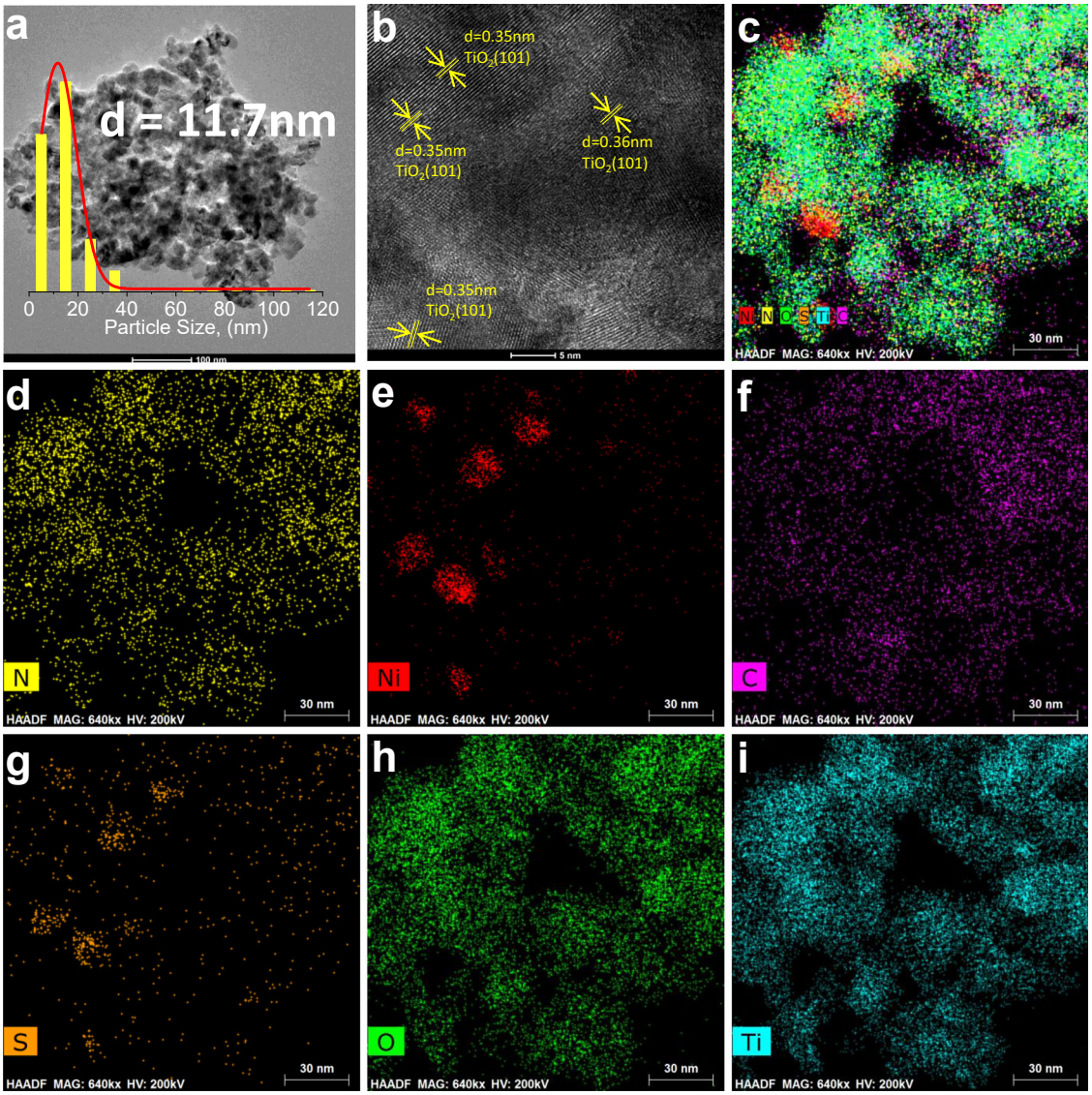

Fig. 3 | Electron microscopy analysis of Ni-L1@TiO_2-800. a, **b** TEM images. In (**a**) it is shown that the particles are distributed on the support with an average diameter of 11.7 nm. The particle size distribution is obtained by measuring more than 200 particles. In (**b**) the lattice spacings are assigned to (101) plane of anatase TiO_2. **c** EDS elemental mapping image, and (**d**–**i**) the visualization of elements: (**d**) N, (**e**) Ni, (**f**) C, (**g**) S, (**h**) O, (**i**) Ti.

4-aminophenol (Fig. 5c). To better understand this observation, in situ XPS characterization experiments of Co-L1@TiO_2-800 and Ni-L1@TiO_2-800 catalysts in presence of nitrogen or hydrogen were performed using a separate reaction cell in the XPS apparatus (Fig. 5d–g, Supplementary Fig. 18). In presence of H_2 at 130 °C, Ni^{2+} is reduced to metallic Ni as shown by the strong increase of the Ni^0 peak together with the decrease of Ni^{2+} intensity (Supplementary Fig. 18). Surprisingly, in addition to Ti^{4+} titanium species Ti^{3+} and Ti^{2+} with a binding energy at ~457 eV and ~455 eV are observed after H_2 treatment (Fig. 5e, g)[53]. Compared with Co-L1@TiO_2-800, more Ti^{2+} and Ti^{3+} species are found in Ni-L1@TiO_2-800 (Fig. 5e, g). In contrast, a clear Ti^{4+} XPS spectrum after a treatment in N_2 atmosphere at 130 °C is observed (Fig. 5d, f). The above analysis indicates that metallic nickel particles are responsible for the reduction of the nitro group to the corresponding aniline[54]. In addition, the subsequent amidation step is also positively influenced by the Ni nanoparticles and low-valent Ti-species. Hence, we propose the reduction of the nitro compound by metallic nickel in presence of hydrogen, subsequently aniline will react with the ester to produce the desired amide facilitated by the support (Fig. 5h).

To understand the role of low-valent Ti-species in the second amidation step, we performed also DFT computations (Fig. 6, details are shown in Supplementary Information). These calculations showed that the most stable configuration of aniline adsorbs on the top of a 5-fold coordinated Ti^{4+} atom (denoted as Ti_{5c}^{4+}, Fig. 6a) and a 5-fold coordinated Ti^{3+} atom (denoted as Ti_{5c}^{3+}, Fig. 6b) sites of anatase-TiO_2 (101) surfaces. In both adsorbed systems, the N atom is bonded on the top of the Ti atom. The accumulation of electron density between N and Ti atom suggests the formation of a N–Ti bond in the two adsorbed systems. The E_{ads} of aniline molecule on Ti_{5c}^{4+} was calculated to be −0.959 eV and the Ti–N bond length was 2.380 Å. The bond length of two N–H bonds were elongated from 1.018 Å in an original aniline molecule to 1.027 Å in the chemisorbed state. The E_{ads} of aniline adsorbed on the top of Ti_{5c}^{3+} was calculated to be −1.153 eV. This suggests that aniline interacts thermodynamically more favorable with the computed Ti^{3+} species compared to the corresponding Ti^{4+} species. The distance of Ti_{5c}^{3+}–N was 2.618 Å and the NH_2 groups in the aniline molecule are slightly leaned to an adjacent bridge oxygen (O_b) on the anatase-TiO_2 (101) surfaces. The hydrogen-bond interactions between O_b and H in the NH_2 group leading to one of the N–H bonds was

https://doi.org/10.1038/s41467-023-40614-1

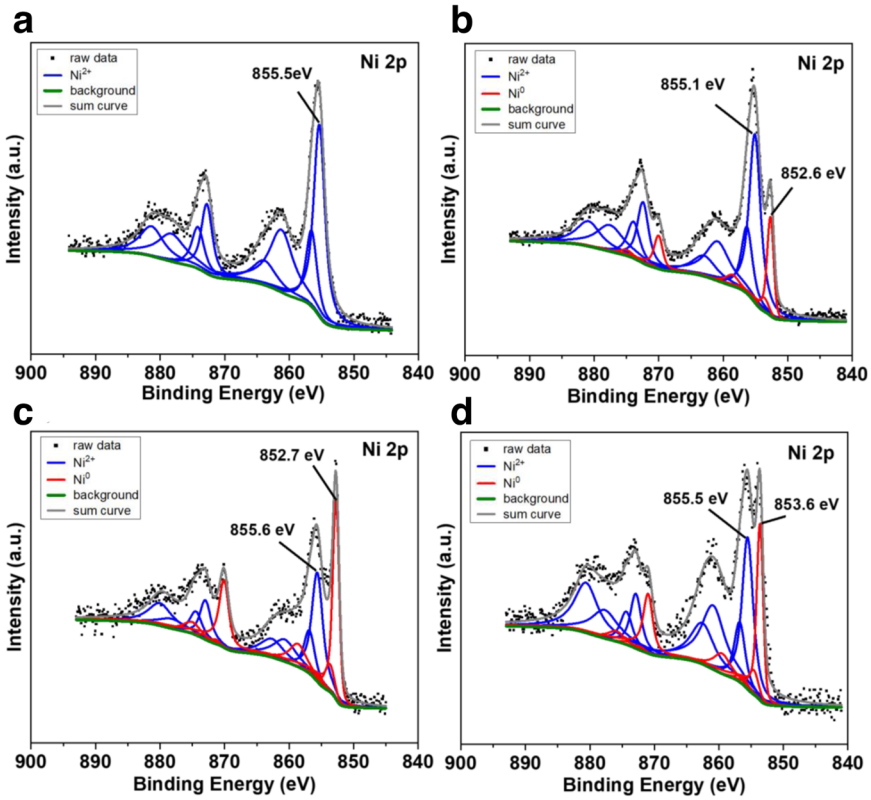

Fig. 4 | XPS Ni 2p spectra of different catalysts. (**a**) Ni-L1@TiO_2-400, (**b**) Ni-L1@TiO_2−600, (**c**) Ni-L1@TiO_2−800 and (**d**) Ni-L1@TiO_2−1000.

elongated to 1.041 and 1.029 Å, respectively. Apparently, the longer bond length of N–H bonds in aniline/ Ti^{3+} suggests that the interaction of aniline with Ti^{3+} promotes the activation and weaken of N–H bonds more effectively than the interaction with the respective Ti^{4+} system.

Next, we aimed to test the general applicability of Ni-L1@TiO_2-800 in various amide syntheses. As shown from the kinetic experiment (Fig. 5a), the second step is relatively slower compared with the nitro reduction. Thus, in order to balance the catalyst loading and reaction rate, we had the idea to speed up the rate determining amidation step by adding cheaper titania support. Indeed, even at low metal catalyst loading in the presence of titania quantitative yield of the desired product can be achieved (Supplementary Fig 19). To further demonstrate the role of the support in this transformation, we pyrolyzed freshly prepared TiO_2 at 400–1000 °C and the resulting five materials were tested in the reaction of 4-aminophenol and ethyl acetate under standard conditions. The following order of activity is observed: fresh TiO_2 > TiO_2-400 > TiO_2-600 > TiO_2-800 > TiO_2-1000 (Supplementary Fig. 20b). Next, all these samples were characterized by XRD (Supplementary Fig. 10b), BET (Supplementary Fig. 15b), and NH_3-TPD (Supplementary Fig. 20a). In general, the specific surface area and the number of acidic sites of these TiO_2 samples decreased significantly with increasing pyrolysis temperature, which also correlates well with the product yield (Supplementary Figs. 15b, 20b). Hence, we believe that both the number of acidic sites and the surface area of TiO_2 are the major factors that affect the amidation process in this model reaction.

Ni-catalyzed synthesis of amides

With an active material for the straight synthesis of paracetamol in hand, we investigated its applicability for other substrates under a standardized set of conditions (30 mg Ni-L1@TiO_2-800, 20 mg TiO_2, 20 bar H_2, 130 °C, 24 h). Diverse nitroarenes with electron-donating (**6**–**11**) or electron-withdrawing groups (**12**–**18**) underwent reductive amidation with ethyl acetate and provided the corresponding amides in up to 89% isolated yield (Fig. 7). Halogenated nitroarenes are well tolerated and produced the corresponding amides (**12**–**17**) without noticeable dehalogenation side reactions. Interestingly, aliphatic nitro compounds, e.g. 1-nitropropane and 1-nitrooctadecane are also converted into amides (**19**–**22**) in 67–72% yield.

For the application of any synthetic methodology, specifically for advanced organic synthesis, it is essential to achieve a high degree of chemoselectivity and functional group tolerance. In this regard, we performed reductive amidation of many functionalized nitroarenes. As shown in Fig. 7, the presented catalytic system tolerates well other potentially reducible groups like ketones (**23**–**24**), carboxylic acids and esters (**25**–**29**), nitrile (**30**), and vinyl substituted derivatives (**37**). In addition, heterocycles (**31**–**36**) were successfully reacted with ethyl acetate and afforded the desired amides in up to 78% yield.

Next, we tested the coupling of different esters (Fig. 8). Apart from ethyl acetate various other alkyl esters including fluorinated ones reacted smoothly to give the corresponding amides (**38**–**48**). Notably, functional groups such as sulfhydryl and nitrile were well tolerated, too (**40**, **44**, **47**, **50**). Interestingly, two carboxylic diesters reacted selectively to provide the mono-amide derivatives (**45**, **54**). Utilizing 4-nitroaniline it is also possible to obtain the corresponding diamide, which is interesting for the preparation of polyamides (**48**). To show that the reductive amidation is possible without excess of ester, we performed further test reactions in solvents and varied the ratio between nitro compound and ester (Supplementary Table 4). As shown in Supplementary Table 4, utilizing toluene as solvent gave the best results, and the optimal ratio between nitro compound and ester is 1:4. This variation of reaction conditions was tested with five selected substrates (**38**–**40**, **49**, **54**) to demonstrate the general applicability. In all cases, the corresponding amides were produced with good yield.

To showcase the utility of this synthetic protocol, we carried out the preparation of selected drug molecules (Fig. 9a). Specifically, Acedoben (**55**), Actarit (**56**), Phenacetin (**57**), and Propanil (**58**) are produced smoothly without further optimization. From a synthetic

https://doi.org/10.1038/s41467-023-40614-1

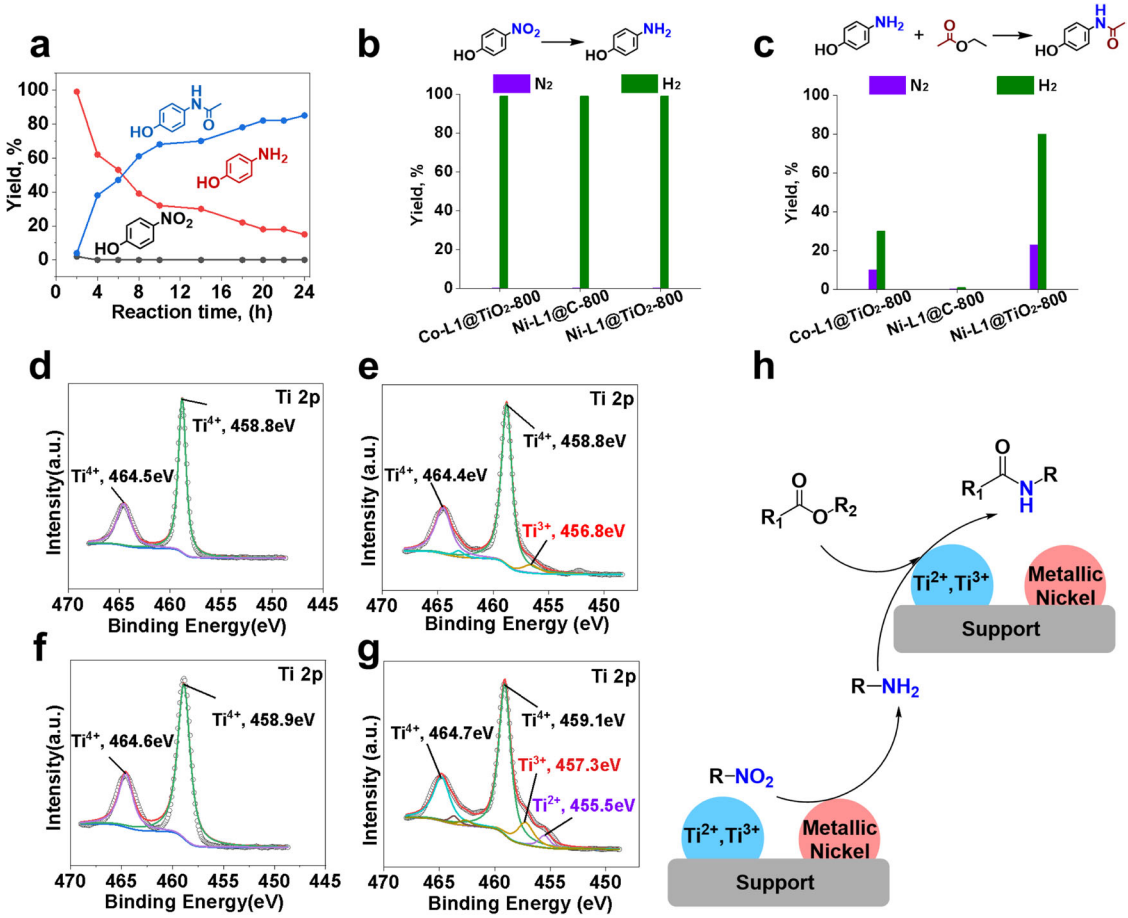

Fig. 5 | Mechanistic investigations. a Kinetic studies. Reaction conditions: 0.5 mmol 4-nitrophenol, 1 mL ethyl acetate, 60 mg Ni-L1@TiO_2−800, 20 bar H_2, 130 °C, 24 h. **b**, **c** Control experiments. Reaction conditions: (**b**) 0.5 mmol 4-nitrophenol, 1 mL ethanol, 60 mg Ni-L1@TiO_2−800, 20 bar H_2, 130 °C, 24 h. (**c**) 0.5 mmol 4-aminophenol, 1 mL ethyl acetate, 60 mg Ni-L1@TiO_2−800, 20 bar H_2, 130 °C, 17 h. In situ XPS characterization was performed at 130 °C under 1 bar N_2 (**d**, **f**) and H_2 (**e**, **g**) for 1 h, (**d**, **e**) Ti 2p for Co-L1@TiO_2−800, (**f**, **g**) Ti 2p for Ni-L1@TiO_2−800. (**h**) Proposed reaction pathway.

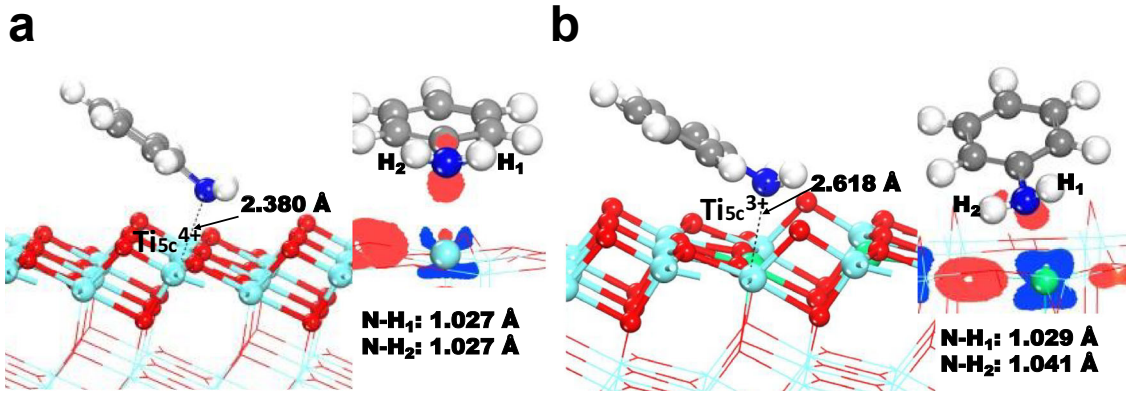

Fig. 6 | The most stable configuration of aniline adsorbed on anatase-TiO_2 (101) surface. a aniline is interacting with a Ti^{4+} ion, and (**b**) aniline is interacting with a Ti^{3+} ion in anatase-TiO_2 (101) surfaces. The inset was the different charge density of the complex. Blue areas represent electron depletion and red areas means electron accumulation with an isosurface value of 0.1 electrons/Å^3.

point of view, late-stage modification of bioactive compounds is interesting, too (Fig. 9b). Hence, MCPA-methylester, a common herbicide, was converted directly to amide (**59**). Similarly, rhodamine fluorescent probe[55] can be successfully transformed into the corresponding amide (**60**). Likewise, amidation of nimesulide, a non-steroidal anti-inflammatory drug (NSAID), and nimodipine afforded the desired products in 72–75% yield (**61**–**62**). Finally, we performed upscaling reactions of selected products on 1–10 g scale (Fig. 9c). No significant deviations of the products yields were observed compared to the 0.5 mmol-scale experiments.

Discussions

In conclusion, a practical reductive amidation methodology has been developed for the direct synthesis of amides from nitro compounds

https://doi.org/10.1038/s41467-023-40614-1

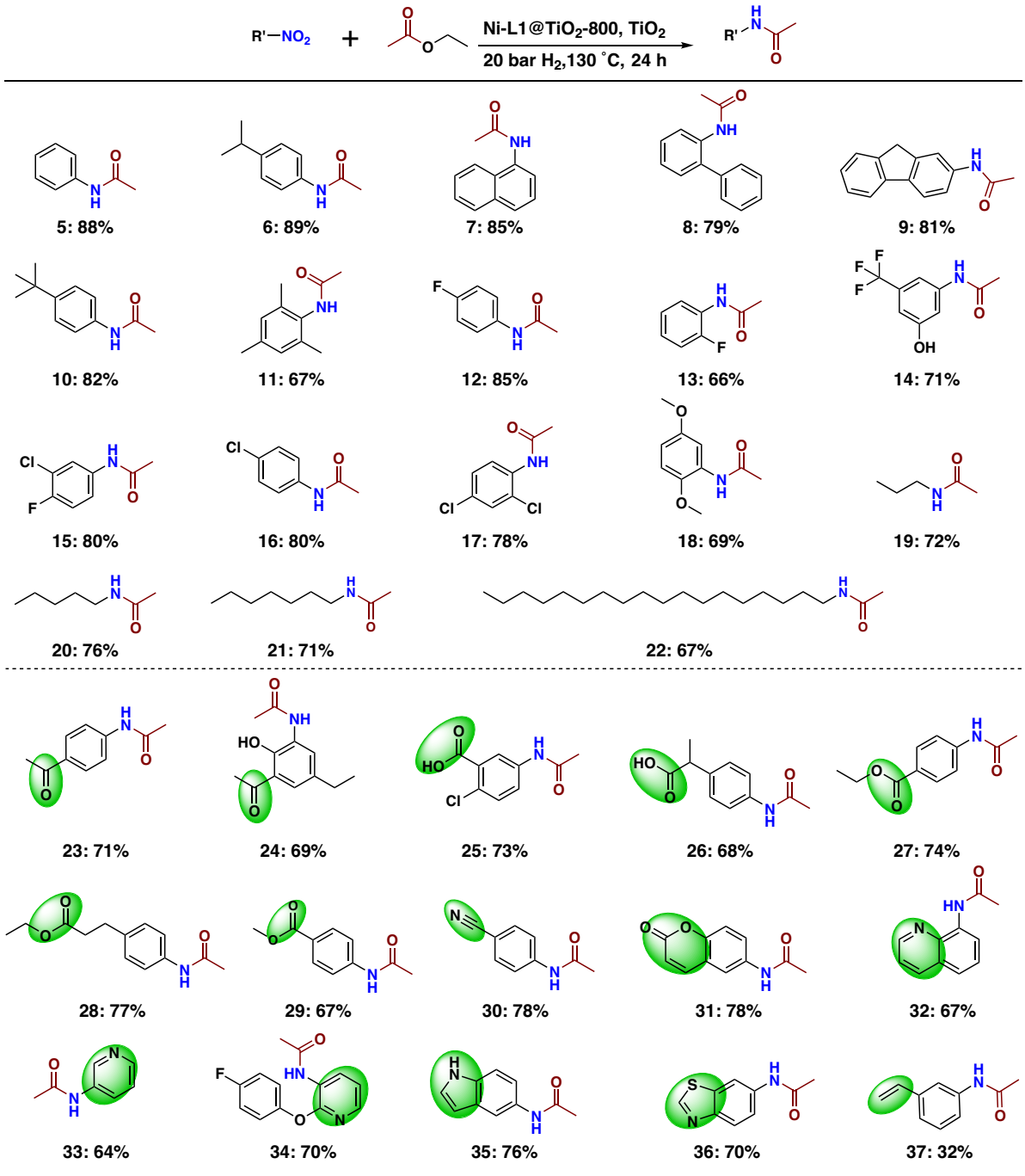

Fig. 7 | Ni-L1@TiO_2–800 catalysed synthesis of amides: scope of nitro compounds. Reaction conditions: 0.5 mmol nitro compound, 1 mL ethyl acetate, 30 mg Ni-L1@TiO_2–800, 20 mg TiO_2, 20 bar H_2, 130 °C, 24 h. Isolated yields based on nitro compound.

and esters using nickel-based nanostructured catalyst. Direct cascade transformation of nitro compounds to amides was realized utilizing molecular hydrogen as green reductant in the presence of a heterogeneous catalyst and to the best of our knowledge no previous examples exist. The presented catalytic material showed excellent substrate scope and high functional group tolerance. The utility of this methodology is demonstrated by a more efficient synthesis of industrially relevant fine chemicals and selected drug molecules including paracetamol. Further, the method allows for fast and clean modifications of many bioactive compounds. The utility of the catalyst material is also demonstrated by gram-scale reactions and recycling experiments. By performing control experiments, material characterizations, and DFT computation, we found metallic nickel and low-valent Ti-species are two crucial factors that allow for this straightforward amide synthesis. We envision that the established methodology will inspire other scientists both in industry and academia to develop even more efficient amide syntheses.

Methods

Materials and methods

All esters and nitro compounds were obtained commercially from various chemical companies and used directly without further purification. Nickel(II) nitrate hexahydrate [$Ni(NO_3)_2{\cdot}6H_2O$, cat no. 203874-20 G], cobalt(II) nitrate hexahydrate [$Co(NO_3)_2{\cdot}6H_2O$, cat no. 239267-5 G] and iron(III) nitrate nonahydrate [$Fe(NO_3)_3{\cdot}9H_2O$, cat no. 216828-100 G] were purchased from Sigma Aldrich. Ni_3S_2 (CAS

https://doi.org/10.1038/s41467-023-40614-1

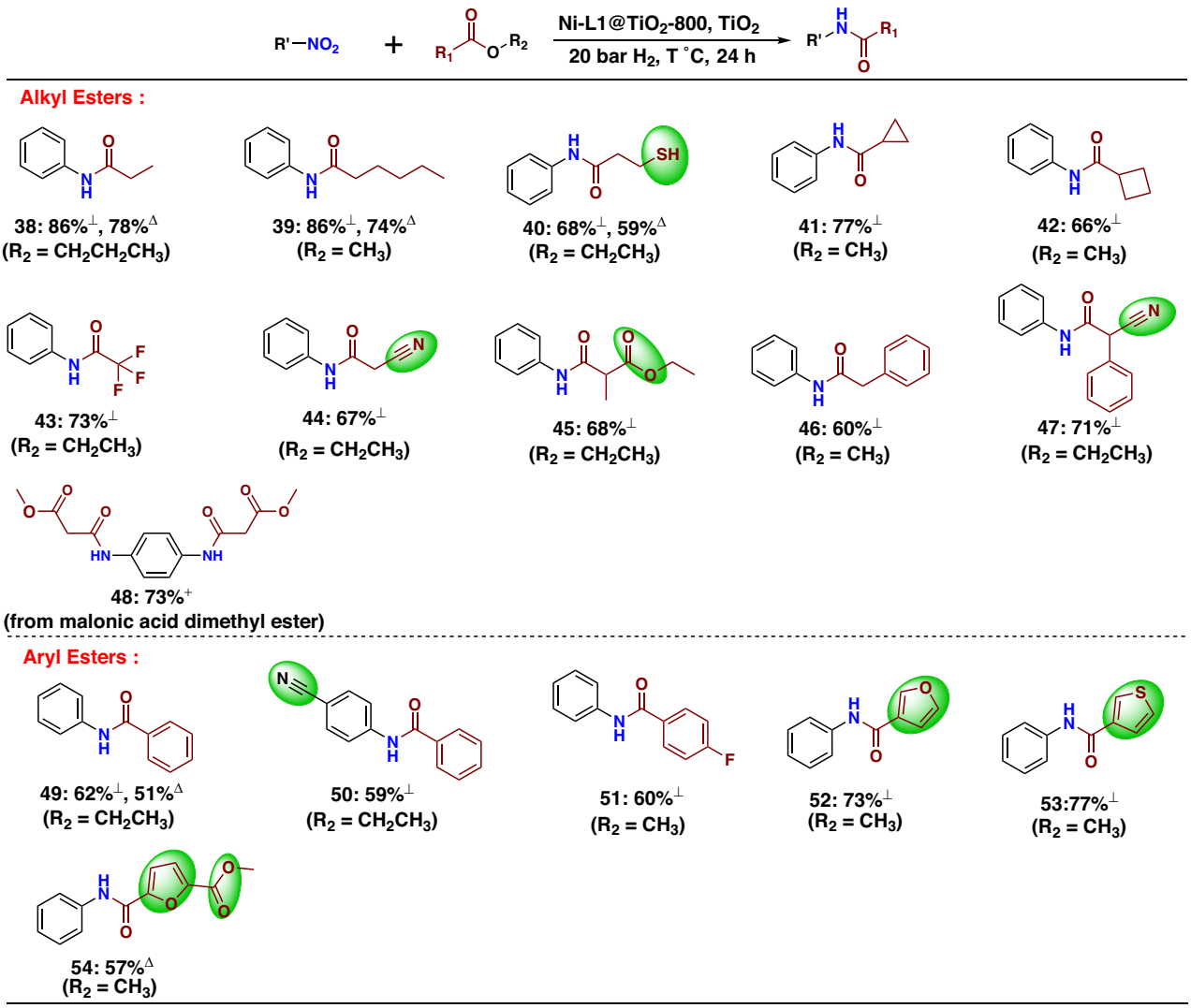

Fig. 8 | Ni-L1@TiO_2–800 catalysed synthesis of amides: scope of esters. ⊥Reaction conditions: 0.5 mmol nitro compound, 1 mL ester, 30 mg Ni-L1@TiO_2–800, 20 mg TiO_2, 20 bar H_2, 130 °C, 24 h. ΔReaction conditions: 0.5 mmol nitro compound, 2 mmol ester, 1 mL toluene, 30 mg Ni-L1@TiO_2–800, 20 mg TiO_2, 20 bar H_2, 140 °C, 24 h. +Reaction conditions: 0.5 mmol 4-nitroaniline, 1 mL ester, 30 mg Ni-L1@TiO_2-800, 20 mg TiO_2, 20 bar H_2, 130 °C, 48 h. All are isolated yields based on nitro compound. The detailed information of these esters is provided in Supplementary Fig. 21.

No.12035-72-2, Lot: C12Y018) was obtained from Thermo Fischer Scientific. Ethyl acetate (HPLC grade, cat no. 5582024) and toluene (HPLC grade, cat no. 10109731) were obtained from Thermo Fisher Scientific. Carbon powder, VULCAN® XC72R with Code XVC72R and CAS No. 1333-86-4 was obtained from Cabot Corporation Prod. The catalyst support γ-Al_2O_3 (cat no. 199443-100 G) and SiO_2 (cat no. 85356-100 G) were purchased from Sigma Aldrich. The pyrolysis experiments were performed using the tube furnace (Bayferrox® 110, LANXESS, GmbH).

XRD powder pattern were recorded on a Panalytical X'Pert θ/2θ -diffractometer equipped with Xcelerator detector using automatic divergence slits and Cu kα1/α2 radiation (40 kV, 40 mA; λ = 0.15406 nm, 0.154443 nm). Cu beta-radiation was excluded using a nickel filter foil. Measurements were performed with either 0.021 or 0.005°s^{-1}. Finely pestled samples were mounted on silicon zero background holders. After data collection obtained intensities were converted from automatic to fixed divergence slits (0.25°) for further analysis. Peak positions and profile were fitted with Pseudo-Voigt function using the HighScore Plus software package (Panalytical). Phase identification was done by using the PDF-2 database of the International Center of Diffraction Data (ICDD).

The XPS measurements were performed on an ESCALAB 220iXL (ThermoFischer Scientific) with monochromated Al Kα radiation (E = 1486.6 eV). Samples are prepared on a stainless-steel holder with conductive double-sided adhesive carbon tape. The electron binding energies were obtained without charge compensation leading a main C 1 s peak at around 284.6 eV. For quantitative analysis the peaks were deconvoluted with Gaussian-Lorentzian curves using the software Unifit 2021, the peak areas were divided by the transmission function of the spectrometer and the element specific sensitivity factor of Scofield. To determine the relative Ni^0 content the Ni 2p spectra are deconvoluted using an experimentally gained peak shape of metallic Ni from a sputter cleaned Ni foil together with peaks corresponding to Ni^{2+}.

In-situ XPS was conducted using a Thermofischer ESCALAB 250Xi X-ray photoelectron spectrometer with a pass energy of 40.00 eV and an Al Kα excitation source (hv = 1253.6 eV). The analysis chamber pressure is $8*10^{-10}$Pa. The Operating Voltage is 12.5 kV. The filament current is 16 mA, and the signal is accumulated 5–10 times. The step size is 0.1 eV. To characterize the effect of gas on the sample structure, the catalyst was placed in a reaction chamber connected to the XPS equipment and exposed to H_2 or N_2 (20 mL/min) at room temperature.

https://doi.org/10.1038/s41467-023-40614-1

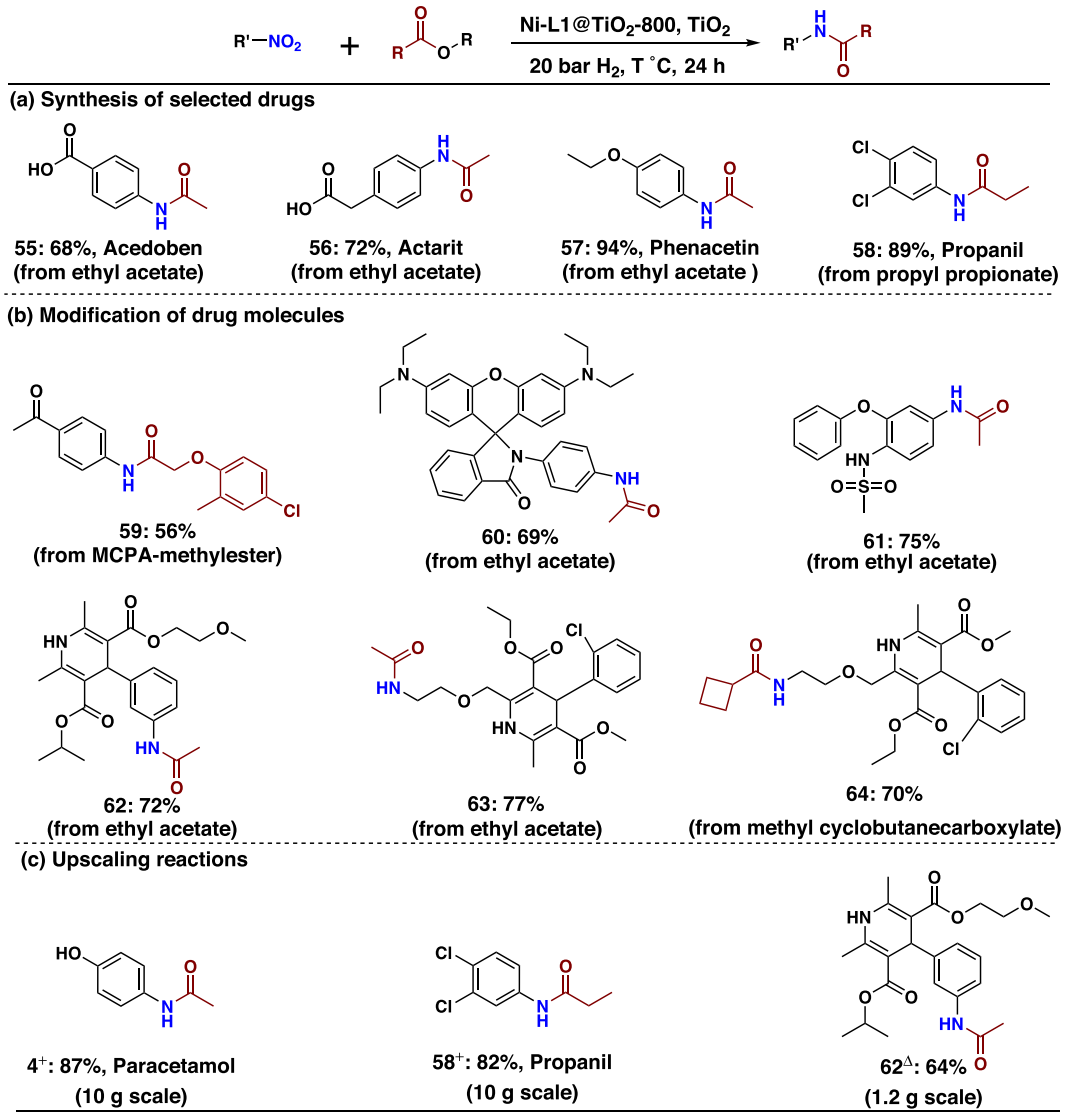

Fig. 9 | Applications of nickel-catalysed amidation. a Synthesis of selected drugs. Reaction conditions: 0.5 mmol nitro compound, 1 mL ester, 30 mg Ni-L1@TiO_2-800, 20 mg TiO_2, 20 bar H_2, 130 °C, 24 h. Isolated yields based on nitro compound. **b** Amidation of nitro and ester containing drugs. Reaction conditions: 0.5 mmol nitro compound, 1 mL ester, 30 mg Ni-L1@TiO_2-800, 20 mg TiO_2, 20 bar H_2, 130 °C, 24 h. Isolated yield based on nitro compound. **c** Scale-up reactions. [+]Reaction conditions: 10 g nitro compound, 30 mL ethyl acetate, required amount of catalyst and TiO_2 (30 mg of Ni-L1@TiO_2-800 and 20 mg TiO_2 for each 0.5 mmol nitro compound), 20 bar H_2, 130 °C, 24 h. [Δ]1.2 g nitro compound, 4 mL ethyl acetate, required amount of catalyst and TiO_2 (30 mg of Ni-L1@TiO_2-800 and 20 mg TiO_2 for each 0.5 mmol nitro compound), 20 bar H_2, 130 °C, 24 h. Isolated yields based on nitro compound. The detailed information of these esters is provided in Supplementary Fig. 22.

Then, once the chamber is heated to 130 °C with 10 °C/min, the sample is treated for 1 h. Afterward, the treated sample was directly transferred into the analysis chamber in vacuum (8×10^{-10}Pa) to avoid exposure to air.

The TEM measurement, the high-angle annular dark-field scanning transmission electron microscopic (HAADF-STEM) images were collected on a FEI Talos F200x S/TEM instrument at 300 kV accelerating voltage. HAADF-STEM images were acquired using a HAADF detector. To prepare the TEM samples, an appropriate amount of sample powder was dispersed in ethanol and then dropped on a 3 mm TEM Cu grid. The images of energy dispersive spectroscopy (EDS) elemental mapping in the STEM mode were obtained from the Titan electron microscope using SuperX system.

Surface area and porosity are carried out by the N_2 adsorption isotherm using the Brunauer-Emmett-Teller (BET) method on an ASAP 2020 Micromeritics instrument. Before analysis, all samples are degassed at 200 °C for 6 h to desorb moisture and impurities from their surfaces.

NH_3-TPD and CO_2-TPD measurements were done using a Micromeritics Autochem II 2910 instrument. A 150 mg sample was loaded in U shaped quartz reactor and heated from RT (room temperature) to 150 °C with 10 K/min in He (50 mL/min) to remove adsorbed water from the surface of the solid material. The temperature remained constant for 60 min, then cooled down to 100 °C in a flow of He (50 mL/min). Following, the sample was exposed to 1% NH_3 or 5% CO_2 in He (50 mL/min) for 60 min at 100 °C, followed by removal of physisorbed NH_3 or CO_2 by flushing with He (50 mL/min) for 60 min at 100 °C. The temperature was decreased for 70 °C for 10 min. The sample was then ramped to 650 °C at a heating rate of 10 K/min in flowing of He (50 mL/min). The temperature was held at 650 °C for 60 min. The analysis of the effluent gases was performed with Quadrupol mass spectrometer (Balzers Omnistar).

NMR spectra were recorded on Bruker AV 300 and 400 spectrometers. Chemical shifts are reported in parts per million relatives to $CDCl_3$ (7.26 and 77.16 ppm for ^1H and ^{13}C respectively) or DMSO-d6 (2.50 and 39.52 ppm for ^1H and ^{13}C respectively). Chemical shifts δ are reported in ppm relative to the solvent resonance signal as an internal standard. The following abbreviations were used to designate chemical shift multiplicities: s = singlet, d = doublet, t = triplet, q = quartet, sept = septet, m = multiplet, br = broad; coupling constants are given in Hertz (Hz).

HRMS data were recorded on (1) ESI-HRMS: HPLC System 1200 /ESI-TOF-MS 6210 (Agilent) and (2) EI-HRMS: Mass Spectrometer MAT 95XP (Thermo Electron), 70 eV. GC-MS was performed on an ISQ Trace 1300 in the electron ionization (EI) mode.

GC analyses was performed on an Agilent 7890 A instrument (Column: Agilent 19091J-413: 30 m × 320 µm × 0.25 µm, carrier gas: H_2, FID detection.

Details of DFT computations can be found in Supplementary Information. DFT Computational details.

All catalytic reactions were carried out in 300- and 100-mL autoclaves (PARR Instrument Company).

Preparation of catalytic materials

Preparation of TiO_2. TiO_2 slurry/gel prepared via sulfate process was commercially obtained from Kronos International, Inc., Research and Development, Germany and labelled as GL102/10826. The following procedure has been used to prepare final form of TiO_2 powder with significantly high surface area: The TiO_2 gel was added to distilled water and the dispersed solution was stirred for 20 min. Then, the mixture was allowed to settle for overnight or for several hours and then the upper layer of water was decanted. This procedure was repeated for 3 to 4 times until almost all soluble components in the slurry were removed by washing. Next, the resulting slurry was centrifuged for 15 min at a speed of 4240 rpm on Heraus instrument, Model: Sepatech 6000, Germany to obtain the solid material, which was then oven dried for 72 h (at 100 °C/24 h, at 150 °C/24 h and at 200 °C/24 h). The obtained TiO_2 clumps were powdered to get fine powder. The surface area of TiO_2 (oven dried at 200 °C) was found to be 295–315 m^2/g. In addition, the preparation of TiO2 support is reproducible and the elemental analysis result is show in Supplementary Table 5.

Preparation of Ni-L1@TiO_2-800 and other catalytic materials. In a 50 mL round bottomed flask, 576 mg $Ni(NO_3)_2$•$6H_2O$ and 300 mg ligand (L1, o-phenylenediamine) were stirred in 50 mL methanol at room temperature for 5 min. Then 2 g of TiO_2 support was added and stirring was continued for 12 h. Then, the methanol was removed by rotary evaporation and the solid material was dried in oven at 60 °C. The resulting material was grounded to a fine powder and transferred to quartz boat. The material was placed in tube furnace and pyrolyzed at 800 °C for 2 h under argon with a heating rate of 5 °C/min and then tube furnace was cooled to room temperature. After cooling the furnace to room temperature, the catalytic material was taken out from the furnace and stored in glass vial. In addition, we repeated the preparation of Ni-L1@TiO_2-800 and its catalytic performance is reproducible (see Supplementary Table 7).

Similar procedure was applied for the preparation of other materials such as Fe-L1@TiO_2-800, Co-L1@TiO_2-800, Ni-L1@C-800, Ni-L1@SiO_2-800 and Ni-L1@γ-Al_2O_3-800.

Note: Elemental analysis of ligands, $Ni(NO_3)_2$•$6H_2O$, TiO_2 and Ni-L1@TiO_2-800 are shown in Supplementary Table 5.

General procedure for the amidation of nitro compounds and esters

Solvent free condition. A magnetic stirring bar and 0.5 mmol nitro compound were transferred to 4 mL reaction vial and then 1 mL ethyl acetate or respective ester was added. Then, 30 mg catalyst (Ni-L1@TiO_2-800) and 20 mg TiO_2 were added, and the vial was fitted with septum, cap, and needle. Next, reaction vials (9 vials with different substrates at a time) were placed into a 300 mL autoclave. The autoclave was flushed with hydrogen for two times with 20 bar and then it was pressurized with 20 bar H_2. The autoclave was placed into an aluminium block preheated at 150–160 °C (placed 30 min before counting the reaction time to attain reaction temperature) and the reactions were stirred for required time. During the reaction the inside temperature of the autoclave was measured to be 130 °C–140 °C and this temperature was used as the reaction temperature. After the completion of the reactions, the autoclave was cooled to room temperature. The remaining H_2 gas was discharged slowly, and the reaction mixture were taken out from the autoclave. The reaction mixture was analysed by GC and GC-MS. The corresponding products were purified by column chromatography (silica, *n*-hexane, ethyl acetate). The purified products were analysed by NMR (^1H, ^{13}C), HRMS, and GC-MS.

Using toluene as solvent. For the reactions conducted in toluene solvent, similar experimental procedure was applied with 0.5 mmol nitro compound, 2 mmol corresponding ester and 1 mL toluene.

Scale-up reactions. 10-gram scale reactions were performed in Teflon fitted 300 mL autoclave. 10 g of respective nitro compound and 30 mL ethyl acetate were added to the Teflon fitted 300 mL autoclave and then required amount of Ni-L1@TiO_2-800 catalyst and TiO_2 (30 mg of Ni-L1@TiO_2-800 and 20 mg TiO_2 for each 0.5 mmol nitro compound). The autoclave was flushed with hydrogen for two times and then it was pressurized with 20 bar H_2. The autoclave was placed into an aluminium block preheated at the desired temperatures (placed 20 min before counting the reaction time to attain reaction temperature) and the reaction was stirred for required time. After the completion of the reactions, the autoclave was cooled to room temperature. The H_2 gas was released slowly, and the reaction mixture was taken out from the autoclave and analysed by GC and GC-MS. The corresponding products were purified by column chromatography (silica, *n*-hexane, ethyl acetate). The purified products were analysed by NMR (^1H, ^{13}C) and HRMS.

Note: for 1.2 g scale reaction carried out in 100 mL autoclave and similar procedure mentioned above has been applied.

Catalyst recycling. A 4 mL dried glass vial was charged with 0.5 mmol 4-nitrophenol and magnetic stirring bar. Then, 1 mL ethyl acetate was added followed by the addition of 60 mg Ni-L1@TiO_2-800. Then, the vial was fitted with septum, cap and needle and placed into a 300 mL autoclave. Then autoclave was flushed with 20 bar H_2 for two times, and it was pressured with 20 bar H_2. The autoclave was placed into an aluminium block preheated at 150 °C (placed 30 min before counting the reaction time to attain reaction temperature) and the reactions were stirred for required time. During the reaction the inside temperature of the autoclave was measured to be 130 °C and this temperature was used as the reaction temperature. After the completion of the reactions, the autoclave was cooled to room temperature. The H_2 gas was discharged slowly, and the reaction vials were taken out from the autoclave. The catalyst was separated by centrifugation and washed with ethel acetate. Then the recycled catalyst was dried and used for the next run without any reactivation.

Data availability

The data that support the findings of this study are available from the corresponding authors (M.B. and R.V.J.) upon request.

References

1. Wang, X. Challenges and outlook for catalytic direct amidation reactions. *Nat. Catal.* **2**, 98–102 (2019).

2. Lundberg, H., Tinnis, F., Selander, N. & Adolfsson, H. Catalytic amide formation from non-activated carboxylic acids and amines. *Chem. Soc. Rev.* **43**, 2714–2742 (2014).
3. Williams, R. E. & Marshall, C. M. Top 200 brand name drugs by retail sales in 2022. https://njardarson.lab.arizona.edu/sites/njardarson.lab.arizona.edu/files/NjardarsonGroup2022Top200PosterV5.pdf.
4. Sarak, S. et al. One-pot biocatalytic synthesis of nylon monomers from cyclohexanol using Escherichia coli-based concurrent cascade consortia. *Green. Chem.* **23**, 9447–9453 (2021).
5. Yokozawa, T., Ogawa, M., Sekino, A., Sugi, R. & Yokoyama, A. Chain-growth polycondensation for well-defined aramide. Synthesis of unprece dented block copolymer containing aramide with low polydispersity. *J. Am. Chem. Soc.* **124**, 15158–15159 (2002).
6. Zhang, D. W., Zhao, X., Hou, J. L. & Li, Z. T. Aromatic amide foldamers: structures, properties, and functions. *Chem. Rev.* **112**, 5271–5316 (2012).
7. Gnanaprakasam, B. & Milstein, D. Synthesis of amides from esters and amines with liberation of H_2 under neutral conditions. *J. Am. Chem. Soc.* **133**, 1682–1685 (2011).
8. Kumar, V., Kumar, M., Sharma, S. & Kumar, N. Highly selective direct reductive amidation of nitroarenes with carboxylic acids using cobalt(II) phthalocyanine/PMHS. *RSC Adv.* **4**, 11826 (2014).
9. Wang, S. P., Cheung, C. W. & Ma, J. A. Direct amidation of carboxylic acids with nitroarenes. *J. Org. Chem.* **84**, 13922–13934 (2019).
10. Mahjour, B., Shen, Y., Liu, W. & Cernak, T. A map of the amine-carboxylic acid coupling system. *Nature* **580**, 71–75 (2020).
11. Cheung, C. W., Leendert Ploeger, M. & Hu, X. Amide synthesis via nickel-catalysed reductive aminocarbonylation of aryl halides with nitroarenes. *Chem. Sci.* **9**, 655–659 (2018).
12. Allen, C. L., Chhatwal, A. R. & Williams, J. M. Direct amide formation from unactivated carboxylic acids and amines. *Chem. Commun.* **48**, 666–668 (2012).
13. Krause, T., Baader, S., Erb, B. & Goossen, L. J. Atom-economic catalytic amide synthesis from amines and carboxylic acids activated in situ with acetylenes. *Nat. Commun.* **7**, 11732 (2016).
14. Valeur, E. & Bradley, M. Amide bond formation: beyond the myth of coupling reagents. *Chem. Soc. Rev.* **38**, 606–631 (2009).
15. Constable, D. J. C. et al. Key green chemistry research areas—a perspective from pharmaceutical manufacturers. *Green. Chem.* **9**, 411–420 (2007).
16. Zheng, Y.-L. & Newman, S. G. Methyl esters as cross-coupling electrophiles: direct synthesis of amide bonds. *ACS Catal.* **9**, 4426–4433 (2019).
17. Ben Halima, T., Vandavasi, J. K., Shkoor, M. & Newman, S. G. A cross-coupling approach to amide bond formation from esters. *ACS Catal.* **7**, 2176–2180 (2017).
18. Ben Halima, T., Masson-Makdissi, J. & Newman, S. G. Nickel-catalyzed amide bond formation from methyl esters. *Angew. Chem. Int. Ed. Engl.* **57**, 12925–12929 (2018).
19. Cheung, C. W., Ploeger, M. L. & Hu, X. Direct amidation of esters with nitroarenes. *Nat. Commun.* **8**, 14878 (2017).
20. Ning, Y. et al. Site-specific umpolung amidation of carboxylic acids via triplet synergistic catalysis. *Nat. Commun.* **12**, 4637 (2021).
21. Ploeger, M. L., Darù, A., Harvey, J. N. & Hu, X. Reductive cleavage of azoarene as a key step in Nickel-catalyzed amidation of esters with nitroarenes. *ACS Catal.* **10**, 2845–2854 (2020).
22. Lundberg, H. et al. Mechanistic elucidation of zirconium-catalyzed direct amidation. *J. Am. Chem. Soc.* **139**, 2286–2295 (2017).
23. Ling, L., Chen, C., Luo, M. & Zeng, X. Chromium-catalyzed activation of acyl C-O bonds with magnesium for amidation of esters with nitroarenes. *Org. Lett.* **21**, 1912–1916 (2019).
24. Runikhina, S. A. et al. Catalytic utilization of converter gas - an industrial waste for the synthesis of pharmaceuticals. *Chem. Sci.* **14**, 4346–4350 (2023).
25. Gao, J. et al. Cobalt single-atom catalysts for domino reductive amination and amidation of levulinic acid and related molecules to N-heterocycles. *Chem. Catal.* **2**, 178–194 (2022).
26. Gao, J. et al. Ambient hydrogenation and deuteration of alkenes using a nanostructured ni-core-shell catalyst. *Angew. Chem. Int. Ed. Engl.* **60**, 18591–18598 (2021).
27. Murugesan, K., Beller, M. & Jagadeesh, R. V. Reusable Nickel nanoparticles-catalyzed reductive amination for selective synthesis of primary amines. *Angew. Chem. Int. Ed. Engl.* **58**, 5064–5068 (2019).
28. Murugesan, K. et al. Cobalt-nanoparticles catalyzed efficient and selective hydrogenation of aromatic hydrocarbons. *ACS Catal.* **9**, 8581–8591 (2019).
29. Hernandez Mejia, C., van der Hoeven, J. E. S., de Jongh, P. E. & de Jong, K. P. Cobalt-Nickel nanoparticles supported on reducible oxides as Fischer-Tropsch catalysts. *ACS Catal.* **10**, 7343–7354 (2020).
30. Kim, S. S., Lee, H. H. & Hong, S. C. The effect of the morphological characteristics of TiO_2 supports on the reverse water–gas shift reaction over Pt/TiO_2 catalysts. *Appl. Catal. B: Environ.* **119-120**, 100–108 (2012).
31. Sarmah, B. & Srivastava, R. Simple and economical synthesis of alkyl phenyl ethers by the reaction of phenols and alkyl esters using nanocrystalline beta. *ACS Sustain. Chem. Eng.* **3**, 210–215 (2015).
32. Biswas, S. et al. Expedient synthesis of bridged bicyclic nitrogen scaffolds via orthogonal tandem catalysis. *Angew. Chem. Int. Ed. Engl.* **60**, 21988–21996 (2021).
33. Winn, M. et al. Discovery, characterization and engineering of ligases for amide synthesis. *Nature* **593**, 391–398 (2021).
34. Huang, Z. et al. Mn-catalyzed selective double and mono-n-formylation and n-methylation of amines by using CO_2. *ChemSusChem* **12**, 3054–3059 (2019).
35. Liu, W. et al. A durable Nickel single-atom catalyst for hydrogenation reactions and cellulose valorization under harsh conditions. *Angew. Chem. Int Ed. Engl.* **57**, 7071–7075 (2018).
36. Hahn, G., Kunnas, P., de Jonge, N. & Kempe, R. General synthesis of primary amines via reductive amination employing a reusable nickel catalyst. *Nat. Catal.* **2**, 71–77 (2018).
37. Jagadeesh, R. V. et al. MOF-derived cobalt nanoparticles catalyze a general synthesis of amines. *Science* **358**, 326–332 (2017).
38. Jagadeesh, R. V. et al. Nanoscale Fe_2O_3-based catalysts for selective hydrogenation of nitroarenes to anilines. *Science* **342**, 1073–1076 (2013).
39. Gao, J. et al. Probing the enhanced catalytic activity of carbon nanotube supported Ni-LaOx hybrids for the CO_2 reduction reaction. *Nanoscale* **10**, 14207–14219 (2018).
40. Pews-Davtyan, A. et al. Biomolecule-derived supported cobalt nanoparticles for hydrogenation of industrial olefins, natural oils and more in water. *Green. Chem.* **21**, 5104–5112 (2019).
41. Nie, R. et al. Recent advances in catalytic transfer hydrogenation with formic acid over heterogeneous transition metal catalysts. *ACS Catal.* **11**, 1071–1095 (2021).
42. Ambrosi, A. & Denmark, S. E. Harnessing the power of the water-gas shift reaction for organic synthesis. *Angew. Chem. Int. Ed. Engl.* **55**, 12164–12189 (2016).
43. Wang, T. et al. Engineering catalytic interfaces in $Cu(\delta+)/CeO_2$-TiO_2 photocatalysts for synergistically boosting CO_2 reduction to ethylene. *ACS Nano* **16**, 2306–2318 (2022).
44. Tarditi, A. M. et al. XPS study of the surface properties and Ni particle size determination of Ni-supported catalysts. *Surf. Interface Anal.* **46**, 521–529 (2014).
45. Kang, L. et al. Photo-thermo catalytic oxidation over a TiO_2 -WO_3 -supported platinum catalyst. *Angew. Chem. Int. Ed. Engl.* **59**, 12909–12916 (2020).

46. Wang, G., Liu, Y., Ye, J. & Qiu, W. Synthesis, microstructural characterization, and electrochemical performance of novel rod-like Ti_4O_7 powders. *J. Alloy. Compd.* **704**, 18–25 (2017).
47. Biesinger, M. C., Payne, B. P., Lau, L. W. M., Gerson, A. & Smart, R. S. C. X-ray photoelectron spectroscopic chemical state quantification of mixed nickel metal, oxide and hydroxide systems. *Surf. Interface Anal.* **41**, 324–332 (2009).
48. Grosvenor, A. P., Biesinger, M. C., Smart, R. S. C. & McIntyre, N. S. New interpretations of XPS spectra of nickel metal and oxides. *Surf. Sci.* **600**, 1771–1779 (2006).
49. Zhang, K. et al. Levulinic acid hydrogenation to γ-valerolactone over single Ru atoms on a TiO_2@nitrogen doped carbon support. *Green. Chem.* **23**, 1621–1627 (2021).
50. Liang, Z. et al. Highly curved nanostructure-coated Co, N-doped carbon materials for oxygen electrocatalysis. *Angew. Chem. Int. Ed. Engl.* **60**, 12759–12764 (2021).
51. Xiao, X., Lim, S. H., Chu, W. & Liu, Y. Chitosan-derived porous N-doped carbon as a promising support for ru catalysts in one-pot conversion of cellobiose to hexitol. *ACS Sustain. Chem. Eng.* **9**, 12655–12662 (2021).
52. Huang, L. et al. Tuning the electron density of metal Nickel via interfacial electron transfer in Ni/MCM-41 for efficient and selective catalytic hydrogenation of halogenated nitroarenes. *ACS Sustain. Chem. Eng.* **10**, 2947–2959 (2022).
53. Hanawa, T. A comprehensive review of techniques for biofunctionalization of titanium. *J. Periodontal. Implant Sci.* **41**, 263–272 (2011).
54. Hauser, J. L. et al. A mesoporous aluminosilicate nanoparticle-supported Nickel–boron composite for the catalytic reduction of nitroarenes. *ACS Appl. Nano Mater.* **2**, 1472–1483 (2019).
55. Natte, K., Neumann, H., Jagadeesh, R. V. & Beller, M. Convenient iron-catalyzed reductive aminations without hydrogen for selective synthesis of N-methylamines. *Nat. Commun.* **8**, 1344 (2017).

Acknowledgements

We gratefully acknowledge the European Research Council (EU project 670986-NoNaCat) and the State of Mecklenburg-Vorpommern for financial and general support. We thank Drs. Stephan Bartling, Henrik Lund, Nils Rockstroh, and other members of the analytical team of LIKAT for their support and excellent work. Jie Gao and Rui Ma thanks the China Scholarship Council (CSC) for financial support.

Author contributions

R.V.J. and M.B. supervised the project. J.G., R.V.J. and M.B. planned and developed the project. J.G. and R.V.J. designed the experiments. F.P. performed selected experiments. J.G. and R.M. prepared catalysts and performed all catalytic experiments. F.R. and R.M. carried out reproducibility of experiments. L.Z. and N.W. performed the TEM and BET measurements. W.S. performed the DFT computation. H.A. performed the TPD measurements. S.W. supervised BET and TPD measurements. N.V.K. prepared the titania support. D.A.C. involved in the development of this project and corrected the NMR spectra and NMR data. J.G., R.V.J. and M.B. wrote the paper.

Funding

Open Access funding enabled and organized by Projekt DEAL.

Competing interests

The authors declare no competing interests.

Additional information

Supplementary information The online version contains supplementary material available at https://doi.org/10.1038/s41467-023-40614-1.

Correspondence and requests for materials should be addressed to Denis A. Chusov, Ning Wang, Rajenahally V. Jagadeesh or Matthias Beller.

Peer review information *Nature Communications* thanks Longlong Ma, Oleksandr Savateev and the other, anonymous, reviewer(s) for their contribution to the peer review of this work.

6. Curriculum Vitae

Rui Ma

Leibniz Institute for Catalysis e. V., Rostock, Germany

Room No: 2,125, Albert-Einstein-Str. 29a

18059 Rostock, Germany

Phone: (+49) 1744822362

E-Mail: rui.ma@catalysis.de

Date of birth: 25.06.1993

Place of birth: Sichuan, China

Nationality: Chinese

Education

(1) Leibniz Institute for Catalysis e. V., Rostock, Germany

PhD of chemistry. Advisor: Prof. Matthias Beller, 09. 2020-present

(2) Department of Chemical Engineering & Technology, Sichuan University

Master of Chemical Engineering. Advisor: Prof. Jianhong Luo, 09.2017-07.2020

(3) Department of Chemical Engineering & Technology, Ocean University of China

Bachelor of Chemical Engineering. 09.2012-07.2016

Publications

(1) Rui Ma, Jie Gao, Lan Zhang, Ning Wang, Yue Hu, Stephan Bartling, Henrik Lund, Sebastian Wohlrab*, Rajenahally V. Jagadeesh* and Matthias Beller * *Green. Chem*., DOI: DOI: 10.1039/D3GC03286H

(2) Base-free Selective α-Alkylation and α-Vinylation of Ketones with Alcohols over Fe/Zn Bimetallic Catalysts

Rui Ma, Jie Gao, Lan Zhang, Hanan Atia, Stephan Bartling, Henrik Lund, Ning Wang*, Sebastian Wohlrab*, Rajenahally V. Jagadeesh*, Matthias Beller* (in progress)

(3) Jie Gao, Rui Ma, Lu Feng, Yuefeng Liu, Ralf Jackstell, Rajenahally V. Jagadeesh*, Matthias Beller*. *Angew. Chem. Int. Ed.* 2021, **60**, 18591–18598. DOI:10.1002/anie.202105492

(4) Jie Gao[+], Lu Feng[+], Rui Ma[+], Bing-Jian Su, Asma M. Alenad, Yuefeng Liu*, Matthias Beller*, Rajenahally V. Jagadeesh*. *Chem Catalysis* **2**, 2022, 178–194, DOI: 10.1016/j.checat.2021.12.009 (co-first author).

(5) Jie Gao, Rui Ma, Fairoosa Poovan, Lan Zhang, Hanan Atia, Narayana V. Kalevaru, Sebastian Wohlrab, Ning Wang, Denis A. Chusov*, Rajenahally V. Jagadeesh,* and Matthias Beller*, *Nat. Commun., **14***, Article number: 5013 (2023), DOI: 10.1038/s41467-023-40614-1

(6) Kangkang Sun, Hongbin Shan, Rui Ma, Peng Wang, Helfried Neumann,* Guo-Ping Lu* and Matthias Beller*. *Chem. Sci*., 2022, **13**, 6865-6872. DOI: 10.1039/D2SC01838A.

(7) Rui Ma, Chunxin Fan, Yubin Wang, Jianhong Luo*, Jun Li, Yuzhu Ji. *Chem Eng Process*, **151**, 2020, 107916. DOI: 10.1016/j.cep.2020.107916.

(8) Rui Ma, Chunxin Fan, Yubin Wang, Jianhong Luo*, Jun Li, Sridhar Komarneni. *Chin. J. Chem. Eng.* **28**, (10), 2020, 2523-2532, DOI: 10.1016/j.cjche.2020.05.025.

(9) Rui Ma, Jie Gao, Xinhua Zhu, Yubin Wang, Jun Li, Jianhong Luo*. *Desalination Water Treat.,* **189,** 2020, 367–379. DOI: 10.5004/dwt.2020.25653.

Awards

(1) National Undergraduate Chemical Design Competition, Class 2, Aug 2015

(2) Shandong university students chemical process experiment competition, Class 3, Nov 2015

(3) Excellent student of Sichuan University, Oct 2018

(4) Excellent graduate student of Sichuan University, Oct 2019

Research interest

(1) Heterogeneous catalytic material, amination and amidation and formylation.

(2) Photocatalysis and electrocatalysis in organic chemistry

Research skills

(1) Column separation, GC, GC-MS, HPLC; NMR; XRD; XPS; TEM

(2) Skills with MS Office, ChemOffice, SciFinder, Reaxys

Language Skills

Chinese (mother language), English (fluent), German (not so good)

Rui Ma

7. Selbstständigkeitserklärung

4. Erklärung gemäß § 4 Absatz 1 Buchstaben g und h der Promotionsordnung

Doktorandinnen/Doktoranden-Erklärung gemäß § 4 Absatz 1 Buchstaben g und h der Promotionsordnung der Mathematisch-Naturwissenschaftlichen Fakultät der Universität Rostock

Name ..... Ma, Rui .....

(Name, Vorname)

Anschrift ..... Grossmann street, 01187, Dresden .....

(Straße, PLZ, Wohnort)

Ich habe eine Dissertation zum Thema

Development of non-noble metal-based heterogeneous catalysts for borrowing hydrogen and amidation reaction

an der Mathematisch-Naturwissenschaftlichen Fakultät der Universität Rostock angefertigt. Dabei wurde ich von Frau/Herrn

Prof. Dr. Matthias Beller betreut.

Ich gebe folgende Erklärung ab:

1. Die Gelegenheit zum vorliegenden Promotionsvorhaben ist mir nicht kommerziell vermittelt worden. Insbesondere habe ich keine Organisation eingeschaltet, die gegen Entgelt Betreuerinnen/Betreuer für die Anfertigung von Dissertationen sucht oder die mir obliegenden Pflichten hinsichtlich der Prüfungsleistungen für mich ganz oder teilweise erledigt.

2. Ich versichere hiermit an Eides statt, dass ich die vorliegende Arbeit selbstständig angefertigt und ohne fremde Hilfe verfasst habe. Dazu habe ich keine außer den von mir angegebenen Hilfsmitteln und Quellen verwendet und die den benutzten Werken inhaltlich und wörtlich entnommenen Stellen habe ich als solche kenntlich gemacht.

Rostock, den 19.01.2024 ..... Rui Ma .....

(Unterschrift)